National Library of Canada
Acquisitions and Bibliographic Services Branch
395 Wellington Street
Ottawa, Ontario
K1A 0N4

Bibliothèque nationale du Canada
Direction des acquisitions et des services bibliographiques
395, rue Wellington
Ottawa (Ontario)
K1A 0N4

Your file Votre référence

Our file Notre référence

NOTICE

The quality of this microform is heavily dependent upon the quality of the original thesis submitted for microfilming. Every effort has been made to ensure the highest quality of reproduction possible.

If pages are missing, contact the university which granted the degree.

Some pages may have indistinct print especially if the original pages were typed with a poor typewriter ribbon or if the university sent us an inferior photocopy.

Reproduction in full or in part of this microform is governed by the Canadian Copyright Act, R.S.C. 1970, c. C-30, and subsequent amendments.

AVIS

La qualité de cette microforme dépend grandement de la qualité de la thèse soumise au microfilmage. Nous avons tout fait pour assurer une qualité supérieure de reproduction.

S'il manque des pages, veuillez communiquer avec l'université qui a conféré le grade.

La qualité d'impression de certaines pages peut laisser à désirer, surtout si les pages originales ont été dactylographiées à l'aide d'un ruban usé ou si l'université nous a fait parvenir une photocopie de qualité inférieure.

La reproduction, même partielle, de cette microforme est soumise à la Loi canadienne sur le droit d'auteur, SRC 1970, c. C-30, et ses amendements subséquents.

Canada

CHEMICAL PETROLOGY, MINERALOGY AND STRUCTURE OF THE TULAMEEN COMPLEX, PRINCETON AREA, BRITISH COLUMBIA

by
Vera Jacqueline Rublee

A thesis submitted to the School of Graduate
Studies and Research in partial fulfillment of the requirements
for the degree of M.Sc. in Geology

UNIVERSITY OF OTTAWA
OTTAWA, CANADA, 1994

ISBN 0-315-95991-6

UNIVERSITÉ D'OTTAWA
UNIVERSITY OF OTTAWA

Abstract

The Tulameen complex is a structurally disrupted pluton made up of equal proportions of ultramafic and feldspathic rocks that outcrop for over 60 km^2 in southwestern British Columbia. Situated at the western margin of the Intermontane belt, the 14 km length of the Tulameen complex parallels the eastern boundary of the Eagle plutonic complex. Dunite, olivine and hornblende clinopyroxenite are the principle ultramafic rocks; wehrlite, olivine-hornblendite, magnetite clinopyroxenite and hornblendite are subordinate and are not mappable units. Feldspar-bearing rocks underlie the eastern half of the Tulameen complex and exhibit a progressive petrologic zonation from gabbro—proximal to the ultramafic rocks—to syenogabbro and syenodiorite eastwards. Ductile shearing and brittle faulting of the Tulameen complex obscure the relationships between the various rock types, and the widespread faulted lithologic contacts attest that its present distribution does not represent its original entirety.

The Tulameen complex is faulted against Late Triassic to Early Jurassic age (Campbell and Tipper, 1971) lower greenschist grade metasedimentary and metavolcanic rocks of the Nicola Group to the east, and to the west by a one km wide belt of penetratively deformed schistose rocks, correlated with the Nicola Group (Monger, 1985). Contacts are northwest-striking mylonitic shear zones—characterized by sub-horizontal stretching lineations—which extend beyond the ultramafic-syenodioritic body and envelope several smaller ultramafic bodies along the strike to the northwest and southeast of the Tulameen complex. The plutonic rocks become increasingly foliated and, in the case of feldspar-bearing rocks, intensely saussuritized adjacent to these high strain zones. The sense of shear along the northwest-trending ductile faults was determined to be dextral. Tertiary brittle structures overprint the ductile fabric and disrupt all units in the Tulameen area.

The petrology and mineralogy of the Tulameen complex indicates an origin by subduction zone processes. The chemical trends revealed in the olivine, clinopyroxene and hornblende compositions are consistent with the crystallization of the Tulameen complex in a hydrous environment, under relatively high fO_2. Trace element chemistry of the representative rock-types exhibit a subduction-zone signature (enriched LILE and LREE, and depleted HFSE relative to MORB abundances); REE patterns indicate a calc-alkaline affinity of the magma.

The interpreted crystallization age of 209.9 ± 4.7 Ma (U-Pb zircon) for the syenodioritic phase is a minimum crystallization age for the Tulameen complex. This age confirms the contemporaneity between the Tulameen complex and the suite of calc-alkaline and alkaline plutons spatially associated with the Nicola Group. These Late Triassic to Early Jurassic plutons have been interpreted by Mortimer (1987) as the final stages of Nicola related magmatism. The structurally controlled emplacement of many of these intrusions (Barr et al., 1976; Hollister et al., 1975) suggests that the demise of the Nicola arc was coincident with deformation. If the ductile deformation of the Tulameen complex is syn-intrusive—as suggested by the closed system behavior of the hornblendes for argon (McDougall, 1974) and confinement of post-cumulus hornblende to the ductile shear zones which bound and cut through the complex—the dextral shearing of the Tulameen complex may represent a deeper structural equivalent of the Late Triassic to Early Jurassic (210-190 Ma; Mortimer et al., 1990) dextral faulting associated with the emplacement of the Guichon Creek Batholith.

The difference in structural fabrics and K-Ar hornblende data between the Tulameen and Eagle plutonic complexes suggests that the two have experienced different structural and thermal histories prior to the mid-Cretaceous. It is postulated that the formation of the northwest-trending ductile fabric in the Tulameen complex is genetically unrelated to the Middle Jurassic deformation associated with the Eagle shear zone, as proposed by Greig (1992).

Table of Contents

Table of Contents (continued)

Table of Contents (continued)

List of Tables

List of Illustrations

Figures

List of Illustrations

Figures (continued)

Plates

Acknowledgements

The author would like to thank Drs. André Lalonde and Ralph Kretz for their supervision and advice, and Dr. Randy Parrish for his interest and commitment.

Fieldwork was supported by grants obtained from the British Columbia Geological Survey Branch for the 1987 and 1988 field seasons. Graduate research at the University of Ottawa was funded by an Ontario Graduate Scholarship and initial support provided by Dr. R. Kretz (NSERC grant) is gratefully acknowledged. Dr. Bill McMillan from the British Columbia Geological Survey Branch was helpful in defining areas of further study of the Tulameen complex during the planning stages of the project. Dr. Graham Nixon, also from the British Columbia Geological Survey Branch, was generous with sharing both his observations and thoughts on the Tulameen complex as well as logistical support while in the Tulameen area. The field support of Nathalie Prud'homme is acknowledged with gratitude, as are field visits by Dr. Ralph. Kretz and Dr. and Mrs. André Lalonde.

Dr. André Lalonde made access to the microprobe at McGill University possible and selflessly dedicated many hours of his own time during the acquisition of the data. Dr. Randy Parrish and staff of the Geochronology Laboratory of the Lithosphere and Canadian Shield Division of the Geological Survey of Canada carried out the U-Pb chemistry and mass spectrometry for the U-Pb zircon analyses. Assistance from the members of the faculty and staff at the Ottawa-Carleton Geoscience Centre, notably Ron Hartree, Jean-François Tardif, John Loop and Dr. J. Moore is appreciated. The undergraduate and graduate students at the Ottawa-Carleton Geoscience Centre provided enjoyable companionship and greatly enriched the author's experience in Ottawa; in particular, Dr. M. Savard. Computer facilities in the geology department at the University of California at Santa Barbara were made available to the author.

Emotional thanks go to several people whose part in the completion of this thesis is significant. André Lalonde's keen enthusiasm, unfaltering support and friendship is valued deeply. Jack and Nin Rublee's participation in all phases of the study from fieldwork to writing, is acknowledged with appreciation and pride. Jack Rublee's editing greatly clarified and improved the manuscript.

Dave Parkinson is credited with keeping the author enthused and excited about the geology of the Tulameen complex. His contribution is great and includes assistance in the field, discussions about the structural and geochonologic components of the Tulameen complex, and especially support and encouragement. The completion of this work is due in large part to my husband, Dave.

Chapter 1.

Introduction to the Tulameen complex.

Introduction

The Tulameen complex is a structurally disrupted pluton made up of equal proportions of ultramafic and feldspathic rocks that outcrop over 60 km^2 in southwestern British Columbia. Dunite, olivine and hornblende clinopyroxenite are the principle ultramafic rocks; wehrlite, olivine-hornblendite, magnetite clinopyroxenite and hornblendite are subordinate and are not mappable units (Findlay, 1963). Feldspar-bearing rocks underlie the eastern half of the Tulameen complex and exhibit a progressive zonation from gabbro—proximal to the ultramafic rocks—to syenogabbro and syenodiorite eastwards. Ductile shearing and brittle faulting of the Tulameen complex obscures the relationships between the various rock types, and the widespread faulted lithologic contacts intimate that the present map pattern does not represent its original entirety.

On a basis of petrography and mineralogy, the Tulameen complex has been included within the distinct class of ultramafic bodies referred to as Alaskan-type zoned ultramafic intrusions (Noble and Taylor, 1960; Taylor and Noble, 1960). These complexes are distinguished from Alpine-type and stratiform bodies by a crudely concentric zonation of successive shells of peridotite (wehrlite), clinopyroxenite and hornblendite about a plug-like dunite core (Jackson and Thayer, 1972). Their global distribution, which reveals a confinement to regional scale belts within compressional orogenic zones (Taylor, 1967; Snoke et al., 1982), include the 750 km long middle Cretaceous age Klukwan-Duke belt of southeastern Alaska, the 1500 km long Late Triassic to Early Jurassic belt in British Columbia and the Yukon, the 600 km long middle to late Paleozoic belt in the Ural Mountains of Russia, and a 350 km long Middle to Late Jurassic belt in the Sierra Nevada and Klamath Mountains of California (Saleeby, 1992). Solitary zoned ultramafic complexes within arc volcanic terranes

have been described in New Zealand (Mossman, 1973), Ethiopia (Molly, 1959), eastern United States (Butler, 1989), Venezuela (Murray, 1973) and Japan (Onuki, 1963).

The petrologic significance of Alaskan-type zoned ultramafic complexes as the feeder zones to andesitic volcanoes was first recognized by Murray (1972). Conrad and Kay (1984) and Foden and Green (1992), among others, proposed that zoned ultramafic complexes, as well as cumulate xenoliths in mafic arc magmas (Aoki, 1971; Arculus and Wills, 1980; Conrad and Kay, 1984; Debari et al., 1987 and Takahashi, 1986), represent the early stages of arc evolution and constitute a petrologic Moho.

A major focus of this study is the petrogenesis of the Tulameen complex, and its relevance to the evolution of the southwestern Intermontane belt in British Columbia.

Location of the Tulameen complex

The Tulameen complex is located 175 km due east of Vancouver and 23 km northwest of Princeton (Fig. 1.1). It is reached by a three hour drive from Vancouver along networks of unpaved logging roads which branch southeastwards off of the Coquihalla highway, and westwards off of the Princeton-Tulameen road. The Tulameen River road crosses the body 7 km due east of the town of Tulameen. Most of the logging roads are actively used by the logging companies working within the area and are generally well maintained.

Physiography and history of the Tulameen River area

The high, rolling landscape of the Thompson plateau of the interior plateau physiographic province characterizes the topography of the Tulameen area. This 1200 to 1500 m high Thompson plateau is deeply cut by rivers which drain into either the Fraser or Columbia rivers. The Tulameen River, which is a tributary of the Columbia River, traverses the Tulameen complex and exposes 1200 vertical metres of ultramafic rock. Grasshopper, Olivine and Lodestone Mountains rise above the plateau with heights of 1470, 1770 and 1865 metres respectively.

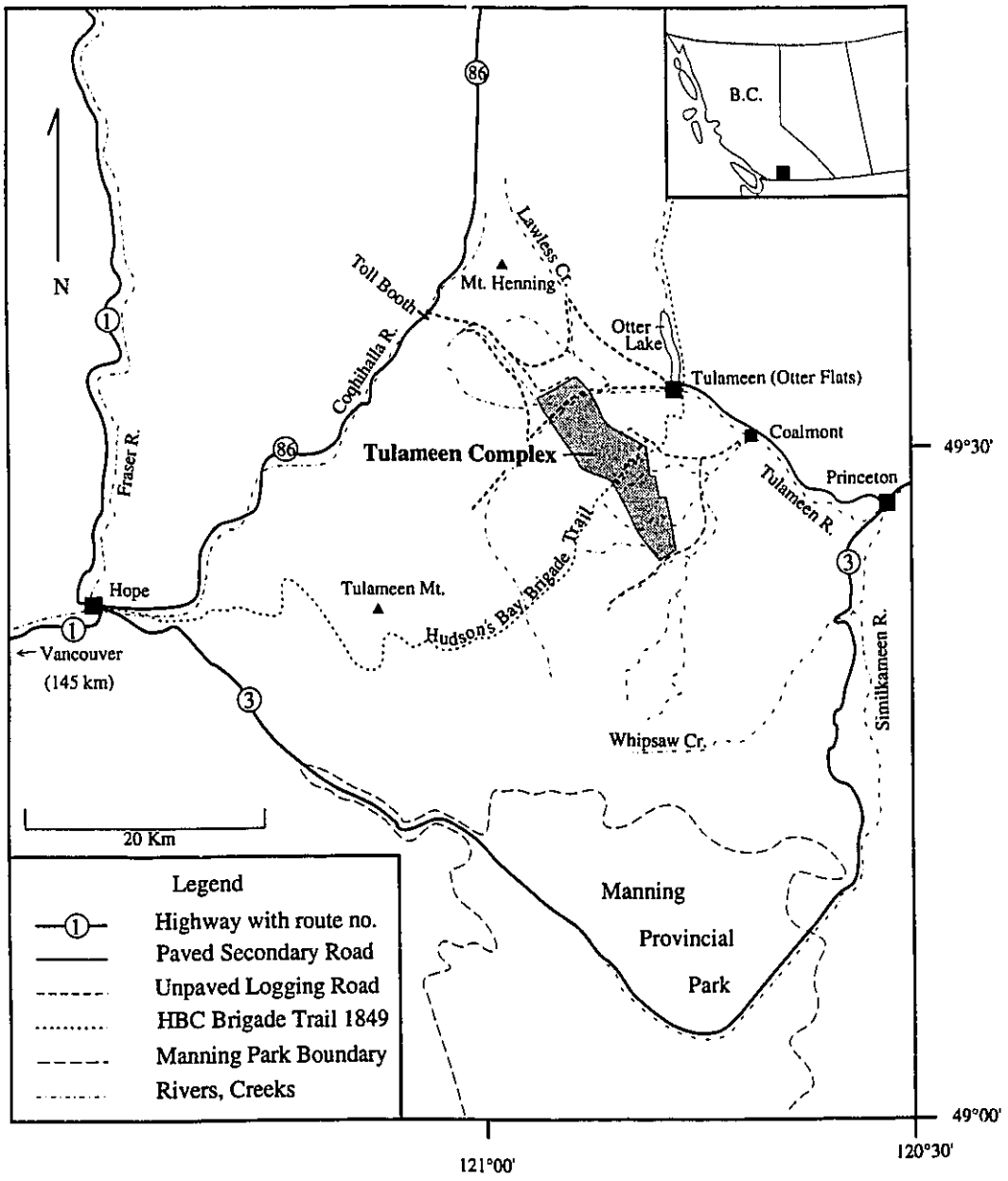

Figure 1.1. Map of the Hope-Princeton area in southern British Columbia showing the location of, and access to, the Tulameen complex. The historic Hudson Bay brigade trail bisects the Tulameen complex and was a major transportation route in the Tulameen valley during the mid- to late 1800's. Modified after Akrigg and Akrigg (1970).

The name "Tulameen" is derived from a North American Indian (Salish) word for "red earth " (Akrigg and Akrigg, 1969). The red ochre, exposed along the banks of the Tulameen River, was used for pictographs and face paint by North American aboriginal people from as far away as the great plains (Bryan, 1981). During the early to mid 1800's, the Tulameen valley became a transportation corridor for the Hudson's Bay company. Stiff customs duties imposed by the Americans forced the Hudson's Bay company to seek an all-British route for its fur brigade to travel between the interior and coast. The Hudson's Bay brigade trail, completed between 1846 and 1847, used the Indian Blackeye's trail which carried the fur brigades over Lodestone Mountain to an Indian campsite called Otter Flats on the Tulameen River near Otter Lake. The settlement of Campement des Femmes was established at Otter Flats, where the wives and children of the fur brigade men would stay when the men journeyed into the mountains (Camsell, 1913; Fig. 1.1).

The Hudson's Bay brigade trail had grown into a larger transportation route for livestock by the late 1800's. In 1885, the discovery of placer gold by a cowboy named Johnny Chance brought a rush of placer miners into the Tulameen Valley (Bryan, 1981). From the late 1880's to 1920's approximately 685,714 grams/tonne of placer platinum was mined from the Tulameen River and its tributaries which drain the area of the ultramafic rocks of the complex (Rublee, 1986). The Tulameen Valley during this time was the sole North American source for platinum. Tertiary coal deposits within the Tulameen basin, known since 1885 (Donaldson, 1973), were mined by underground methods from 1919 to 1940, and by opencast mining from 1954 to 1957 (Goodharzi and Van Der Flier-Keller, 1988).

Previous geological studies within the Tulameen River area.

Among the earliest published geological investigations of the Princeton area were those carried out by the International Boundary Commission Expedition led by Bauerman from 1859-1861 (Dawson, 1879) and Daly from 1901-1906 (Camsell, 1913). G.M. Dawson of the

Geological Survey of Canada, explored a large part of southern British Columbia, including the Princeton area in 1877. Monger's (1989a) Geological Survey of Canada open file map (1: 250,000) of the Hope-Ashcroft district is the most recent geological compilation of the region which includes the Tulameen complex.

The first documented field study of the Tulameen area was done by Camsell of the Geological Survey of Canada from 1906-1912. This reconnaissance survey led to a GSC 1913 memoir, containing the first published map of the area and detailed descriptions of the rock units and mineral prospects. Subsequent to this work, the nature and distribution of platinum-group elements, chromite and magnetite, within the ultramafic rocks was the subject of many investigations by the geological surveys of Canada (Rice, 1947; O'Neill and Gunning, 1934; Cabri et al. 1973; Raicevic and Cabri, 1976), United States (Kemp, 1902; Mertie, 1969) and British Columbia (Eastwood 1959).

The Tulameen complex was remapped in detail during the late 1950's as a part of a Ph.D. project undertaken by D.C. Findlay (1963). Subsequent work includes M.Sc. studies by Roddick (Roddick and Farrar, 1971) and St. Louis (1984). At the time the present study was being carried out, G.N. Nixon of the British Columbia Geological Survey Branch examined the Tulameen complex during the 1987 field season to evaluate the chromite and PGE (i.e. platinum group elements) potential (Nixon and Rublee, 1988; Nixon et al., 1990). Findlay's (1963) detailed 1: 20,000 geological map of the Tulameen complex has remained the foundation of all further work, with minor additions and modifications.

Regional geology of the southwestern Intermontane belt.

The geology of British Columbia is fascinating in the extreme diversity of its strata, magmatism, metamorphism and deformational style. This heterogeneity is due to the variedstratigraphy, tectonic pattern and history of the individual terranes which comprise the Canadian Cordillera (Fig. 1.2a). Despite the fundamental differences between the terranes,

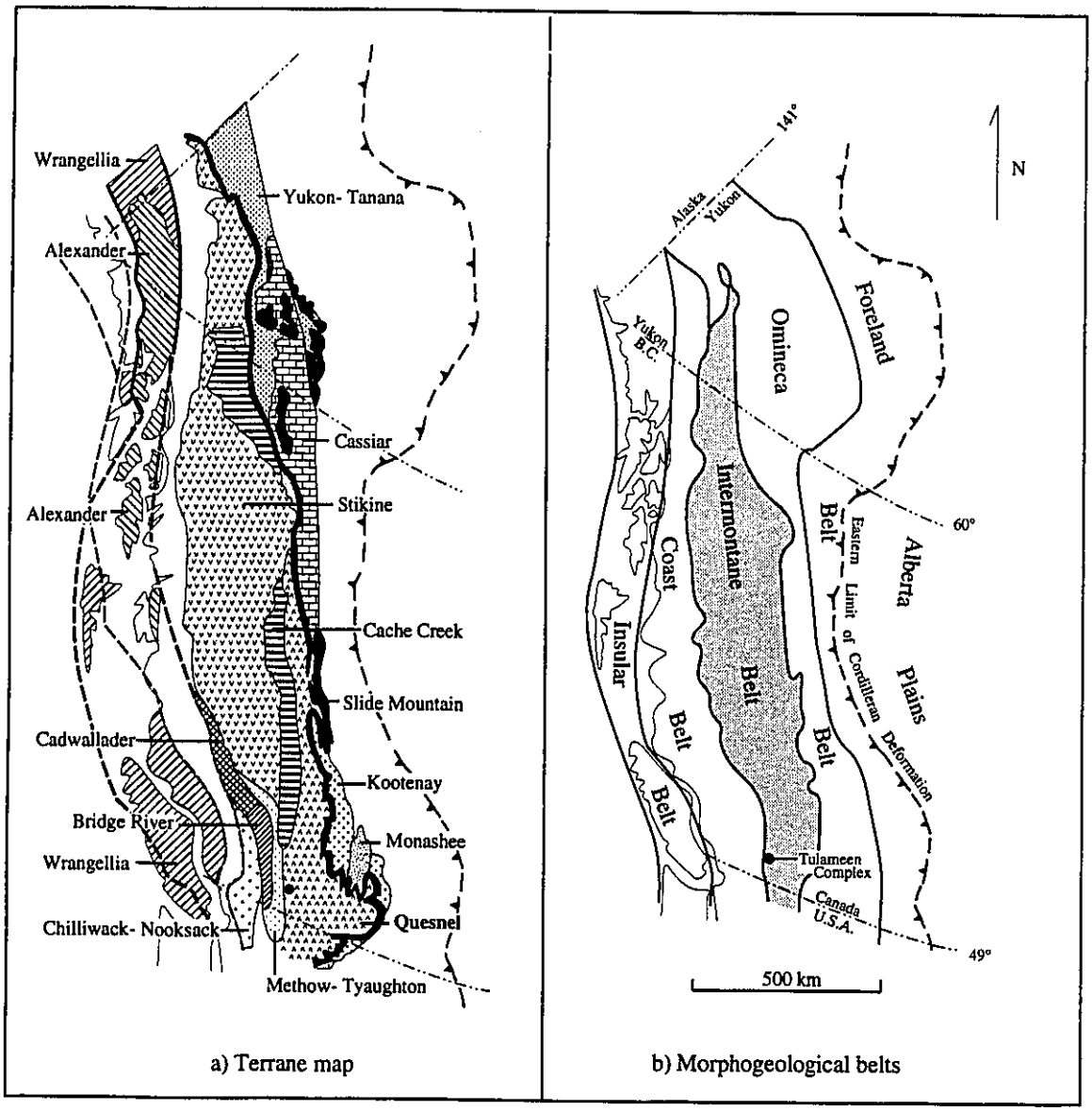

Figure 1.2 Distribution of terranes (a) and morphogeological belts (b) in the Canadian Cordillera. The Tulameen complex is situated at the western margin of Quesnel terrane (a) in the southwest part of the Intermontane belt. Modified after Monger (1989b).

five northwest-trending belts are demarked on the basis of similarity in metamorphism, volcanism and deformation. These morphogeological belts, from east to west, are the Foreland, Omineca, Intermontane, Coast and Insular belts (Price et al., 1985; Fig. 1.2b). The alternate Foreland, Intermontane and Insular belts are distinguished from the intervening, spectacularly rugged Omineca and Coast mountainous belts by a topographically subdued landscape made up of unmetamorphosed stratified rocks, and their low metamorphic grade equivalents, of oceanic and island arc affinities.

The Intermontane belt, which includes the Tulameen complex at its southwest margin (Fig. 1.2b) includes island arc (Stikine and Quesnel) and oceanic (Cache Creek) terranes (Fig. 1.2a). In southern British Columbia, the Quesnel terrane consists of a Paleozoic stratigraphy of marine volcanic and sedimentary rocks of 1) Devonian to Permian Harper Ranch Group (Monger, 1985) and 2) the Devonian through Triassic age Apex Mountain complex (Monger et al., 1982); these are overlain by felsic to mafic volcaniclastic rocks, flows and sedimentary rocks of the Late Triassic to Early Jurassic Nicola Group (Campbell and Tipper, 1971). Several calc-alkaline and alkaline plutons which exhibit a wide range in composition from dunite to diorite and syenite intrude, or are emplaced into, the Nicola strata. Shales, sandstones and conglomerates of the Early to Middle Jurassic Ashcroft Formation (Frebold and Tipper, 1969) unconformably overly the Nicola Group, approximately 100 km north of the Tulameen area (Fig. 1.3).

The Mesozoic stratigraphy of the Quesnel terrane has been interpreted (Mortimer, 1987) as a west-facing volcanic arc built upon an older Paleozoic basement (Read and Okulitch, 1977; Fig. 1.4a). The evidence for east-dipping subduction beneath the Quesnel terrane in the Late Triassic to Early Jurassic, is the distribution of younger (Norian to Sinemurian) shoshonitic lavas to the east of older—Carnian to Norian—calc-alkaline lavas (Mortimer, 1987). The disrupted Pennsylvanian to Middle Jurassic chert, argillite, basalt, limestone and alpine-type

Legend to generalized geological map of the southwestern Intermontane belt (Fig. 1.3) on verso.

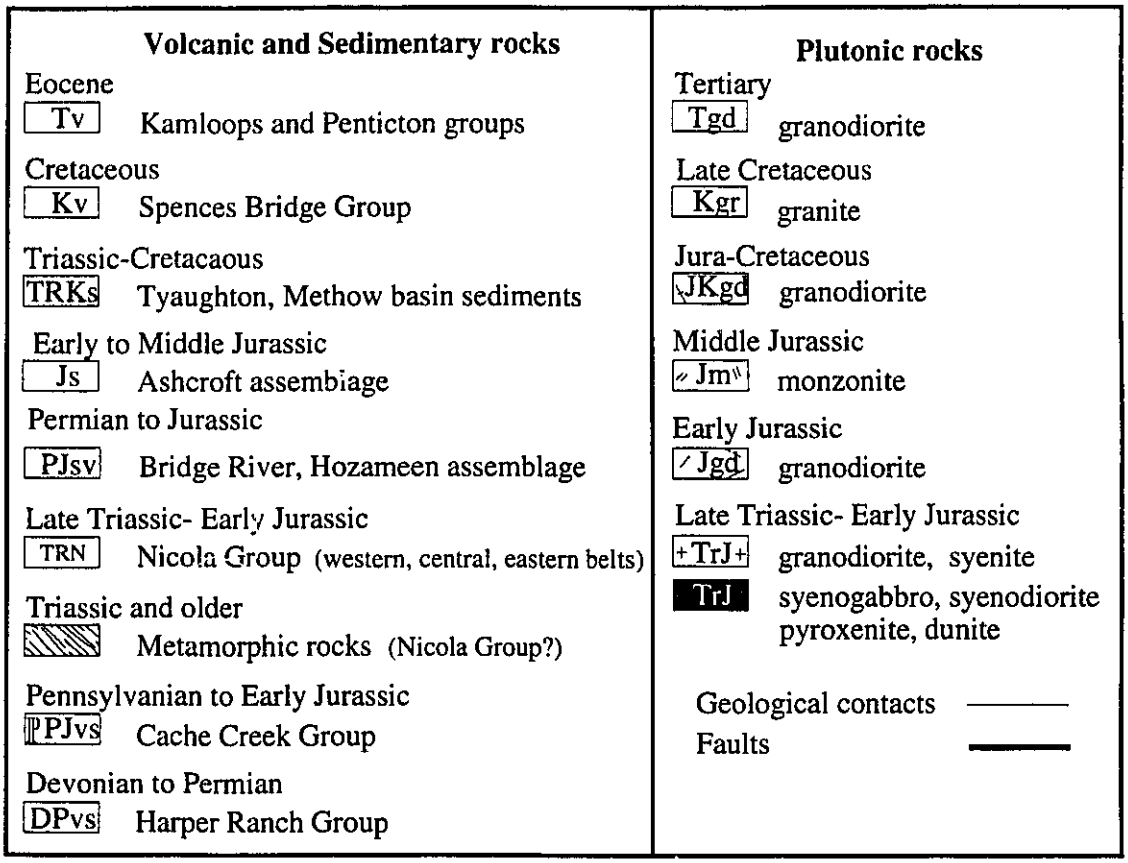
Volcanic and Sedimentary rocks
Eocene
Tv
Kamloops and Penticton groups
Cretaceous
Kv
Spences Bridge Group
Triassic-Cretacaous
TRKs
Tyaughton, Methow basin sediments
Early to Middle Jurassic
Js
Ashcroft assembiage
Permian to Jurassic
PJsv
Bridge River, Hozameen assemblage
Late Triassic- Early Jurassic
TRN
Nicola Group (western, central, eastern belts)
Triassic and older
Metamorphic rocks (Nicola Group?)
Pennsylvanian to Early Jurassic
PPJvs
Cache Creek Group
Devonian to Permian
DPvs
Harper Ranch Group
Plutonic rocks
Tertiary
Tgd
granodiorite
Late Cretaceous
Kgr
granite
Jura-Cretaceous
JKgd
granodiorite
Middle Jurassic
Jm
monzonite
Early Jurassic
Jgd
granodiorite
Late Triassic- Early Jurassic
+TrJ+
granodiorite, syenite
TrJ
syenogabbro, syenodiorite
pyroxenite, dunite
Geological contacts
Faults

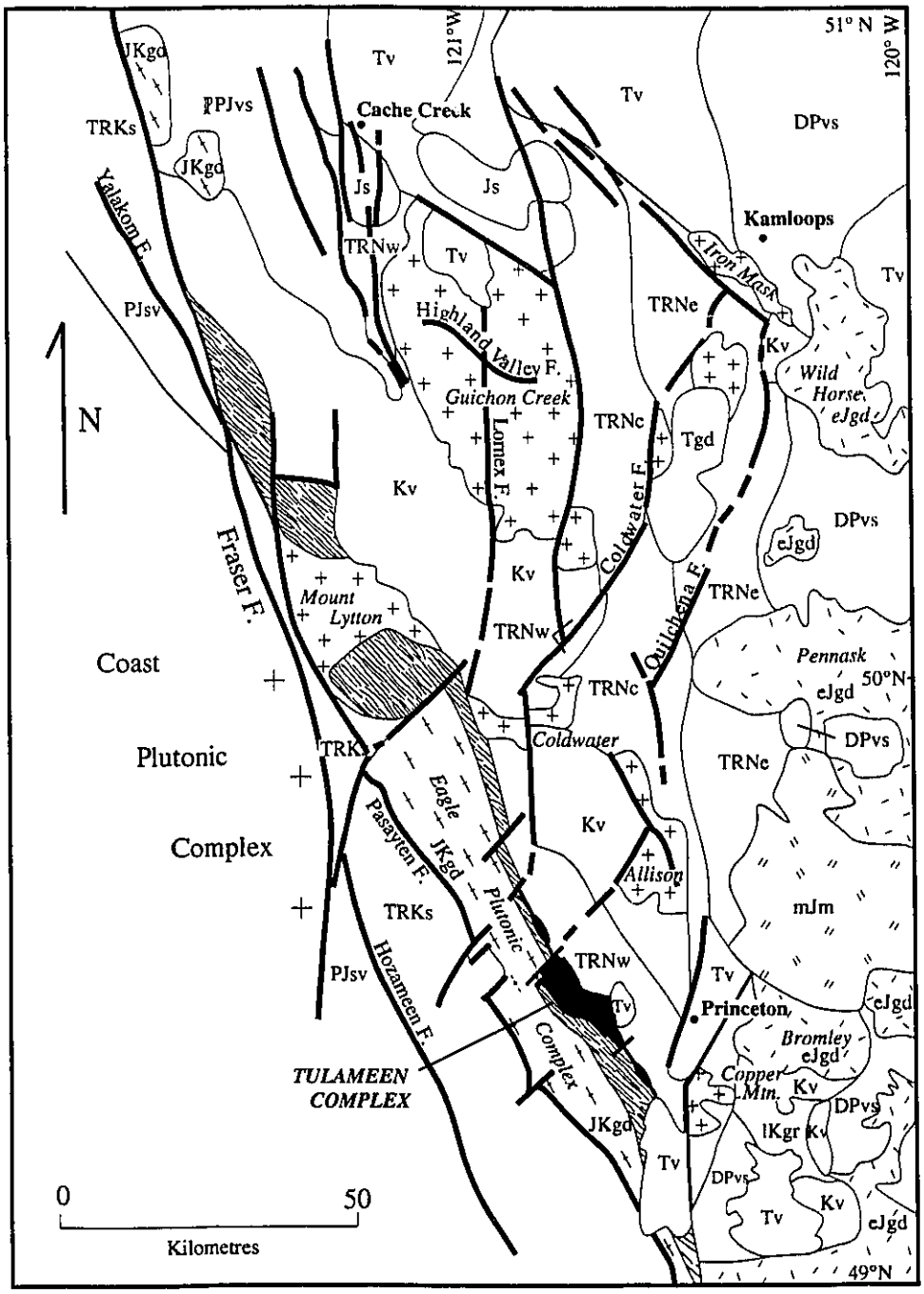

Figure 1.3. Generalized geological map of the southwestern Intermontane belt, modified after Mortimer (1987), Monger (1985) and Parrish and Monger (1992). Legend for map is displayed on page facing.

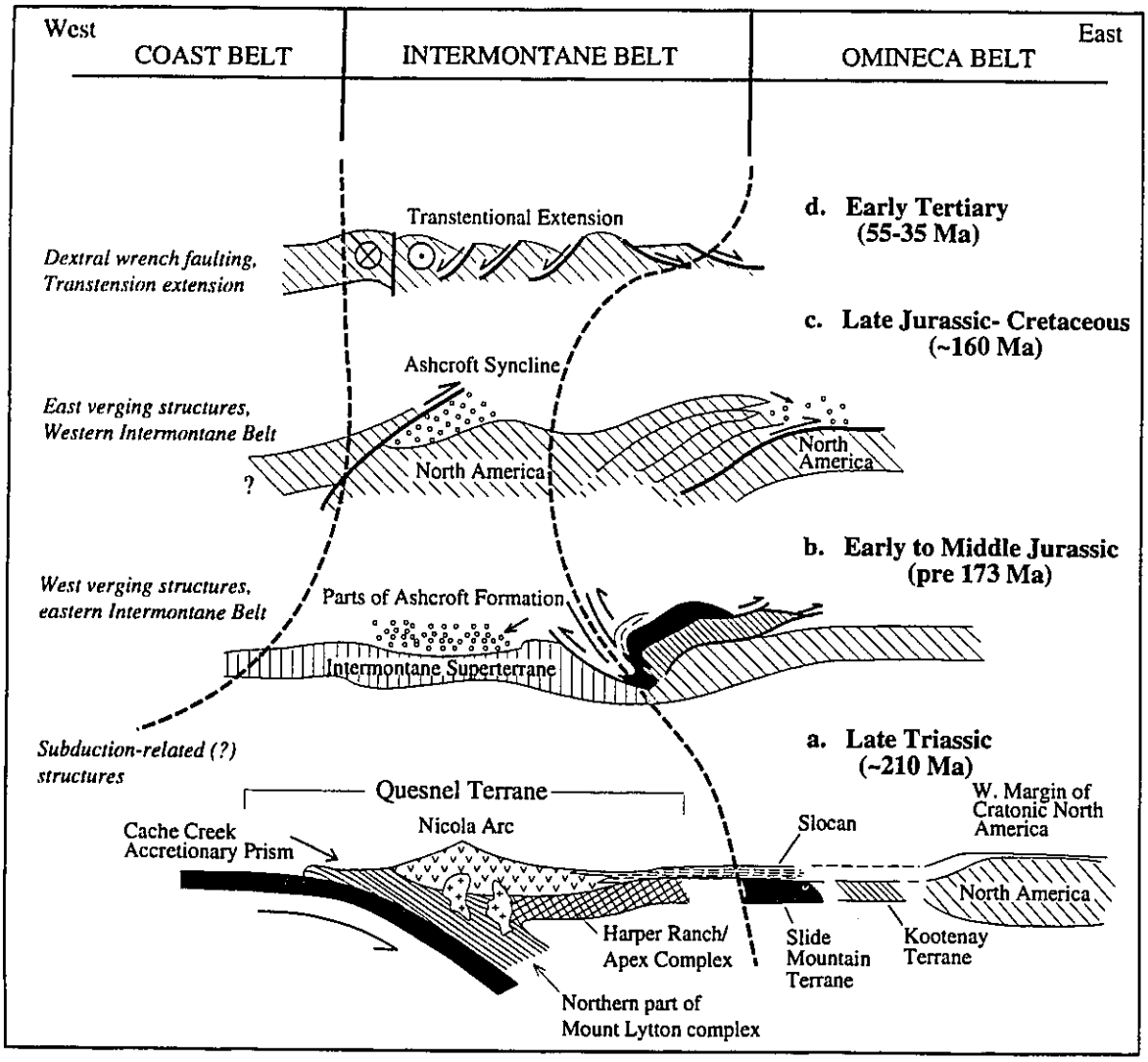

Figure 1.4. Diagrammatic representation of the late Paleozoic to Neogene evolution of the southwest Intermontane belt (modified after Monger, 1989b). a) During the Late Triassic, Quesnel terrane comprises a west facing arc (Nicola) built upon an older Paleozoic basement (Harper Ranch and Apex Complex), and an east dipping accretionary prism (Cache Creek group). Quesnel and oceanic Slide Mountain terranes are obducted onto the North American craton during the Early to Middle Jurassic (b) and are further deformed by Late Jurassic to Cretaceous east directed thrusting (c) and Tertiary brittle faulting (d).

ultramafic rocks of the Cache Creek terrane (Price et al., 1985), are interpreted as the remnants of the west-facing accretionary prism to the Nicola arc (Mortimer, 1986).

The accretion of Quesnel and oceanic Slide Mountain terrane to the east, onto the North American continental margin during the Early to Middle Jurassic (pre 173 Ma.; Parrish and Wheeler, 1983; Fig. 1.4b) preceded the Middle-Late Jurassic eastward thrusting of Cache Creek terrane over Quesnel terrane in southern British Columbia (ca. 160 Ma; Travers, 1982; Mortimer et al., 1990; Fig. 1.4c). Monger (1985) regards the northeasterly-verging structures along the eastern margin of the Eagle complex as the lower level equivalents of this Middle Jurassic Cache Creek-Quesnel terrane deformation. In agreement with Monger (1985), Greig et al. (1992) suggest that the plutonism and deformation related to emplacement of the Eagle tonalite (155 ± 4 Ma; U-Pb zircon) and Falls Lake suite (110.5 ± 2.0 Ma; U-Pb zircon)—and uplift of the Mount Lytton complex—reflect the initial and final stages of the accretion of the Insular superterrane (amalgamated Peninsular, Wrangellia and Alexander terranes) to North America. The Late Jurassic deformation, characterized by northeast verging structures in the Eagle complex (Monger, 1985; Greig 1992), Cache Creek terrane (Mortimer et al., 1990) and Ashcroft Formation (Travers, 1978) (Fig. 1.4c), obscures an earlier late Paleozoic to early Mesozoic subduction-related fabric, preserved in rocks of the Mount Lytton complex (Monger, 1985) and Quesnel terrane (Moore, 1989; Hollister et al., 1975; Fig. 1.4a).

Deposition of the Ashcroft Formation in Early to Middle Jurassic time, upon the Cache Creek and Quesnel terranes, has been related by Travers (1987) to the accumulation of arc detritus in a back-arc setting. McClelland et al. (1992) argue that the Cretaceous Kingsvale-Spences Bridge continental volcanic arc, built across the Intermontane belt, represents the eastward migration of the Late Jurassic Gambier arc above a single subduction zone situated outboard the Insular superterrane. Conversely, Thorkelson and Smith (1989) relate the magmatism to east-directed subduction and closure of a marginal basin east of the Insular

superterrane. This volcanism was followed by two Tertiary episodes of volcanism, producing plateau basalts of the Eocene Kamloops and Princeton groups, and Miocene plateau basalts (Armstrong, 1988).

Tertiary faulting related by Price et al. (1985) and Ewing (1980) to right lateral transform motions of the Fraser River-Straight Creek fault system and crustal extension occurring eastwards within the Intermontane terrane, have extensively disrupted all of the units within the area. Williams and Ross (1979) proposed that the sedimentation and volcanism within the Princeton and Tulameen basins were controlled by a series of northwest-striking faults.

Geology of the Tulameen River area

The Tulameen complex is faulted against Late Triassic to Early Jurassic age (Campbell and Tipper, 1971) lower greenschist grade metasedimentary and metavolcanic rocks of the Nicola Group to the east, and to the west by a one km wide belt of penetratively deformed schistose rocks, correlated with the Nicola Group (Monger, 1985). The metamorphic rocks to the west, separate the Tulameen from the Late Jurassic Eagle tonalite (155 ± 4 Ma, U-Pb zircon; Greig et al., 1992), Eagle tonalitic gneiss (148 ± 6 Ma, U-Pb zircon; Greig, 1992) and middle Cretaceous Falls Lake muscovite-bearing, peraluminous granite (110.5 ± 0.4 Ma; Greig, 1992)—all of which make up the Eagle plutonic complex and form the southern half of the 200 km long Mount Lytton-Eagle metamorphic-plutonic complex.

An elliptical basin of coal-bearing terrigenous strata and volcanic rocks of the Eocene age Princeton Group, referred to as the Tulameen basin, rests in angular unconformity (Camsell, 1913) on Nicola Group volcanic rocks to the east of the Tulameen complex. The Tulameen coal basin is overlain by a Miocene age basaltic cap (Goodarzi and Van der Flier-Keller, 1988). Undeformed basaltic dykes of either the Eocene Princeton Group or Miocene-

Pliocene flood basalts occur as parallel swarms at the northern and southern extremities of the Tulameen complex.

A northwest-striking, southwest-dipping structural fabric characterizes the eastern part of the Eagle plutonic complex and schistose rocks of presumed Nicola Group affinity. The Tulameen complex, itself elongate and parallel to this regional trend, is bounded and dissected by northwest-trending mylonitic shear zones, marked by subhorizontal stretching lineations (chapter 3). Several small ultramafic bodies are linearly distributed along the strike of the Tulameen complex, northwestwards towards Mount Henning, and southeast to Whipsaw Creek. The ultramafic rocks, which range in composition from hornblende clinopyroxenite to hornblendite, occur as highly foliated lenses between mylonitized Nicola Group metavolcanic and metasedimentary rocks and the western belt of schistose rocks (Rublee, 1989).

All of the geologic units within the Tulameen River area are extensively disrupted by Tertiary brittle faults, with both dip-slip and strike-slip movements. Brittle faulting of the Eocene strata of the Princeton Group is spectacularly displayed in the Blakeburn cast of the Tulameen coal basin. Quaternary and Recent glacially derived sediments cover a large portion of the Tulameen area.

Chapter 2.

Geology and petrography of the Tulameen complex.

Introduction

The distribution of mappable units of the Tulameen complex observed during the 1987 and 1988 field seasons was found to be in agreement with that presented by Findlay (1963). The generalized geological map of the Tulameen complex (Fig. 2.1) shows it as a 17 km long, 4 km wide northwesterly elongate body made up of equal proportions of ultramafic and feldspathic rocks. The ultramafic rocks include dunite, wehrlite, olivine clinopyroxenite, hornblendite clinopyroxenite and hornblendite. The southeastern half exhibits an overall compositional spectrum from gabbro to syenogabbro and syenodiorite. Several small ultramafic bodies are linearly distributed along the strike of the complex, running northwestwards towards Mount Henning, and southeast to Whipsaw Creek. These ultramafic outliers range in composition from hornblende pyroxenite to hornblendite and occur as highly foliated lenses within the mylonitized country rocks (Rublee, 1989).

The Tulameen complex is bordered on the west by a narrow belt of highly deformed schistose rocks which have been correlated with the middle Carnian to Sinemurian Nicola Group (Monger, 1985; Greig, 1992), and Nicola Group metavolcanic and metasedimentary rocks on the east. The Nicola Group is a diverse assemblage which forms a 70 km wide belt which extends from Kamloops to the International border. The group was first named and described by G.M. Dawson for a section mapped on the south side of Nicola Lake, 75 km north of Tulameen (Rice, 1947).

Legend to generalized geological map of the Tulameen complex (Fig. 1.2) on verso.

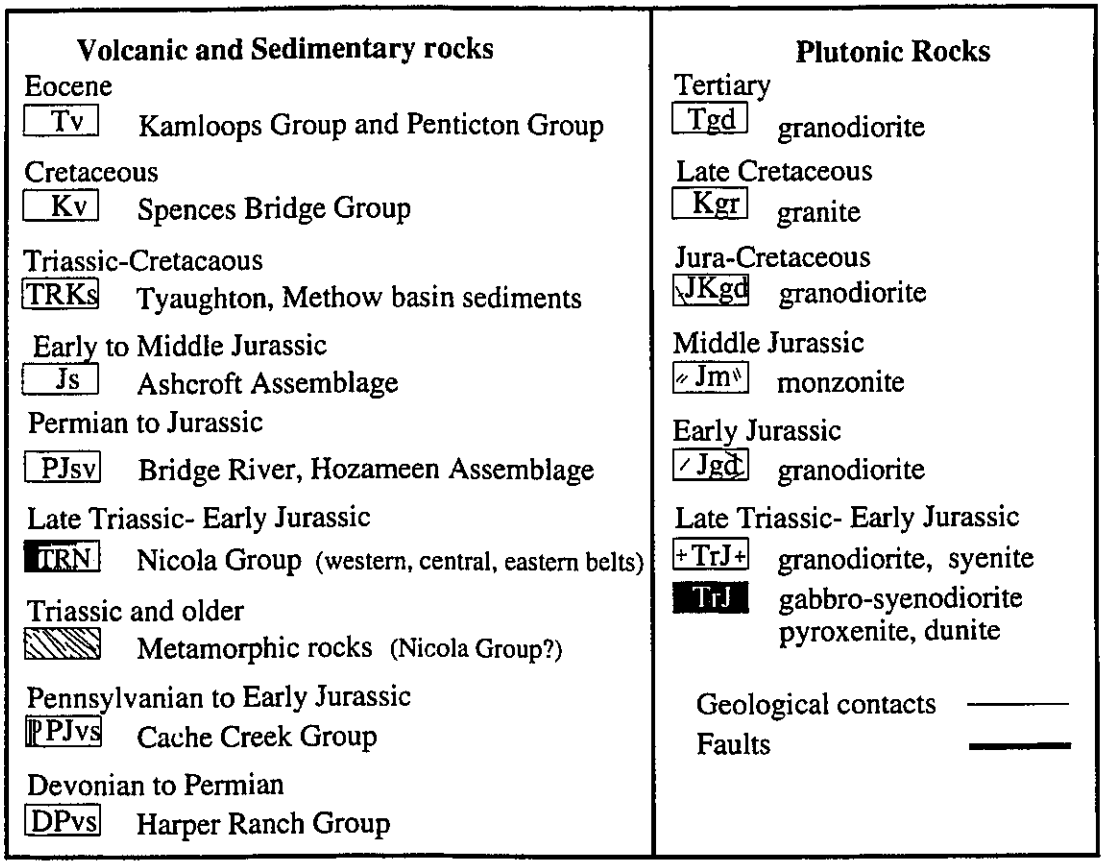
Volcanic and Sedimentary rocks
Eocene
Tv
Kamloops Group and Penticton Group
Cretaceous
Kv
Spences Bridge Group
Triassic-Cretacaous
TRKs
Tyaughton, Methow basin sediments
Early to Middle Jurassic
Js
Ashcroft Assemblage
Permian to Jurassic
PJsv
Bridge River, Hozameen Assemblage
Late Triassic- Early Jurassic
TRN
Nicola Group (western, central, eastern belts)
Triassic and older
Metamorphic rocks (Nicola Group?)
Pennsylvanian to Early Jurassic
PPJvs
Cache Creek Group
Devonian to Permian
DPvs
Harper Ranch Group
Plutonic Rocks
Tertiary
Tgd
granodiorite
Late Cretaceous
Kgr
granite
Jura-Cretaceous
JKgd
granodiorite
Middle Jurassic
Jm
monzonite
Early Jurassic
Jgd
granodiorite
Late Triassic- Early Jurassic
+TrJ+
granodiorite, syenite
TrJ
gabbro-syenodiorite
pyroxenite, dunite
Geological contacts
Faults

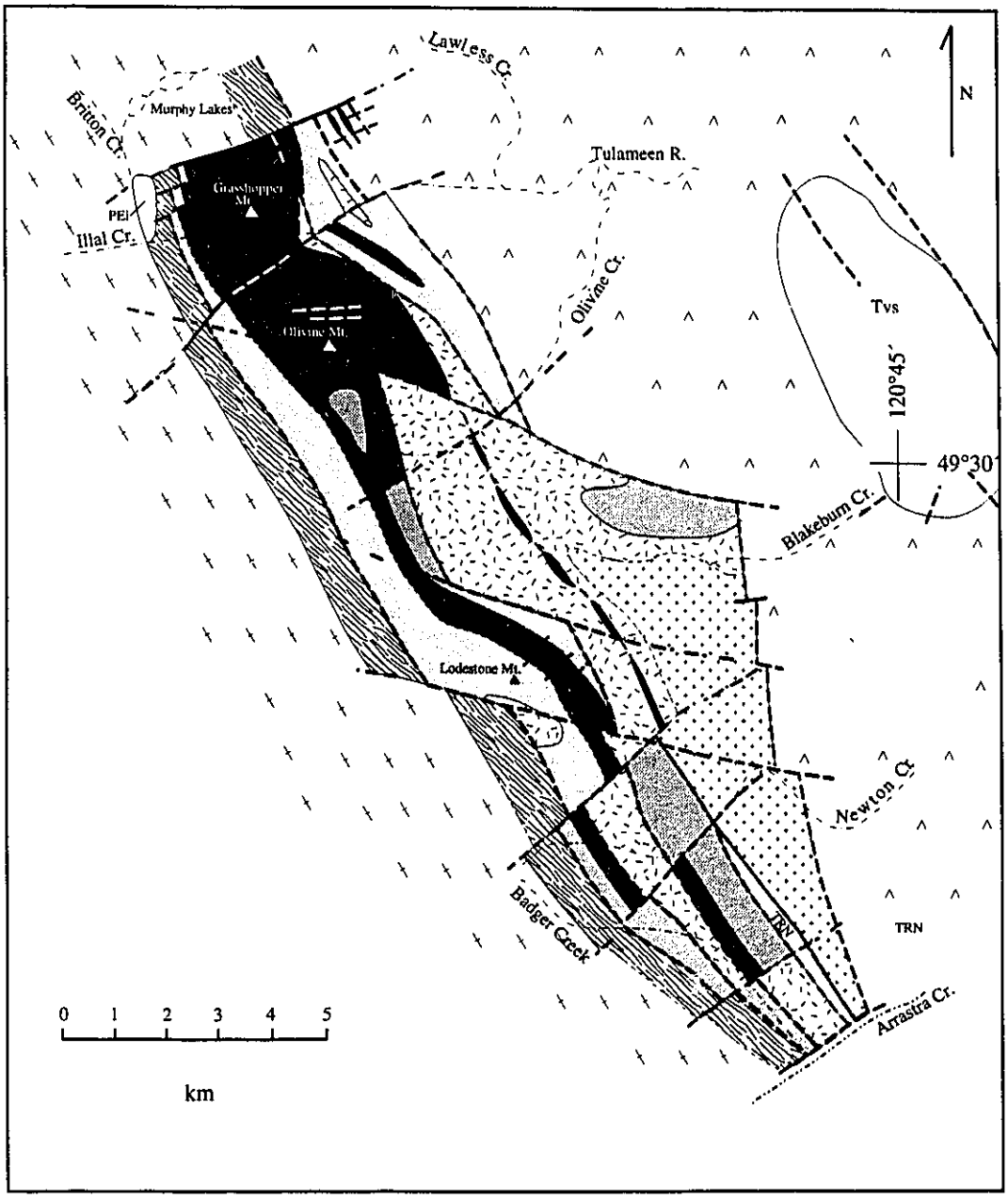

Figure 2.1. Generalized geological map of the Tulameen complex modified after Findlay (1963). Distribution and classification of rock types is that described by Findlay (1963). Ductile and brittle faults discovered in the 1987 and 1988 field seasons are documented and described in this study. Legend for map is on page facing.

Nicola Group rocks east of the Tulameen complex

Lower greenschist grade metavolcanic and metasedimentary rocks of the Nicola Group predominate east of the Tulameen complex. Volcanic rocks from this southeastern part of the Nicola Group, in the vicinity of the Tulameen complex, were not included in either Preto's or Mortimer's petrologic or geochemical study of the Nicola Group and are therefore referred to as undifferentiated Nicola Group on the regional compilation map for the southwestern Intermontane region (Monger, 1989a).

East of the Tulameen complex, Nicola Group rocks include pyroclastic breccias, mafic flows, crystal tuffs, and interbedded argillites and limestones. The pyroxene- and feldspar-rich tuffaceous andesitic breccias predominate over bladed feldspar- and pyroxene -feldspar porphyritic flows and crystal tuffs. Pyroclastic breccias are characterized by angular to sub-rounded lapilli to block-sized volcanic clasts which are supported in a pyroxene and feldspar-rich andesitic tuffaceous matrix. The clasts, which are mafic and pyroxene- and plagioclase-phyric, include calcite-filled amygdaloidal, vessicular and aphanitic varieties. Medium-grained dioritic to monzonitic fragments comprise up to 5% of the clasts. Finely bedded tuffaceous argillites, siltstones and rare limestone are interbedded with fine-grained green-grey crystal tuffs and mafic flows. The most continuous exposure of these metasedimentary packages—which vary from 5 cm to greater than 100 m in width—occurs along the north bank of the Tulameen River, approximately 200 m upstream from its confluence with Lawless Creek. Compositional layering strikes northwest and dips moderately to the southwest.

Schistose rocks west of the Tulameen complex.

The 1 km wide belt of highly foliated rocks of upper greenschist to lower amphibolite metamorphic grade which separates the Eagle plutonic and Tulameen complexes was defined by Camsell (1913) as the western margin of the Nicola Group.

This correlation, which has been continued (Monger, 1985; Greig, 1992), appears to be based on spatial association, because there are no known fossils in this assemblage (Monger, 1989a).

This northwest-striking band of schistose rocks which borders the western contacts of the Tulameen complex, shows an increase in metamorphic grade from upper greenschist to amphibolite grade westward towards the Eagle plutonic complex. Proximal to the Tulameen complex, the Nicola Group rocks are characterized by biotite-chlorite-quartz and sericite schists, epidote-garnet calc-silicates, phlogopite-bearing marbles and biotite-garnet gneisses. At the eastern contact with the Eagle complex, exposed along the Tulameen River road and Briton Creek logging road, foliated marble, biotite amphibolite, and hornblende-schists are in contact with the Eagle tonalite. Sills of foliated granodiorite and aplite dykes are observed within the schists at several locations (Murphy Lakes road, Tulameen River road, Whipsaw Creek road) along the eastern contact of the Eagle plutonic complex.

Contact relationships between Nicola Group and Tulameen complex rocks.

All contacts observed between the Nicola Group and the Tulameen complex are faults and are detailed in the following chapter on the structural features of the Tulameen complex. Evidence for magmatic intrusion of the Tulameen complex into the Nicola Group was not found at the contacts. The lack of a metamorphic aureole within the lower greenschist grade Nicola Group metasedimentary and metavolcanic rocks is striking not only by the lack of new higher temperature mineral assemblages, but also by the preservation of primary features, such as calcite and chlorite filled vesicles in the sheared breccia clasts at the contact. No inclusions of Nicola Group rocks at the margins of the Tulameen complex, nor dykes of dunite to syenodioritic composition within the Nicola Group were found. Findlay (1963, 1969) interpreted foliated hornblendite pods, mapped

within the lower greenschist grade metavolcanic and metasedimentary rocks near the northeastern contact with the plutonic body, to have resulted from the contact metamorphism of Nicola Group rocks by the intrusion. An alternative and more plausible view is that the foliated hornblendite pods are tectonized pods of the ultramafic complex caught up within the northwest trending shear zones that bound and cut through the Tulameen complex. The fabric within these ultramafic lenses is a uniformly oriented, penetrative ductile fabric which is inconsistent with hornfelsing.

The eastern and western contacts between the supracrustal rocks and the ultramafic-gabbroic body are northwest-oriented mylonitic shear zones, whereas northeast to east-trending brittle faults truncate the Tulameen complex to the north and south. A steep strain gradient, towards the northwest-striking ductile shear zone is evidenced by the transformation of foliated rocks to L-tectonites over short (50 m) distances. Stretched volcanic clasts and quartz rodding within the bordering Nicola Group rocks, stretched porphyroclasts of K-feldspar within the syenodiorites and elongated augen of amphibole and pyroxene in mylonitized pyroxenites define lineations which consistently plunge shallowly to the northwest. This increase in deformation towards the contact is clearly observed on the logging road which skirts the northeastern flank of Grasshopper Mountain, the switchbacks south of Olivine Creek, in Newton Creek and along the Whipsaw Creek logging main at mile 13.

The Tertiary brittle faults which juxtapose Tulameen intrusive and Nicola Group rocks to the north and south, are generally steeply dipping breccia, clay gouge and iron carbonate chloritic shear zones. Both country and intrusive rocks are extremely fractured and quartz-carbonate veined in these fault zones. Steps on quartz-fibre slickensides and offsets of marker units (marble layers) indicate both dip-slip and strike-slip movements along these faults.

Tulameen Complex

The areal proportions of rock types calculated by Findlay (1963) reveals that the ultramafic and feldspathic rocks are present in equal amounts (Table 2.1). It is important to note however, that most of the contacts between the lithologic units are faults and therefore the present form of the Tulameen complex may not represent its original entirety.

Dunite, olivine clinopyroxenite and hornblende clinopyroxenite are the principle ultramafic rocks; wehrlite, olivine-hornblende clinopyroxenite, magnetite clinopyroxenite and hornblendite are subordinate and are not mappable units at the scale Findlay mapped (1:20,000). The clinopyroxene-rich rocks make up the bulk of the ultramafic portion and envelop the dunite massif. Hornblende clinopyroxenite is a marginal unit of the ultramafic body and separates it from the feldspathic part as well as the bordering country rocks.

Feldspar-bearing rocks underlie the eastern half of the Tulameen complex and form a northwesterly elongate body which exhibits a progressive petrologic zonation from gabbro—proximal to the ultramafic rocks—to syenogabbro and syenodiorite, with decreasing clinopyroxene and increasing potassic feldspar content eastwards. The minerals of the feldspathic rocks show extensive alteration. Plagioclase and K-feldspar are saussuritized and sericitized and the pyroxene is uralitized. The gabbro to syenodiorite body is extensively sheared at the contacts with the ultramafic rocks. The widespread replacement of clinopyroxene by hornblende in both the clinopyroxene- and plagioclase-rich rocks further obscures the relationship between the two rock suites. Along the eastern contact with Nicola Group pyroclastic rocks, the gabbroic-dioritic rocks are L-tectonites. The contact between the syenodiorite phase and Princeton Group east of Tanglewood Hill is not exposed. The topography of the area underlain by the gabbroic to syenodioritic rocks is low in relief (300 m) and covered with vegetation; a thick (up to 8 m; Findlay, 1963) cover of unsorted Quaternary alluvium covers the terrain below 1500 m elevation.

Table 2.1.

Areal proportions of rock types in the Tulameen complex (modified after Findlay, 1963).

Lithology	Area (sq. km.)	% of Tulameen complex	% of ultramafic part	% of feldspathic part
Feldspathic rocks				
Syenodiorite	10.7 \ 27.1	48		60
Gabbro-syenogabbro	16.4 /			40
Ultramafic rocks				
Hornblende clinopyoxenite	15.3	27	51	
Olivine clinopyroxenite	8.6	15	29	
Dunite	6.0	10	20	

Outcrops are small (< 3 m), discontinuous and exposed in logging scars and along road cuts and creek beds.

The modal compositions of the rock units of the Tulameen complex determined by Findlay (1963) are shown in Table 2.2.

i) Dunite

Massive chromitiferous dunite occupies the central part of the ultramafic mass. It outcrops over a considerable lateral (9 km^2) and vertical (950 m) extent and is well exposed on the topographic highs of Grasshopper (1470 m) and Olivine (1770 m) mountains and where the Tulameen River has deeply incised these features between Illal and Lawless creeks. Outcrops, generally barren of any vegetation, are distinguished by a spalling-type fracturing and 1 cm thick orange-brown weathering rind. Glossy black chromite, easily seen on the dull buff to orange coloured weathered surface, occurs as disseminated grains, wispy bands and lenses.

The medium-grained, granular fresh surface of the dunite varies in colour from buff to black, with increasing extent of serpentinization. Contoured intensities of serpentinization (Findlay, 1963) reveal an asymmetric zonation with greater than 80% serpentine in the northeast and less than 20% serpentine in the southwest (Fig. 2.2). Thin section examination of the freshest samples (less than 15% secondary minerals) reveals that the dunite is an adcumulate—an igneous rock distinguished by a framework of touching mineral crystals with less than 7% intercumulus material (Irvine, 1982)—characterized by a mosaic packing of subequant 2-3 mm olivine and scattered (< 0.5 mm) chromite grains. Rare clinopyroxene and phlogopite crystals occur as intercumulate grains. The olivines, ranging in size from 0.5 to 10 mm, are colourless in plane polarized light and unzoned under cross-polars. Most grains show undulatory and banded extinction. Polygonization of the larger strained crystals is evidenced by the presence of numerous

Table 2.2

Modal composition of the rock units of the Tulameen complex.

Modified after Findlay (1963).

Lithology	Ol.	Px.	Hb.	Cr. + Mt.	Pl.	KFsp	Bt.
Syenodiorite	----	15-25	----	<6	45-55	12-37	<2
Syenogabbro	----	35-50	----	<7	35-50	12-22	<7
Gabbro	5-10	40-50	----	<6	40-50	0-5	<11
Hornblendite	----	----	>70	5-20	----	----	----
Hornblende clinopyroxenite	----	15-85	5-70	5-20	----	----	----
Clinopyroxenite	----	0-10	0-5	0-20	----	----	----
Hornblende-olivine clinopyroxenite	0-10	5-55	5-35	5-15	----	----	----
Olivine clinopyroxenite	10-45	50-85	0-5	0-10	----	----	----
Wehrlite	45-70	10-40	----	5-25	----	----	----
Dunite	90-95	0-2	----	0-5	----	----	----

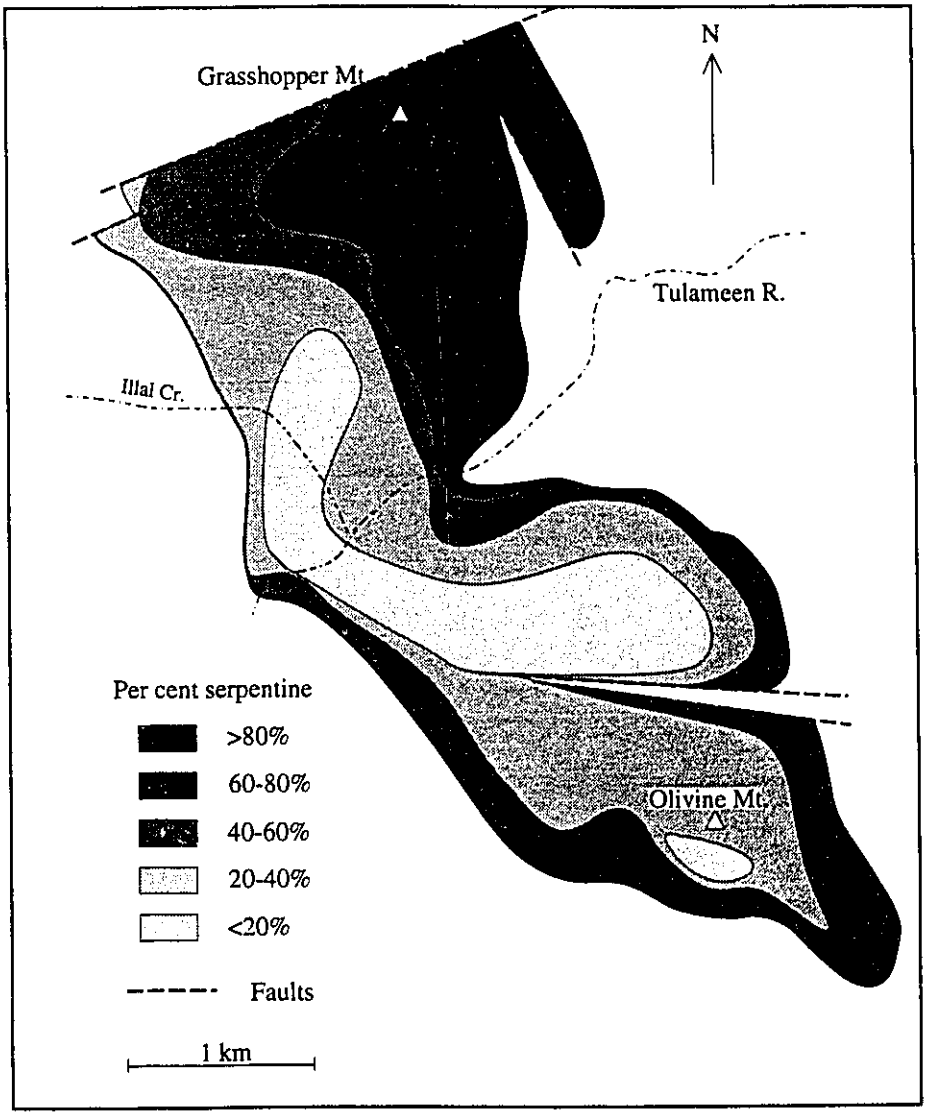

Figure 2.2. Contoured intensities of serpentinization in dunite (modified after Findlay, 1963). Map reveals an asymmetric zonation of serpentine minerals with increasing alteration from southwest to northeast. Contours of serpentine abundances are northwest striking and southwest dipping and parallel the structural grain in the Tulameen area.

distinct domains of random extinction. Grain boundaries are irregular and complexly interlocking. Olivine grains show a progressive replacement by serpentine minerals which, in the least altered samples, occur primarily along rectilinear fractures within the olivine crystals, and along grain boundaries. In extensively serpentinized dunites, the allotriomorphic granular fabric is replaced by a mesh texture of serpentine. Relict olivine occurs as islands surrounded by veinlets of cross and slip fibre, or irregular platy serpentine which pseudomorphs the original grain. Magnetite produced from the metamorphism outlines the grain boundaries, fractures, cleavage and median zones of veinlets. In sheared dunite, magnetite outlines foliation planes which wrap around elongated and pulled apart olivine cores. The cross-fibre serpentine within the foliation is optically aligned within the matrix, as are the cross fibre serpentine veinlets which grow within the olivine pull aparts. This implies that serpentinization occurred with deformation.

A structural variation of the dunite is a dunite breccia, exposed for approximately 150 m along the Tulameen River at its confluence with Illal Creek. The fragmentary nature of this rock type is clearly evident on the water-worn weathered surface where 2 mm to 1 m sized angular clasts of serpentinized dunite protrude above a serpentinized matrix. The clasts are rimmed by a 1-2 mm black, and outer 2-3 mm rusty orange rind. Radiating acicular masses up to 3 cm in diameter of a minty-green amphibole occur within the matrix. The dunite clasts appear to have been serpentinized and fracture-filled by cross and slip-fibre serpentine prior to their incorporation into the breccia.

The contact between dunite and surrounding pyroxenite, viewed on Grasshopper and Olivine Mountains, is gradational, with a narrow (100 m wide) intervening zone of wehrlite. Towards the outer margins of the dunite, clots of large (up to 10 cm) diopside crystals are common. Within 200 metres of the contact between dunite and olivine clinopyroxenite, parallel clinopyroxenite dykes up to 10 cm in width are observed intruding

the dunite on the south flank of Olivine Mountain, Illal Creek and Tulameen River. Dunite is surrounded by olivine pyroxenite along all but its northern contact where the Tulameen complex has been truncated by a northeast-striking Tertiary brittle fault. Exposures of dunite along the logging roads traversing the northern flank of Grasshopper Mountain, are extensively fractured in a brittle fashion as well as serpentinized.

ii) Wehrlite

On the scale mapped by Findlay (1: 20,000), wehrlite, which occurs as a narrow (10 m) intervening band between dunite and olivine clinopyroxenite, is not represented as a mappable unit. This transition from dunite to olivine clinopyroxenite is clearly seen on the weathered surfaces of the outcrops by the increase of contrasting glassy green diopside against the dull orange to buff coloured serpentinized olivine. Discontinuous bands and isolated grains of chromite are evident on the weathered surfaces of the wehrlite as well. In thin section, the diopside and chromite occur as intercumulate grains between serpentinized olivine grains.

iii) Pyroxenite

Pyroxenite underlies 42 volume % of the Tulameen complex (Findlay, 1963; Table 2.1). The broad name of pyroxenite is given to the suite of diopside-dominated ultramafic rocks which include—with increasing proportions of olivine and hornblende—clinopyroxenite, olivine clinopyroxenite, olivine-hornblende clinopyroxenite and hornblende clinopyroxenite. Olivine clinopyroxenite and hornblende clinopyroxenite constitute the larger mappable units which envelope the dunite massif and extend along the southwestern third of the Tulameen complex from Olivine Mountain to Arrastra Creek. Olivine-hornblende clinopyroxenite, magnetite clinopyroxenite and clinopyroxenite occur on the outcrop scale within either of the two larger units. Plagioclase-bearing clinopyroxenite is uncommon but was observed within a 2 m wide layered olivine

clinopyroxenite section in Illal Creek, approximately 1 km upstream from its confluence with the Tulameen River.

Diopside is the major cumulus phase in the pyroxenite and orthopyroxene is conspicuously absent. Olivine, magnetite and hornblende account for the mineralogical variation of these essentially monomineralic rocks. Outcrops of clinopyroxenite are characterized by a blocky fracture pattern, as opposed to the more rounded spalling-type fracturing in dunite. The colour of the weathered surface varies with its composition; serpentinized olivine imparts a blue-grey hue to the ordinarily grassy green pyroxenite surface whereas black hornblende darkens the weathered surface considerably.

a) Olivine clinopyroxenite

The map pattern of olivine clinopyroxenite, is a sinuous, northwest-striking band which encases the dunite and extends the entire 17 km length of the Tulameen complex. Its apparent thickness varies from less than 100 metres, on the western and eastern flanks of Grasshopper Mountain, to a maximum width of approximately 1 km on the well exposed southern side of Olivine Mountain. South of Blakeburn Creek, olivine clinopyroxenite occurs as discontinuous northwest-trending exposures within faulted blocks of sheared pyroxenite. Characteristically, the olivine clinopyroxenite is a coarse-grained and granular-textured, with a distinctive, blue-grey-green mottled appearance. Clinopyroxene accounts for 70-85 % of the modal mineralogy and olivine between 5 and 15%. Recessively weathering grains of olivine pit the surface of the pyroxenite. Sawn surfaces show off the mottled coloring imparted by the dark sub-rounded to irregular shaped clots of serpentine rimmed olivine grains within the allotriomorphic-granular matrix of clinopyroxene (plate 2.1).

Olivine clinopyroxenite is an adcumulate rock made up of a network of touching, unzoned clinopyroxene (50-85%) and olivine (10-45%) crystals (Findlay, 1963). The

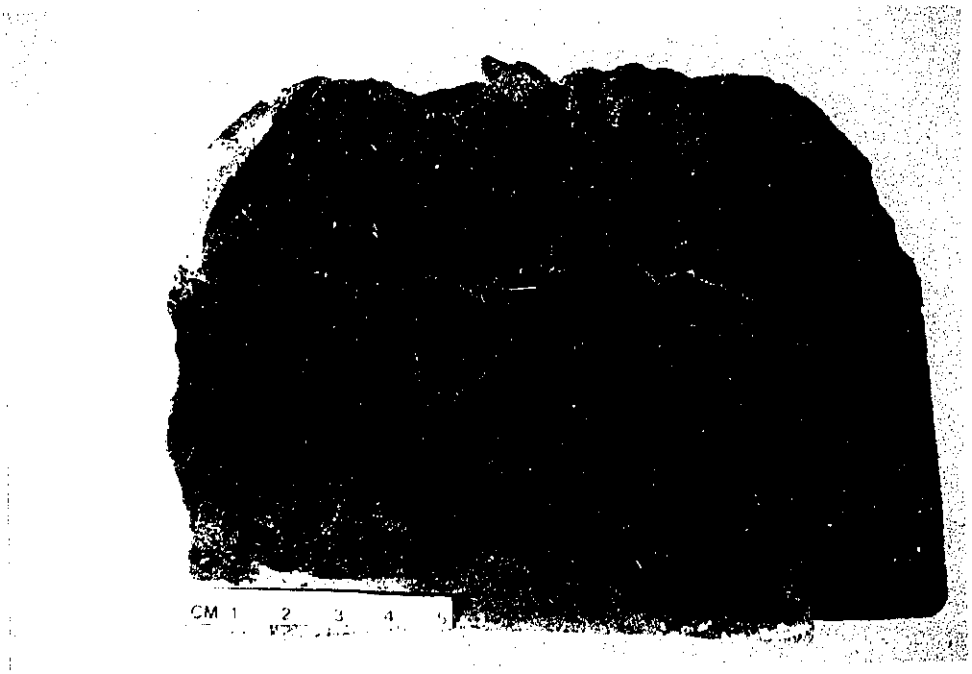

Plate 2.1. Sawn surface of olivine clinopyroxenite shows the characteristic mottled appearance of olivine clinopyroxenite. Blue-grey clots of serpentinized olivine grains stand out against the green, granular clinopyroxene framework. On the outcrop surfaces, olivine grains weather out leaving behind orange-stained boxwork-textured pits.

pyroxene, colourless to very weakly pleochroic diopside, occurs as large (0.5 cm but up to 1 cm) highly strained sub-equant grains and smaller (0.5 mm) inclusion-free grains with straight extinction. The larger crystals exhibit many deformational features in addition to the strained extinction, such as deformation twins and lamellae, kink-banding and polygonization. Grain boundaries are commonly irregular, and in the extreme, sutured between the large crystals. The distribution of the smaller grains—interpreted as recrystallized clinopyroxene because of the straight extinction, lack of inclusions and straight 120° grain boundaries—around the larger cumulus minerals give a mortar texture to the rock. Relict patches of olivine, preserved within the mesh of serpentine veinlets which pseudomorph the original crystal, are rimmed by an orange-coloured isotropic alteration, possibly iddingsite. Radial fractures extend out from the serpentinized olivine grain into adjacent clinopyroxene crystals. Opaque minerals, which range in modal amounts of 0-20% (Findlay, 1963), are present as: 1) anhedral intercumulus crystals (< 2 %), 2) a fine dusting of grains along cleavages, fractures and especially the straight grain boundaries between the sub-grains and 3) platey and anhedral inclusions within the cumulus clinopyroxene. The platey needles are arranged in an orthogonal (parallel to the cleavage planes) grid-like pattern within the clinopyroxene. Trace quantities (<2%) of tan-blue pleochroic plates of chlorite occur at the grain boundaries between the clinopyroxene and olivine grains.

The incorporation of serpentinized dunite xenoliths and megacrysts of clinopyroxene brings about textural variation of olivine clinopyroxenite. Football-sized dunite inclusions are abundant within the olivine clinopyroxenite exposed along Tulameen River approximately 1 km down river from the mouth of Illal Creek. The xenoliths, which range in size from 1 to 30 cm, may be sub-rounded prolate inclusions with sharp contacts or, more rarely, ribbon-shaped with contorted contacts with the host rock (Nixon and

Rublee, 1987). Expansion fractures radiating out from the dunite into the host rock attests to their incorporation prior to serpentinization. Elsewhere, large crystals of diopside, up to 10 cm in length, occur as single euhedral megacrysts, clusters, lens-like bands, and schlieren within the olivine clinopyroxenite. An elongate, dendritic form of the pyroxene megacryst was observed on Grasshopper Mountain.

Findlay (1963) described well developed magnetite layering within the olivine clinopyroxenite near its contact with hornblende clinopyroxenite on Lodestone Mt. These bands, which parallel the northwest-striking, southwest-dipping contact (Findlay, 1963), are more frequently observed within the hornblende-rich pyroxenites.

With the exception of the elevated outcrops on Olivine Mountain and canyon exposures along the Tulameen River, the contact relationships between olivine clinopyroxenite and other units of the Tulameen complex are obscured by a thick cover of Quaternary alluvium. Between olivine clinopyroxenite and dunite, several different types of contact relationships were noted. The previously described transitional contact between olivine clinopyroxenite, wehrlite and dunite was observed along the eastern side of Olivine Mountain and northeastern flank of Grasshopper Mountain. In the absence of wehrlite, the two units are sharply juxtaposed and sheared at their junction. A 100 to 130 m wide (Findlay, 1963) hybrid contact zone, characterized by xenoliths of one rock type in the other, is observed in the Tulameen River. Irregular to clot-like segregations of clinopyroxene crystals occur within the dunite and dunite xenoliths are abundant within the olivine clinopyroxenite. The northwest -striking contacts between olivine clinopyroxenite and hornblende clinopyroxenite are not exposed, but the two units outcrop within metres of each other. In the Badger Creek area, Findlay (1963) noted intermediate hornblende-olivine clinopyroxenite as a gradational unit between the two. Where the contact between olivine clinopyroxenite and gabbroic border phase of the syenogabbro to syenodiorite body

was seen (Tulameen River), the rocks were highly sheared, and in the case of the feldspar-rich rocks chloritized and saussuritized. This contact is a northwest-striking, southwest-dipping quartz-carbonate shear zone and the penetrative fabric within both units is a northwest-striking, southwest-dipping schistosity.

b) Hornblende clinopyroxenite and variants

Hornblende clinopyroxenite, one of the more extensive units of the Tulameen complex, occurs as an outer marginal phase to the ultramafic portion, separating the olivine and clinopyroxene-rich cumulus rocks from the feldspathic suite, Nicola Group and schistose country rocks. It forms parallel northwest-oriented belts—approximately 0.25- 1 km wide, which extend discontinuously along the length of the complex—and fault-bounded lenses within and at the margins of the Tulameen complex. Outcrops within the forested slopes of Grasshopper, Olivine and Lodestone mountains display a blocky fracturing and a dark olive green mottled weathered surface, due to the stubby black prisms of hornblende within the clinopyroxene-rich groundmass.

Hornblende clinopyroxenite is composed of clinopyroxene (50-75%), hornblende (10-45%), magnetite (5-20%) and minor (<2%) amounts of apatite, plagioclase and mica. The unweathered surface reveals subhedral stubby black prisms of hornblende, up to 1 cm in length, occurring more often as glomerocrysts than solitary minerals, along with disseminated grains to irregular clots of magnetite in a granular fine- to medium-grained grass-green coloured matrix of clinopyroxene crystals. In thin section, hornblende is a green to tan coloured, moderately pleochroic, unzoned mineral which replaces diopside and olivine (Findlay, 1963) along cleavage planes, fractures and grain boundaries (plate 2.2). This replacement may take the form of patches or large twinned and unzoned oikocrysts of hornblende. Findlay (1963) noted that magnetite replaces hornblende along cleavage directions. Clinopyroxene is unzoned with straight grain boundaries and varies little from

Plate 2.2. Photomicrographs showing hornblende (magnesiohastingsite) replacing clinopyroxene (diopside) along: a) cleavage planes, b) as patches within clinopyroxene and c) along grain boundaries. The upper photomicrograph is taken under plane polarized light, and the lower under cross nicols. Hornblende appears tan-green and clinopyroxene colorless in plane polarized light. Field of view is 5 mm.

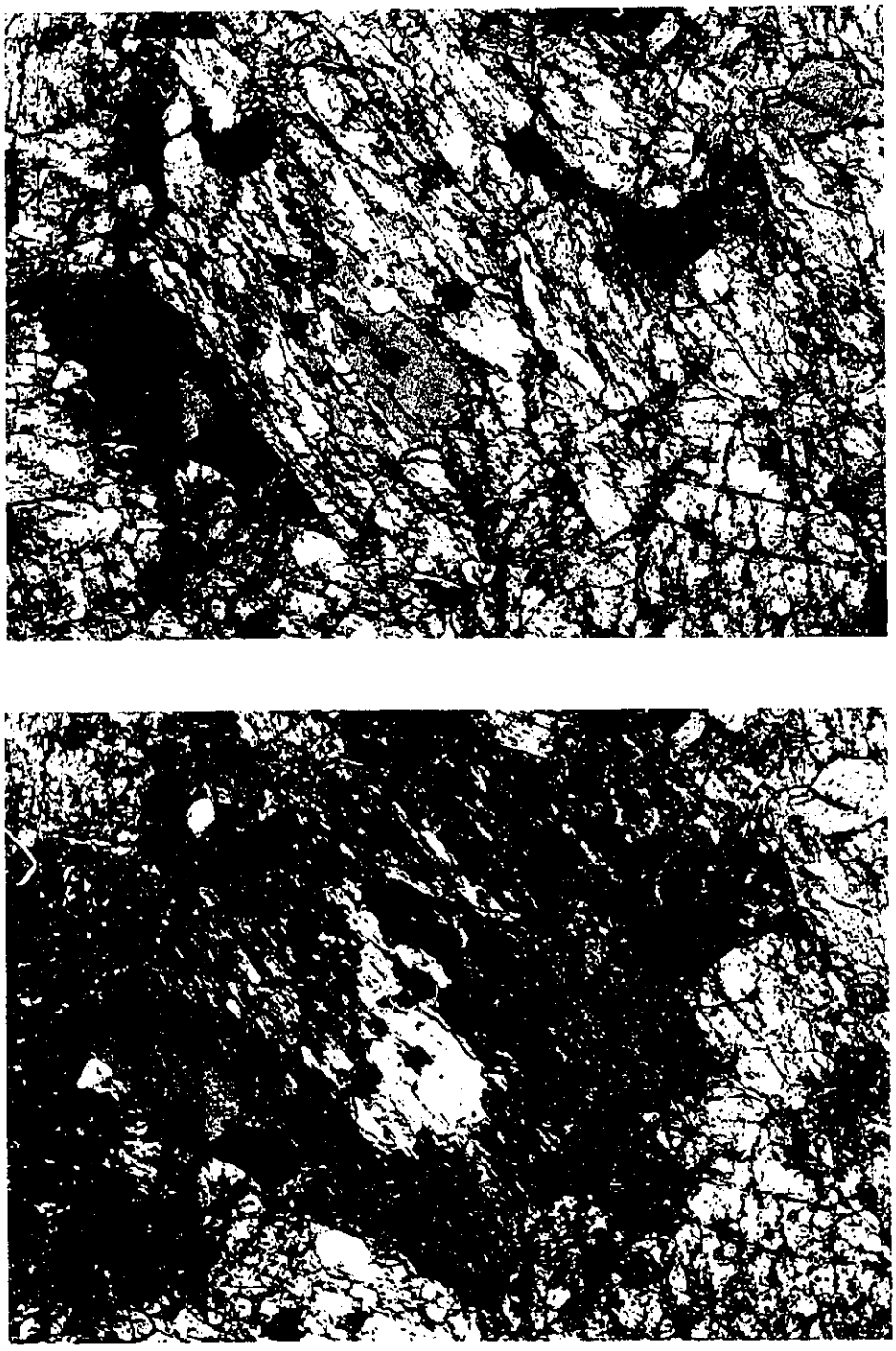

Plate 2.2a

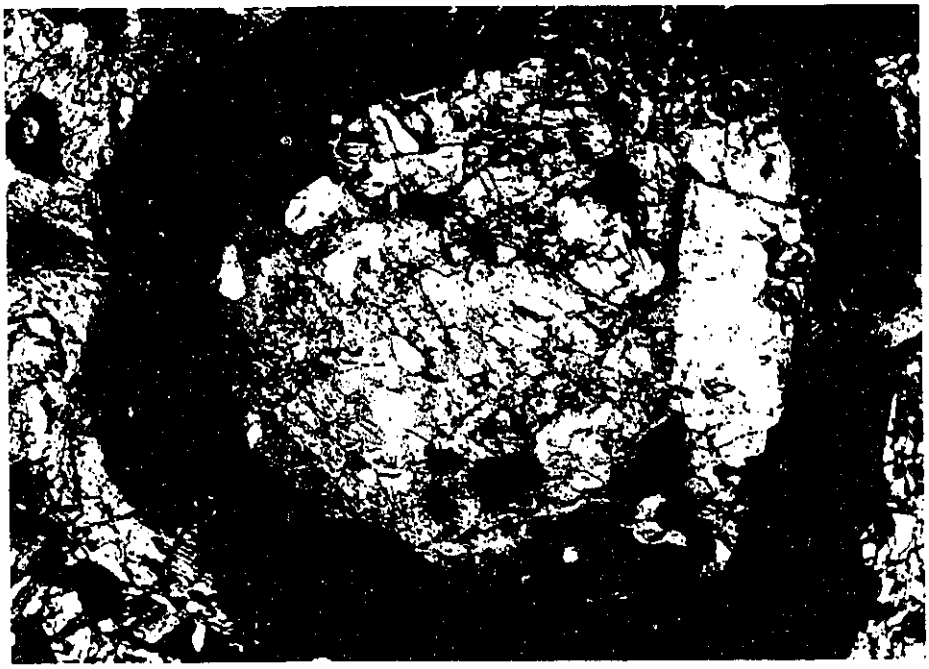

Plate 2.2b

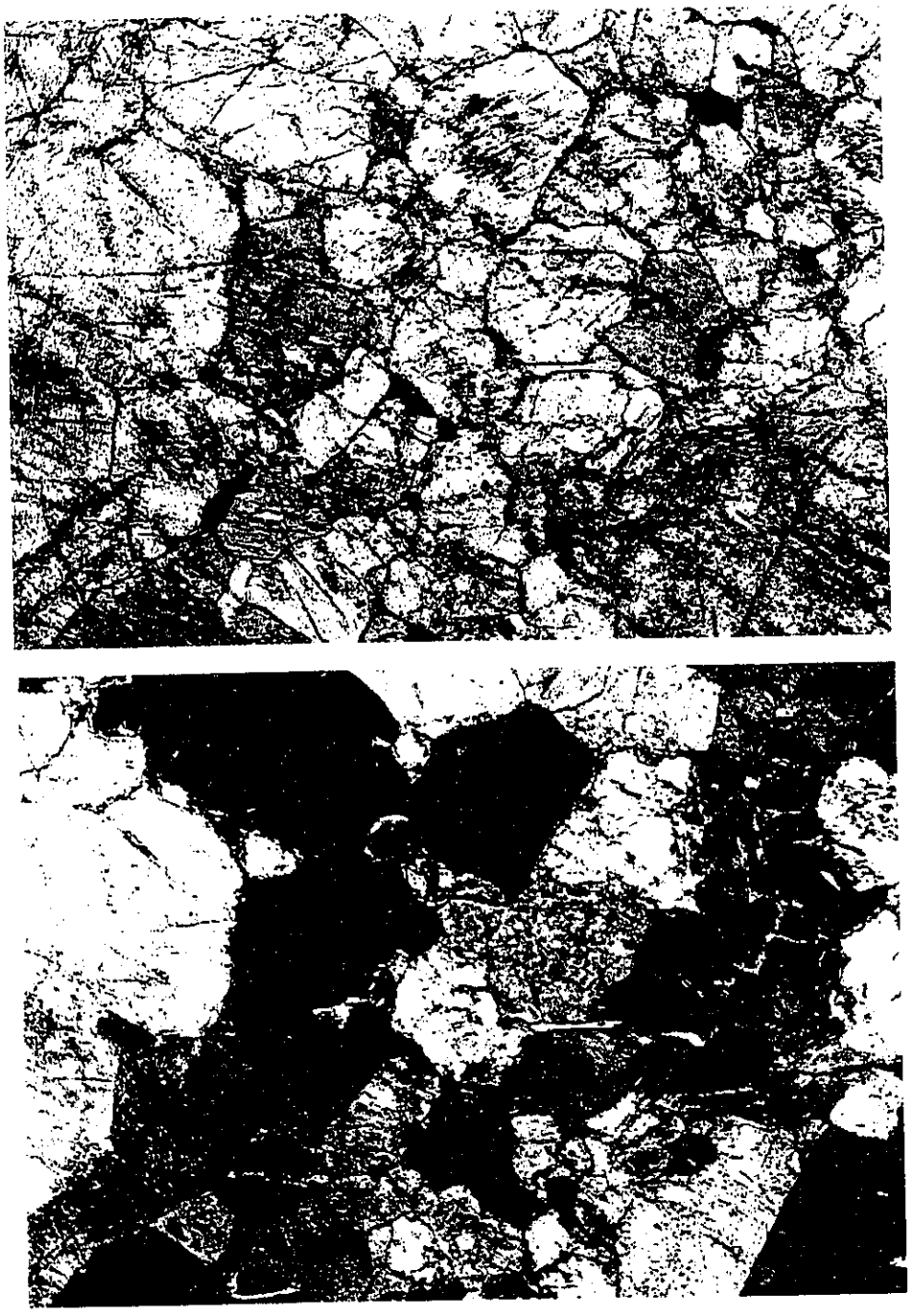

Plate 2.2c

clinopyroxene in the olivine clinopyroxenite. Anhedral magnetite grains are intercumulate to clinopyroxene. Mica, is present in trace amounts as euhedral plates at the grain boundaries between clinopyroxene crystals.

This rock type exhibits a wider range of texture than other phases of pyroxenite. The variation in hornblende size accounts for many of the textural variations observed within hornblende clinopyroxenite. Pegmatitic hornblende clinopyroxenite occurs as small pockets within the hornblende clinopyroxenite near the contact with the gabbroic body. Towards the contact, the modal proportion of hornblende increases to the extent that hornblende clinopyroxenite grades into clinopyroxene hornblendite and hornblendite. Hornblendite occurs as iron stained, discontinuous lenses which parallel the northwest-striking contacts. They are often more resistant than the other contact rocks and protrude as tabular bodies above the surrounding rocks. Magnetite and apatite abundances increase markedly in the hornblende-rich rocks. Lens and vein-like masses of magnetite occur within hornblende pyroxenite on Lodestone Mountain and Tanglewood Hill. Findlay (1963) noted that magnetite veins posses a distinct planar orientation with the strike of the layering paralleling the contact between the ultramafic and feldspar-bearing units in the Lodestone area (350° dipping 65-70°SW). The magnetite bodies exhibit a wide range in dimension, the greatest of which was estimated by Eastwood (1959) to be approximately 100 m in length with an average thickness of 3 m. Chalky-white weathering apatite crystals, up to 1 cm in length, are clearly visible in the black coloured clinopyroxene hornblendite and hornblendite. These crystals, with modal abundances as high as 5%, are subhedral prisms which appear to be concentrated along the grain boundaries of the hornblende crystals, and as inclusions within pegmatitic crystals.

The contact relationships of the hornblende clinopyroxenite unit are difficult to determine because many of the contacts are poorly exposed or are obscured by post-

cumulus hornblende, magnetite, and apatite. The gabbroic and dioritic rocks are sheared and extensively saussuritized and uralitized (tremolite alteration rims on clinopyroxene) towards the contact with the ultramafic rocks. Hornblende replaces the altered (tremolite-fringed) clinopyroxene—within both the ultramafic and feldspathic rocks at their contact—rims xenoliths of both rocks types, and occurs within veins which parallel the contact. The hornblende is pristine and devoid of alteration.

iv) Gabbro

Gabbro outcrops as narrow (100-200 m) northwest-oriented, southwest-dipping belts which are confined to the margins of the gabbro-syenodiorite body in contact with the ultramafic rocks. It is possible that this unit is more widely present but is concealed by the extensive hornblende-magnetite-apatite mineralization at the contact. Map scale gabbro zones include two parallel bands which intersect the Tulameen River east of the dunite massif, a narrow strip along the eastern slope of the ridge which extends from Olivine to Lodestone mountains, and a discontinuous belt of gabbro at the western contact between the Tulameen complex and the schistose country rocks.

Outcrops are small (1-5 m), with streaky black and white weathered surfaces. The gabbro has a northwest-striking mylonitic foliation; feldspar rodding in the plane of the foliation imparts a subhorizontal, northwest-directed stretching lineation. Well developed C/S fabrics (Simpson and Schmid, 1983) are observed in sheared gabbro, which outcrops along the Lodestone Road. These structural fabrics are described in the following chapter which relates to the structural features of the Tulameen complex.

In less deformed outcrops of gabbro, larger cumulus plagioclase crystals protrude above the waterworn surfaces exposed in the Tulameen River. Clinopyroxene and feldspar are of equal proportion (40-50%) , and magnetite (trace-6%), olivine (<5%) and secondary biotite (<7%) are present in minor amounts. Potassic feldspar accounts for approximately

10% of the groundmass feldspar in the sheared samples. Clinopyroxene occurs as faintly pleochroic pale green to pale yellow-green coloured stubby subhedral grains within a sheared groundmass of mosaic calcium and minor potassium feldspar (plate 2.3). The clinopyroxenes are generally isolated but when touching show penetrative relationships. Subordinate prismatic clinopyroxene crystals exhibit sector zoning, defined by optically distinct triangular segments, the apices of which meet at the centre of the prismatic crystal. Opposite sectors are optically, and chemically identical (plate 2.4). Clinopyroxenes contain abundant inclusions of euhedral apatite, biotite and oxide minerals—with both anhedral and platey habits—which are preferentially distributed along concentric and sector zones (plates 2.4). Olivine is present in minor amounts (<5%) in one of the thin sections (87-JR-28-01), as colourless, fractured grains which are rimmed by fine grained reddish-brown mica and fine-grained opaque minerals. The feldspars, which account for approximately 45-50% of the rock are strained, sericitized and saussuritized. The large protruding cumulus plagioclase are polygonized and recrystallized. Clay material marks the outlines of recrystallized subgrains in the mortar-textured and ribbonned groundmass (plate 2.3). Fibrous dark green hornblende partially rims and replaces clinopyroxene along cleavage planes in sample 88-JR-16-05. Apatite and magnetite are present in minor amounts as anhedral 2 mm grains, as well as inclusions.

Very few contacts between the gabbroic and ultramafic rocks are exposed. However, the intense deformation, observed as a northwest-striking ductile foliation, within each of the units towards their contact, indicates that the contact is structural. The relationship between the ultramafic and feldspathic suites is concealed by the extensive overprinting of hornblende within both the pyroxenites and gabbros, as previously discussed. Despite the lack of continuous outcrop within the feldspathic portion of the Tulameen complex, the relationship between gabbro and adjacent syenogabbro appears to

Plate 2.3. Photomicrograph of gabbro (sample 87-JR-28-01) under plane polarized light (top) and cross nicols (bottom). Pale green, faintly pleochroic clinopyroxene (diopside; observed as both stubby subhedral and prismatic sector-zoned crystals) and minor (<5%) biotite and opaque-rimmed olivine occur as isolated and inter-penetrating crystals in a sheared and partially recrystallized groundmass of potassium-feldspar and plagioclase. The clinopyroxenes contain abundant inclusions of euhedral apatite, biotite and oxide minerals—both anhedral and platey habits—which are preferentially concentrated along concentric and sector zones. Field of view is 5 mm.

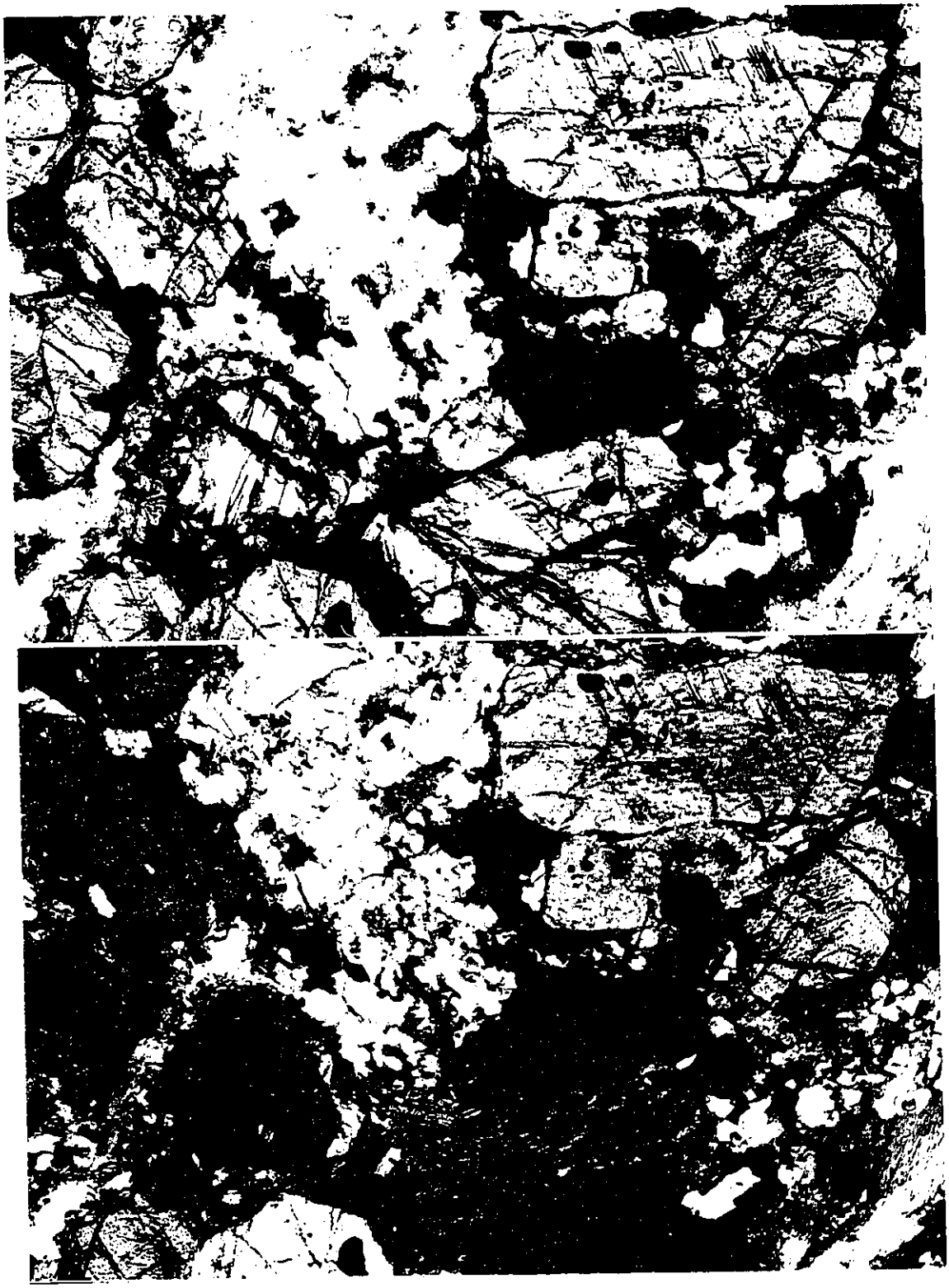

Plate 2.3

Plate 2.4. Sector-zoned clinopyroxene in gabbro (sample 87-JR-28-01) under plane polarized light (top) and crossed nicols (bottom). Sector-zoning (also referred to as "hourglass"-zoning) in prismatic clinopyroxene is revealed under polarized light where the optical (and chemical; Fig. 5.11) differences between the sectors define 4 triangular segments, the opposites which are optically and chemically identical. Platey oxides are preferentially concentrated along the boundaries of the sectors. Dark circle around grain is an ink track. Field of view is 5 mm.

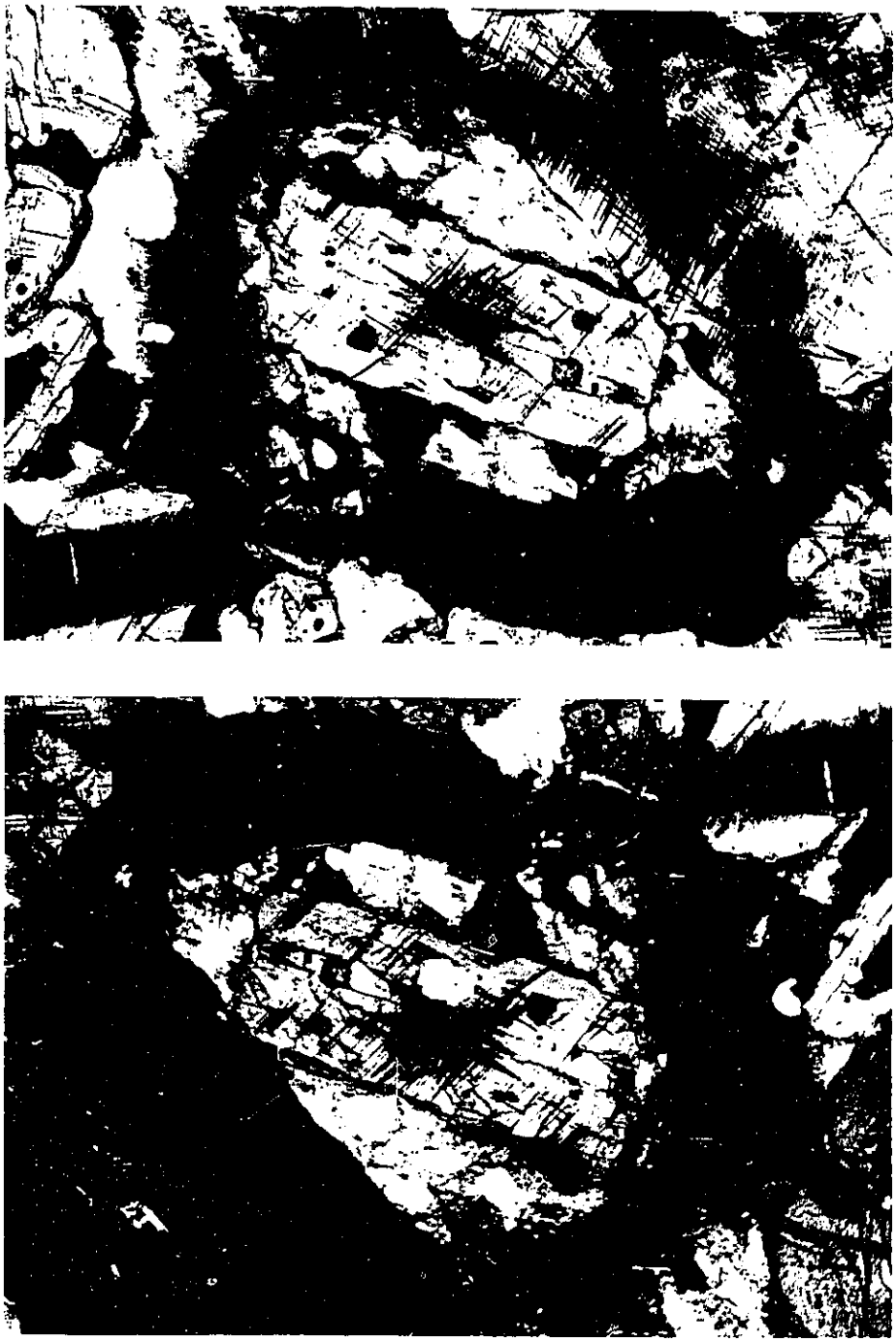

Plate 2.4

be gradational, evidenced by the systematic decrease of modal clinopyroxene, absence of olivine and concomitant increase in feldspar content.

An unusual outcrop of hornblende gabbro, distinct from the clinopyroxene gabbro, outcrops along the north bank of Tulameen River, approximately 1 km downstream from Illal Creek. The hornblende gabbro occurs as a 2 m wide dyke-like body within olivine clinopyroxenite; it has sharp contacts and is northwest striking. The northwestern half of the hornblende gabbro has the appearance of a breccia intrusion, and the southeastern part is homogeneously modally layered. Ovate inclusions of pyroxene gabbro are aligned within a medium-grained hornblende pyroxene gabbroic matrix. A set of northwest trending, southwest dipping clinopyroxene-phyric mafic dykes intrude the brecciated and modally layered hornblende gabbro and parallel the contacts.

v) Syenogabbro

Despite the absence of recognizable plagioclase with compositions of $>An_{50}$, Findlay (1963) defined this rock type as syenogabbro on the basis its general chemical, mineralogical (pyroxene as the dominant mafic mineral) and paragenetic nature.

Syenogabbro is centrally distributed in the region between Olivine and Blakeburn creeks. It is distinguished from the gabbro by a decrease in modal clinopyroxene (35%), absence of olivine and the predominance of plagioclase (35-50%) and potassium feldspar (12-22%). Outcrops are small with heavy limonite and manganese staining along fractures. The rounded weathered surface is a mottled creamy buff and green colour, although in the sheared outcrops the colour changes to a dull olive green , due to extensive saussuritization of the plagioclase and uralitization of the clinopyroxene.

Syenogabbro exhibits varying intensities of structural fabric development. In the vicinity of the northwest-striking ductile shear zones which cuts through the centre of the Tulameen complex, as well as the bounding shear zones with the Nicola Group rocks and

ultramafic rocks, the syenogabbro is intensely foliated. This lithologic unit is further disrupted by numerous brittle crush and gouge zones.

The rock is of a medium grain with crudely aligned 0.5 cm long laths of plagioclase, orthoclase and tremolite-mantled clinopyroxene. Aggregates of altered clinopyroxene impart a clotted green appearance to both fresh and weathered surfaces. This fabric parallels the northwest-oriented schistossity developed within sheared syenogabbro

Hand samples belie the degree of alteration. Tabular plagioclase and orthoclase crystals are almost completely saussuritized and sericitized—as revealed in several representative thin sections. Plagioclase compositions from unaltered crystals yield An_{45}, An_{47} (Findlay, 1963) and An_{30}. Resorbed clinopyroxene cores are rimmed by a fringe of tremolite, epidote and calcite. The remnant clinopyroxene is pale green in colour and possesses a faint pale green to pale yellow pleochroism. In sections of syenogabbro from the hornblende-rich contact zone with hornblende clinopyroxenite southwest of Lodestone Mountain, the hornblende replaces the tremolite-rimmed relict clinopyroxene grains.

vi) Syenodiorite

Syenodiorite forms the easternmost phase of the gabbroic body. It extends along a northwest-trending zone south of Tanglewood Hill, stopping just short of Arrastra Creek. In the field syenodiorite is distinguished from syenogabbro by its higher proportion of potassium feldspar (up to 35%) and by its coarse grain size. Subparallel laths of salmon-coloured feldspar impart a trachytic texture to the rock (plate 2.5). Outcrops are small and often extensively fractured; the weathered surface is a mottled buff-green shade with distinctive chalky-coloured apatite crystals, up to 0.5 cm in length. In comparison, highly

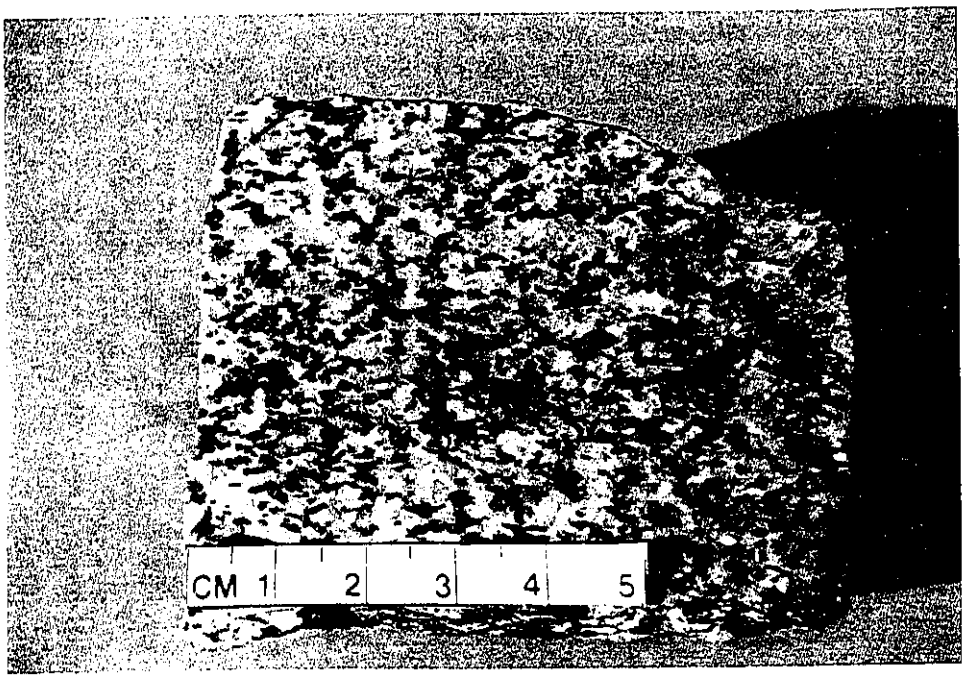

Plate 2.5. Sawn surface of hand sample of syenodiorite. The alignment of tremolite-fringed clinopyroxene and laths of K-feldspar impart a subhorizontal, northwest trending mineral lineation which parallels the mineral stretching lineation measured along the ductile shear zones which bound and cut through the Tulameen complex.

foliated outcrops of syenodiorite are dark grey in colour with streaked out to augen shaped potassium feldspar porphyroclasts.

The mineralogy and petrography of the syenodiorite are similar to those observed for the syenogabbro with the addition of chloritized biotite, large (1 cm) apatite crystals, poikilitic orthoclase, and secondary microcline and rare fluorite. The feldspars are of approximately equal modal abundances and are highly altered tabular and poikilitic (orthoclase) grains. Tremolite and epidote fringed clinopyroxene (7-10 %) occurs as clots with anhedral blebs of magnetite and chloritized biotite. Apatite occurs as highly fractured and sericite-altered crystals of impressive size (1 cm). The occurrence of hornblende in the syenogabbro is confined to contact zones between syenodiorite and hornblende clinopyroxenite (Newton Creek, Badger Creek).

Chapter 3.

Structural geology of the Tulameen Area.

Introduction

Ductile and brittle processes have extensively modified the Tulameen complex. Observed contacts between the lithologic units are sheared and parallel the mylonitic shear zones which bound and cut through the plutonic body. New road exposures and logged clearings in the 30 years since Findlay's field work, have aided in the discovery of the mylonitic shear zones which appear to be of overwhelming significance to the evolution and ultimate understanding of the Tulameen complex. The Tertiary brittle faults disrupt all units within the Tulameen area are subordinate in importance to the ductile structures.

For a better understanding of the structural fabrics observed in the Tulameen complex and how they relate to the structural evolution of the southwestern Intermontane belt, a brief description of the four episodes of regional deformation follows.

Structural features of the southwestern Intermontane belt.

Monger (1985) recognized 4 episodes of regional deformation in the southwestern Intermontane belt: 1) post-Permian to pre-Middle Jurassic ductile deformation, 2) Early and Middle Jurassic folding and metamorphism, 3) Late Jurassic to Early Cretaceous plutonism, metamorphism and ductile deformation and 4) early to middle Tertiary strike-slip and extensional faulting which is the predominant structural feature of the southwestern Intermontane belt. These Cenozoic faults obscure the older structural features in this area.

The structural domains associated with each episode, and their spatial relationship to the Tulameen complex, are shown in Figure 3.1. The northwest-elongate Tulameen Complex is situated to the east of the Eagle shear zone—an informal name given by Greig (1992) to a 100

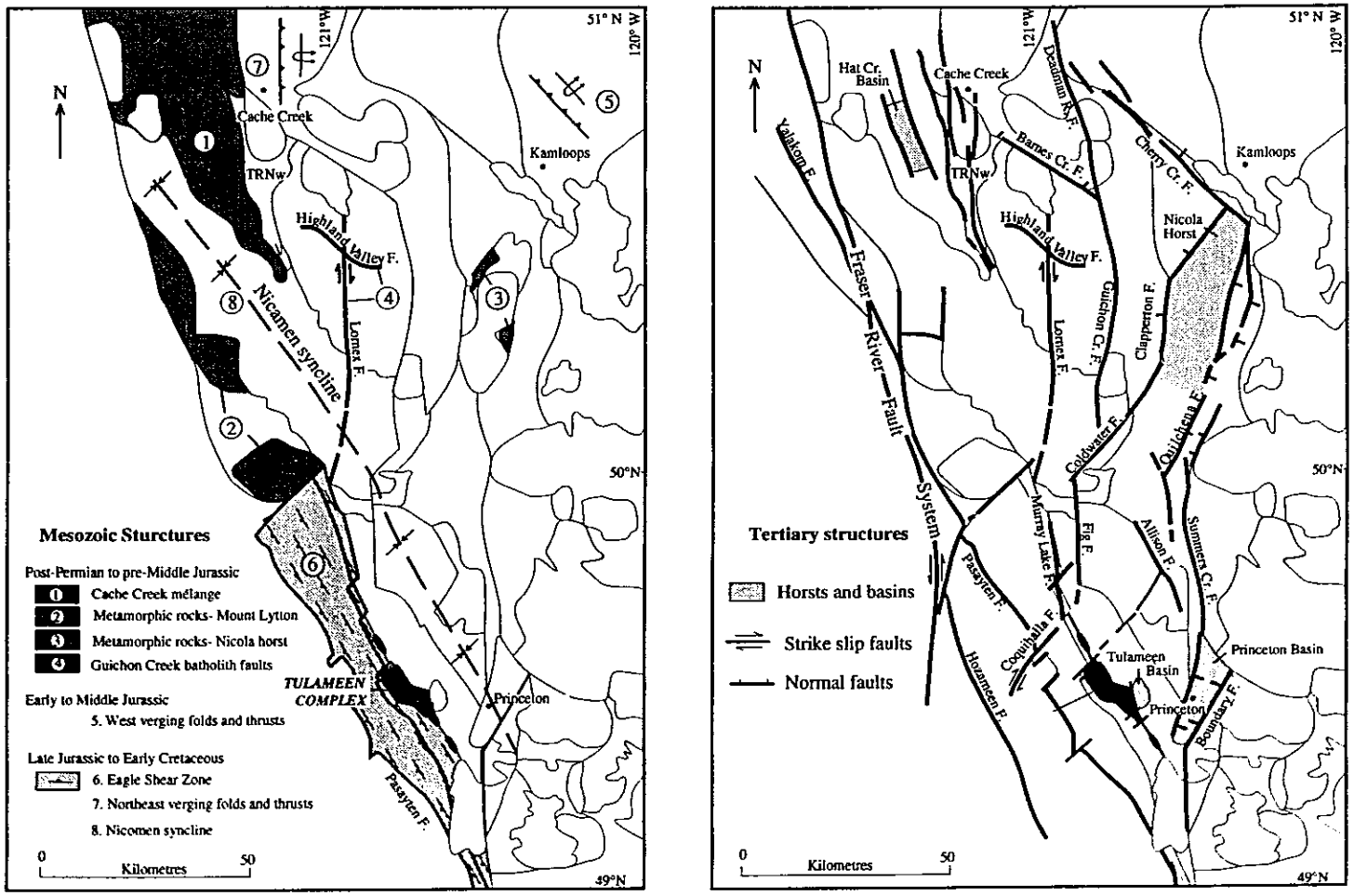

Figure 3.1. Mesozoic (a) and Tertiary (b) structural elements in the Intermontane belt (modified after Monger, 1989a).

km long, >1 km wide belt of rocks made up of deformed Nicola Group and Eagle tonalite—and is extensively disrupted by Tertiary faulting.

i) Post-Permian to pre-Middle Jurassic deformation

The late Paleozoic to early Mesozoic structures shown in Fig. 3.1a include blueschist mélange in the Cache Creek, metamorphic fabrics in the northern part of the Mount Lytton complex and interior of the Nicola horst, and faults in the Nicola Group and Guichon Creek batholith (Gabrielse, 1992).

The tectonic mélange along the eastern margin of Cache Creek contains blocks of highly disrupted Cache Creek (with fossiliferous clasts indicating an age range from Late Pennsylvanian to Late Permian; Monger et al., 1982) and Nicola Group volcanic rocks in a Late Permian to Late Triassic mélange matrix (Monger et al., 1982). Late Triassic radiometric ages have been obtained from blueschist minerals in the mélange (Gabrielse and Yorath, 1992).

In the southwestern Intermontane belt, the Late Triassic Nicola Group is typified by low metamorphic grade (sub-greenschist grade) and a structural fabric dominated by brittle faulting and fracturing (Preto, 1977). Ductile fabrics, although rare throughout most of the Nicola belt, are preserved within the deeper crustal rocks of the Mt. Lytton complex and Nicola horst, both interpreted by Monger (1985) as exhumed Nicola arc basement. The timing of the early Mesozoic ductile deformation has been determined in the Mount Lytton complex by U-Pb zircon dates obtained from a locally foliated granodiorite (212 ± 1 Ma; Parrish and Monger, 1992) which crosscuts northwest trending mylonitic fabrics within paragneisses and orthogneisses dated at 225 ± 5 Ma (Parrish and Monger, 1992). Moore (1989) similarly describes high grade (lower amphibolite) Nicola Group metavolcanic rocks that are penetratively deformed by a northwest-striking foliation with a moderate west plunging mineral stretching lineation within the core of the Nicola horst.

Additional evidence of early Mesozoic deformation is the fault bounded nature of many of the very Late Triassic to Early Jurassic plutons within the Nicola Group; this has led many workers to speculate that plutonism was accompanied by faulting (Preto, 1977; Barr et al., 1976; Monger, 1985). Hollister et al. (1975) held that the Guichon Creek batholith differentiated during simultaneous movements along the dextral Lornex and Highland Valley faults. Ages obtained on sericite, from structurally controlled mineralized veins associated with these fault zones, yield 210-190 Ma K-Ar cooling ages (Mortimer et al., 1990). Mortimer et al. (1990) interpreted the age of crystallization to be 210 ± 3 Ma (U-Pb zircon) for the pluton. Preto (1977) proposed that the sedimentation and volcanism of the Nicola Group was controlled by an older fault system which includes the Summer Creek, Allison and Quilchena faults within the central part of the Nicola Group.

Monger (1989a) relates the formation of these post-Permian to pre-Middle Jurassic structures to the late Paleozoic to early Mesozoic, eastward directed subduction of Cache Creek beneath the Nicola arc (Fig. 1.4a). He speculates that the sheared mélange formed in the accretionary complex and the brittle faulting associated with the Guichon Creek batholith, occurred in the upper part of the upper plate, and the ductile fabrics exposed in the northern Mount Lytton complex originated in the lower part of the upper plate.

ii) Early to Middle Jurassic folding and faulting

Structures derived from this Early to Middle Jurassic episode of deformation are confined to the juncture of the Intermontane and Omineca belts (Monger, 1985), at the northeastern corner of Fig. 3.1a. Strata from each belt are caught up in the west-verging backfolds and thrusts that formed as a result of the obduction of the Eastern Assemblage and part of Quesnel terrane onto the North American craton (185-175 Ma; Fig. 1.4b). Monger (1985) relates the deposition of the Jurassic Ashcroft Formation to the uplift and erosion of the Omineca belt during this deformational event.

iii) Late Jurassic and Early Cretaceous age deformation

The Late Jurassic to Early Cretaceous structures, which are confined to the western margin of the southern Intermontane belt, record the protracted accretion of the Insular terranes (Alexander, Wrangellia, Peninsular) to the North American margin (Monger, 1985; McClelland et al., 1992; Fig. 1.4c).

Late Jurassic structures have been described in supracrustal rocks in the Ashcroft area and deeper level plutonic rocks of the Eagle plutonic complex (Travers, 1978; Greig, 1989). Monger (1985) suggested that the northeast-verging thrust faults and folds, which involve the Cache Creek and Nicola Group supracrustal rocks in the Ashcroft area, are higher level expressions of the plutonism, metamorphism and ductile shearing occurring within the Eagle shear zone (Greig, 1992), 100 km to the south.

Middle Jurassic deformation of the Eagle plutonic complex is confined to a narrow 100 km long belt of deformed rocks along the eastern margin of the complex (Fig. 3.1a). The Eagle tonalite and schistose rocks—of presumed Nicola derivation—are penetratively deformed, with a northwest-striking, southwest-dipping foliation. On the basis of coplanar fabrics between the tonalite and schists, the presence of foliated tonalite sills, within the deformed country rock near the contact, and geometry of mylonitized inclusions, Greig (1992) argues that the emplacement of the 155 ± 4 Ma (U-Pb zircon; Greig et al., 1992) Eagle tonalite was simultaneous with contractional ductile deformation, and that the formation of the penetrative foliation is related to the emplacement of this intrusion. The timing determined for the northeast verging structures within the Ashcroft Formation has been bracketed by the discovery of Callovian (169-163 Ma) fossils within the Ashcroft Group (Travers, 1978) and a K-Ar whole rock date from the Ashcroft Formation of 162 ± 5 Ma reported by Mortimer et al (1990).

The development of Early Cretaceous structures within the southwestern Intermontane belt is related to the activation of the Pasayten fault circa 105 Ma (Greig, 1992). Sinistral, east-side-up, reverse movement along this fault accommodated the uplift of the Mt. Lytton, Eagle and Okanogan plutonic complexes and formation of a northwest trending structural depression (Nicomen syncline) into which the Spences Bridge Group was deposited (Monger, 1985). An additional result of this rapid uplift was the regional middle Cretaceous resetting of K-Ar and Rb-Sr dates of Cretaceous and older rocks east of the Pasayten fault (Greig et al., 1992).

iv) Tertiary brittle faulting

The late Eocene to Oligocene (46 to 34 Ma; Coleman and Parrish, 1991) Fraser River-Straight Creek dextral fault system forms the western border of the Intermontane belt and offsets an older (Late Cretaceous to early Tertiary) network of northwest trending dextral strike-slip faults (Harrison, Ross Lake, Hozameen, Yalakom and Pasayten) by 80 to 100 km (Monger 1986). Normal faulting in the western Intermontane belt is believed by Monger (1989a) to follow the Basin and Range style Eocene (58-45 Ma; Parrish et al., 1988) extensional deformation which occurred farther to the east in the southern Omineca belt (Parrish et al., 1988).

The mixed strike-slip and dip-slip nature of faulting is evident within the area of the Intermontane represented in Fig. 3.1b. The north to northeast trending Coquihalla and Murray Lake (called the Zoa fault by Greig, 1992) faults dextrally offset the Eagle shear zone to the north of the Tulameen complex. The Coldwater-Clapperton and Quilchena normal faults bound the Nicola horst, and the Boundary normal fault forms the eastern margin of the Princeton basin (Fig. 3.1b).

Structural geology of the Tulameen area

Three distinct structural domains are defined by their structural fabrics in the Tulameen area (Fig. 3.2). These three domains are northwest trending and divided into: 1) a western belt

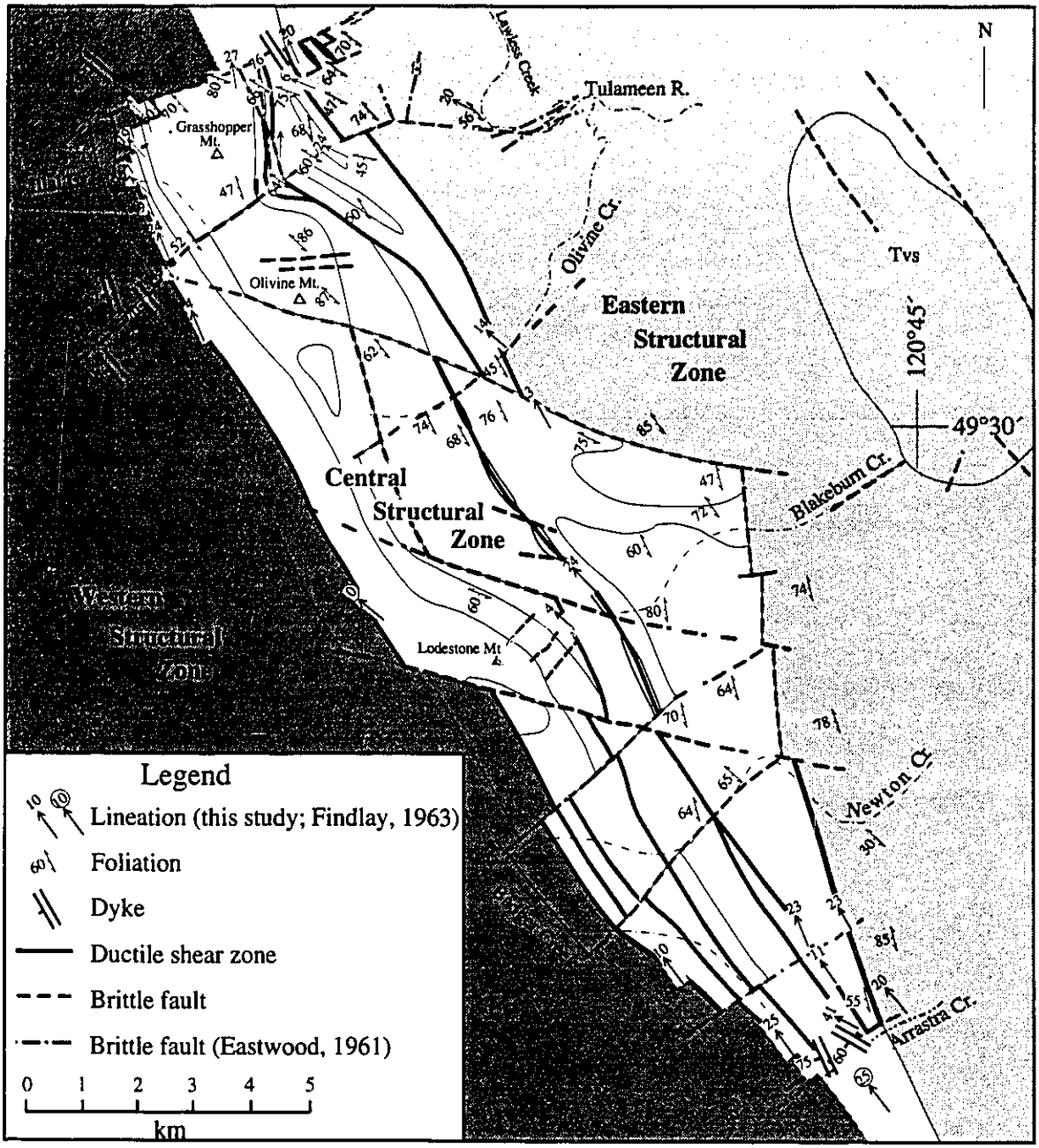

Figure 3.2. Structural features of the Tulameen complex.

of penetratively deformed, upper greenschist to lower amphibolite grade schistose rocks west of the Tulameen complex, 2) a central zone defined by the Tulameen complex and outlying ultramafic rocks aligned along a northwest striking ductile shear zones and 3) non-penetratively deformed, sub-greenschist grade Nicola Group mafic volcanic and sedimentary rocks which occur to the east of the Tulameen complex. Tertiary brittle faults cut across all three structural tracts.

i) Western zone structures

The schistose rocks which form a narrow belt separating the Tulameen and Eagle complexes are differentiated from the Nicola Group rocks to the east, by a pervading northwest-striking, southwest-dipping foliation and higher metamorphic grade. The increase in metamorphic grade westwards towards the Eagle plutonic complex is demonstrated by the change from biotite-chlorite-quartz and sericite schists proximal to the Tulameen complex to hornblende-biotite and siliceous amphibolites one km to the west.

The foliation remains remarkably consistent in orientation throughout the 100-km-long strike length of this region (Monger, 1985). Variable lineation directions however are measured at the Eagle and Tulameen contacts of the schistose rocks. Lineations measured by Greig (1989) in the schistose rocks towards the Eagle plutonic complex have down-dip plunges which sweep from the southeast to west (Fig. 3.3a); proximal to the Tulameen complex, mineral lineations consistently plunge moderately to the northwest (Fig. 3.3b). The ductile nature of this deformation is suggested by pinch and swell forms of quartz veins, sheared and rotated garnets within calc-silicate layers and boudinaged and folded granodioritic dykes of presumed Eagle tonalite.

ii) Eastern zone structures

In sharp contrast to the western contact rocks, steeply dipping breccia, clay gouge and iron-carbonate chloritic brittle shear zones dominate the structure of the Nicola Group

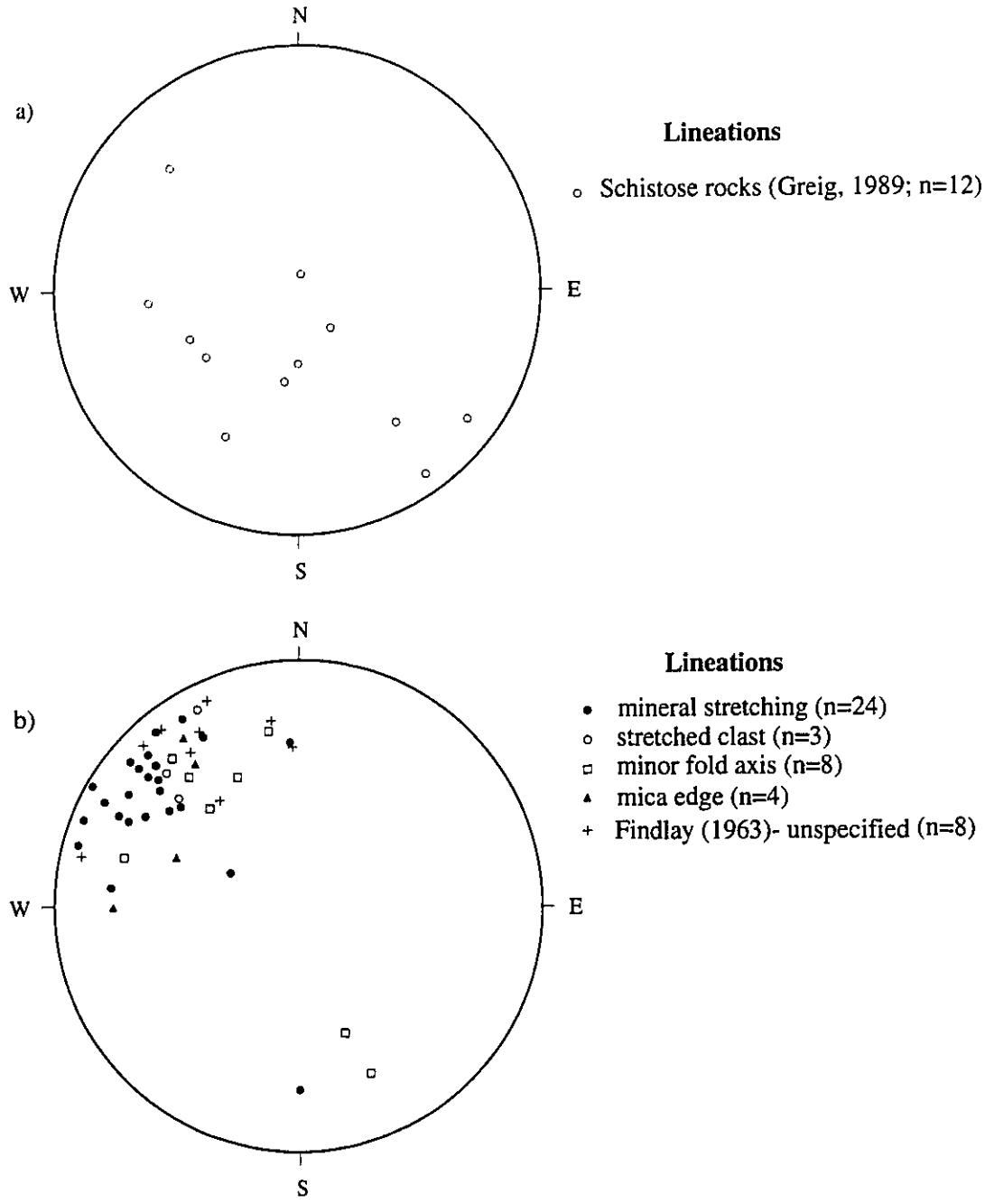

Figure 3.3. Stereoplot of lineations measured in: a) the schistose rocks at the eastern margin of Eagle plutonic complex in Law's camp and to the south (Greig, 1989), and b) in the schists, Tulameen complex and Nicola Group rocks along the northwest striking ductile shear zones which bound and cut through the Tulameen complex.

pyroclastic breccias, mafic flows, crystal tuffs, and interbedded argillites and limestones bounding the Tulameen complex to the east. Penetrative ductile fabrics are absent and foliations measured within the interbedded phyllites and argillites are confined to discrete, northwest-trending, chloritic shear zones which parallel northwest-trending, southwest dipping-compositional planes.

Ductile structures within the supracrustal rocks are restricted to the mylonitized margins of the Tulameen complex and outlying ultramafic bodies. A steep strain gradient in the Nicola Group rocks proximal to the shear zones is evidenced by the transformation of S-tectonites to L-tectonites over short (50 m) distances. Volcanic clasts within the pyroclastic breccia, and pyroxene crystals within the matrix, become progressively elongated (up to 10:1 aspect ratio) and impart a well developed mineral stretching lineation to the sheared rocks. These lineations (Fig. 3.3b), measured in the plane of the foliation, plunge shallowly to moderately towards the northwest. The more homogeneous volcanic flows and tuffaceous units become highly foliated chlorite schists. This increase in deformation within the Nicola Group towards the contact, is observed along the length of the Tulameen complex; it can be examined on exposed contacts which crop out along the logging road skirting the northeastern flank of Grasshopper Mountain and the switchbacks south of Olivine and Newton creeks. It is significant that calcite and chlorite filled vesicles in the bomb and lapilli sized clasts inside the pyroclastic rocks are not replaced by any higher temperature minerals in the high strain zones. This indicates that the sheared Nicola Group rocks along the eastern boundary of the Tulameen complex have not been elevated above their regional lower-greenschist metamorphic grade.

iii) Central zone structures.

The intermediate structural domain within the Tulameen area is a 45-km-long by 5-km-wide northwest-trending shear zone which encompasses the Tulameen complex and several smaller (200 m long) ultramafic bodies. Northeast- to east-trending brittle faults slice up and

truncate the Tulameen complex. These regionally extensive ductile and brittle faults produce the apparent conformity of the northwest elongate Tulameen complex to the regional structural grain and mask older structures unique to it.

The Tulameen complex has experienced several episodes of deformation since its crystallization. Primary igneous structures such as graded bedding and rhythmic or modal layering are rare within this large mass of cumulus material. Discontinuous blebs, clots and schlieren of chromite, diopside and olivine are ubiquitous within the ultramafic units and imply that any original magmatic stratigraphy has been extensively disrupted.

a) Igneous structures within the Tulameen complex.

Measurable and laterally continuous modal layering was observed only in two localities within the Tulameen complex: 1) within feldspathic pyroxenite exposed in Illal Creek, approximately 200 m upstream from its confluence with the Tulameen River and 2) within hornblende gabbro cropping out on the north bank of the Tulameen River, approximately 1 km downstream from Illal Creek. Although the vergence of the layering was inferred to face to the southwest in the Tulameen River section (Nixon and Rublee, 1988) and northwest in the Illal creek outcrop, importance put upon these determinations is suspect due to the degree of both ductile and brittle faulting within the Tulameen River area.

Pods and schlieren of chromite are easily distinguished on the orange-buff weathered surfaces of dunite and peridotite on Olivine and Grasshopper mountains. Measurements by Findlay (1963) and Nixon et al. (1990) of the orientation of these chromite segregations reveal a randomness to their distribution. In the predominantly monomineralic units such as dunite and olivine clinopyroxenite, clots to discontinuous bands of the second mineral phase (e.g. diopside within dunite and olivine within pyroxenite) are ubiquitous and impart a mottled, heterogeneous appearance to the weathered surfaces.

Other planar igneous features exposed on Lodestone Mountain and Tanglewood Hill include mineral (magnetite, hornblende and plagioclase) banding—confined to the contact between the ultramafic and feldspathic rocks—and lens and vein-like masses of magnetite within olivine pyroxenite and hornblende pyroxenite. Findlay (1963) noted that magnetite veins possess a distinct planar orientation with the strike of the layering, paralleling the contact between the ultramafic and feldspar-bearing units in the Lodestone area (350° dipping 65-70°W). The magnetite bodies exhibit a wide range in dimension, the greatest of which was estimated by Eastwood (1959) to be approximately 100 m in length with an average thickness of 3 m. On Lodestone Mountain, northeast trending brittle faults offset the magnetite layering (Findlay, 1963). Millimetre to dm wide hornblende-rich layers within hornblende pyroxenite are commonplace at the contact between the ultramafic and feldspathic rocks. Findlay (1963) noted that the long axes of the amphibole crystals parallel the walls of the bands. Alternating bands of hornblende- and feldspar-rich layers were also documented by Findlay (1963) in the syenogabbro and were found to parallel the northwest strike of the contacts.

Breccias of differing varieties are common throughout the Tulameen complex. Dunite breccia, first described by Camsell (1913), is spectacularly exposed for over 1 km, along the waterworn outcrops of Illal Creek and Tulameen River at their confluence. Clasts were serpentinized prior to breccia lithification, as indicated by the confinement of randomly oriented serpentine veins to the interiors of the clasts. A mixed ultramafic breccia is exposed in a logging scar on the west flank of Grasshopper Mountain. Elongated clasts of hornblende-olivine pyroxenite, dunite and olivine pyroxenite are supported within a hornblende-rich, fine-grained matrix. In the same logging scar, although genetically unrelated to the polylithic ultramafic breccia, there are impressive exposures of an intrusive breccia of coarse-grained to pegmatitic hornblende pyroxenite fragments, cemented by undeformed granodiorite—presumably the late Paleocene or early Eocene Illal stock (Greig, 1989)—which crops out 500

m to the west. An interesting, although local igneous breccia, of gabbroic composition, is visible along the north bank of the Tulameen River, approximately 200 m upstream from the olivine pyroxenite and gabbro contact. Ovate inclusions of pyroxene gabbro are aligned within a medium-grained hornblende pyroxene gabbroic matrix. The northwest-striking breccia is approximately 2 metres in width and has sharp contacts with the olivine pyroxenite and modally layered hornblende gabbro. A set of northwest-oriented, southwest-dipping pyroxene basaltic dykes intrude the gabbro and parallel the contacts.

The contact between the ultramafic and feldspathic parts of the Tulameen complex is frequently exposed as an intrusive breccia. The nature of the breccia is ambiguous; fragments of both hornblende-rimmed pyroxenite in gabbro and diorite—as well as gabbro and diorite within hornblende-pyroxenite, are common.

b) Ductile structures

The mylonitic shear zones described in this chapter were undocumented prior to this study, although sheared Tulameen and Nicola rocks were alluded to by Findlay (1963) and Eastwood (1961), respectively. Findlay (1963) noted a widespread foliation and sparse lineation in the saussuritized gabbros at the margin of the ultramafic body but attributed the fabric to contact metamorphism.

Northwest-striking mylonitic shear zones, with sub-horizontal stretching lineations, bound the Tulameen complex—and several smaller ultramafic bodies which are linearly aligned with it—and cut through it. The plutonic rocks become increasingly foliated and, in the case of feldspar-bearing rocks, intensely saussuritized adjacent to these high strain zones (Plate 3.2) . At several exposures the fabric is an L-tectonite, lacking a measurable foliation but displaying distinct mineral stretching lineations. As little as 50 meters away from the shear zone, the ductile fabric in the rock diminishes.

Plate 3.1. Photographs of sheared plutonic rocks of the Tulameen complex adjacent to the northwest striking ductile shear zones which bound and cut through the ultramafic-gabbroic body. a) Mylonitic foliation in gabbro on northwest flank of Grasshopper Mountain (sample 88-JR-06-08). b) Mylonitic foliation observed in sheared syenogabbro along the medial northwest trending shear zone approximately 1.5 km southeast of Olivine creek (sample 87-JR-08-09). c) Sheared syenodiorite along the southeast contact of the Tulameen complex with the Nicola Group (Newton Creek; sample 87-JR-21-09).

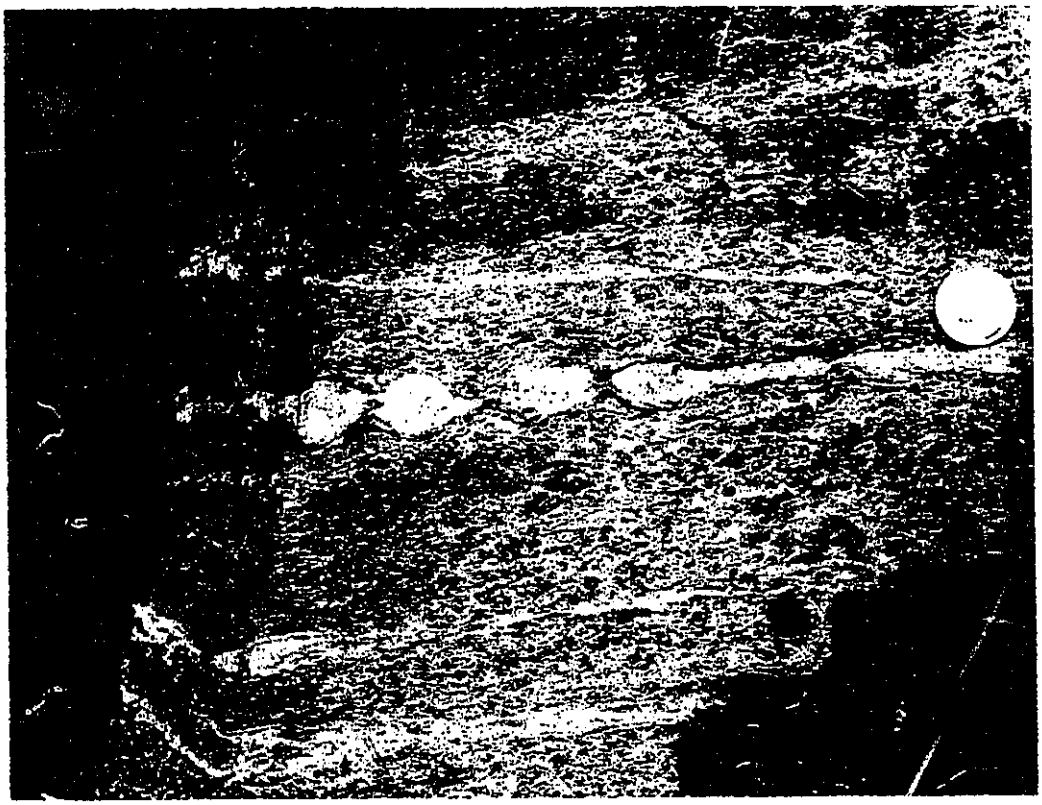

Plate 3.1a

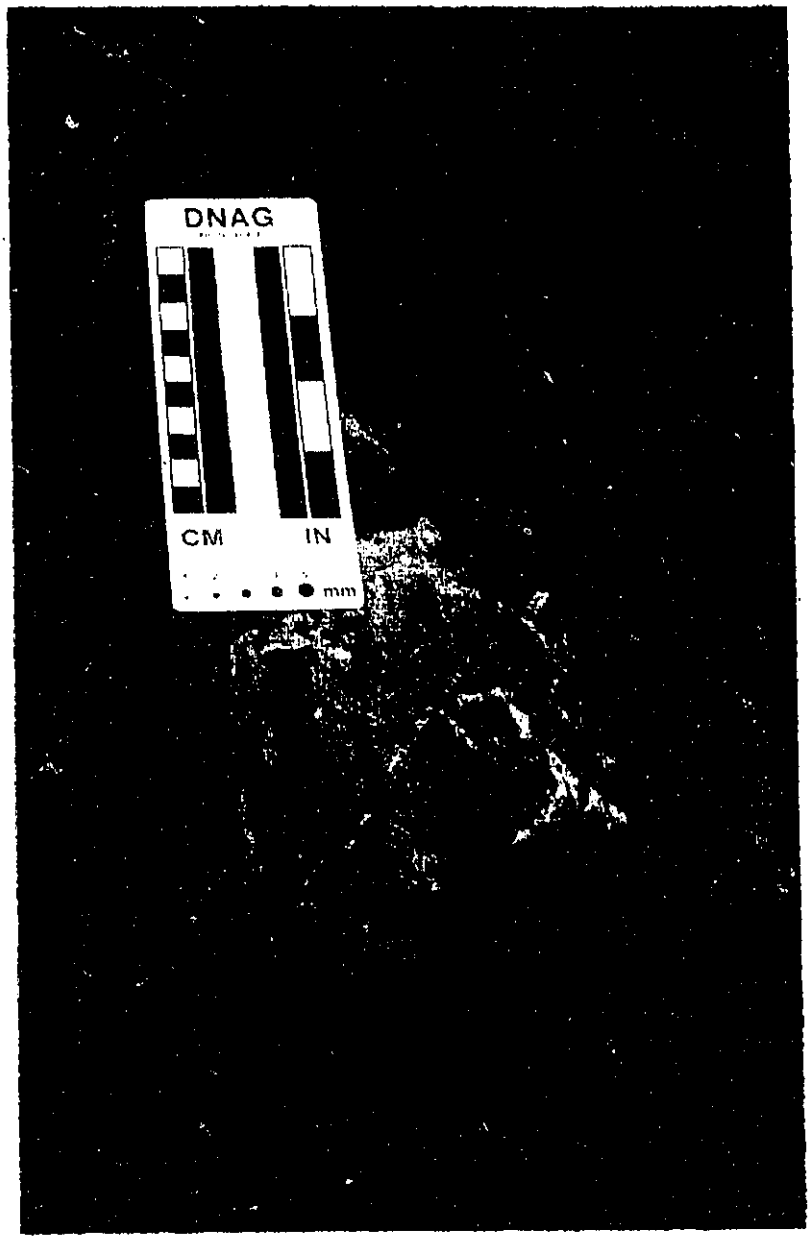

Plate 3.1b

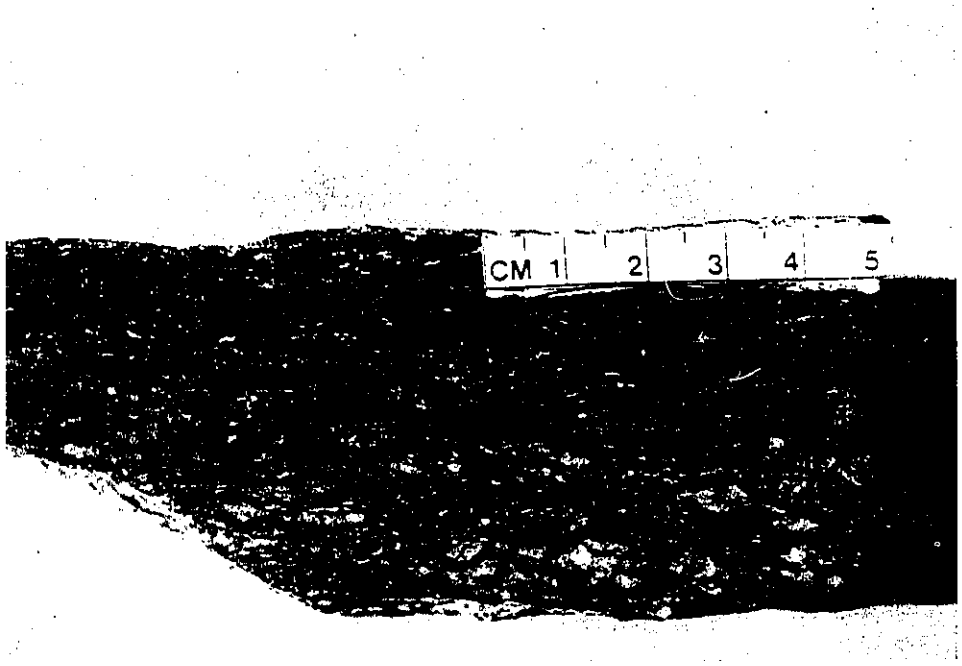

Plate 3.1c

This foliation generally strikes between 140° and 150° and dips moderately to steeply southwestwards, although in areas disrupted by Tertiary faulting it is deflected northwards (110°-120°; Fig. 3.4). The stretching lineations (Fig. 3.3b), which consistently plunge towards the northwest in the plane of the foliation, are defined by stretched porphyroclasts of potassium feldspar within syenodiorite, and elongated augen of hornblende and clinopyroxene in the mylonitized pyroxenites. These fabrics are generally much better displayed in the gabbro, syenogabbro and syenodiorite as opposed to the monomineralic dunites and pyroxenites. Spectacular feldspar rodding, within the foliation plane of mylonitized hornblendite lenses, is exposed at mile 18 on the north side of the Whipsaw Creek main road.

The smaller outliers of ultramafic rock, which range in composition from olivine pyroxenite and hornblende pyroxenite to hornblendite, occur as highly foliated northwest-striking, southwest-dipping lenses, within mylonitized Nicola Group and schistose rocks. The margins of the 5 to 100 m wide lenses are intensely sheared to mylonitized. At the northeastern mylonitic contact on the north side of Grasshopper Mountain, several small (1-2 metre wide), highly sheared blocks of hornblendite are bounded by chloritic shear zones within the sheared Nicola pyroclastic assemblage.

The sense of shear along the northwest-trending ductile faults was determined to be dextral on the basis of the consistency of shear sense indicators observed in the outcrop and in oriented thin sections. Each outcrop and thin section from which this decision was made, offered several types of kinematic indicators (Simpson, 1986; Simpson and Schmid, 1983; i.e. C/S fabrics, asymmetric pressure shadows, broken and rotated inclusions, drag folds), which were all compatible. Representative shear-sense indicators are shown in Fig. 3.5 and Plate 3.2.

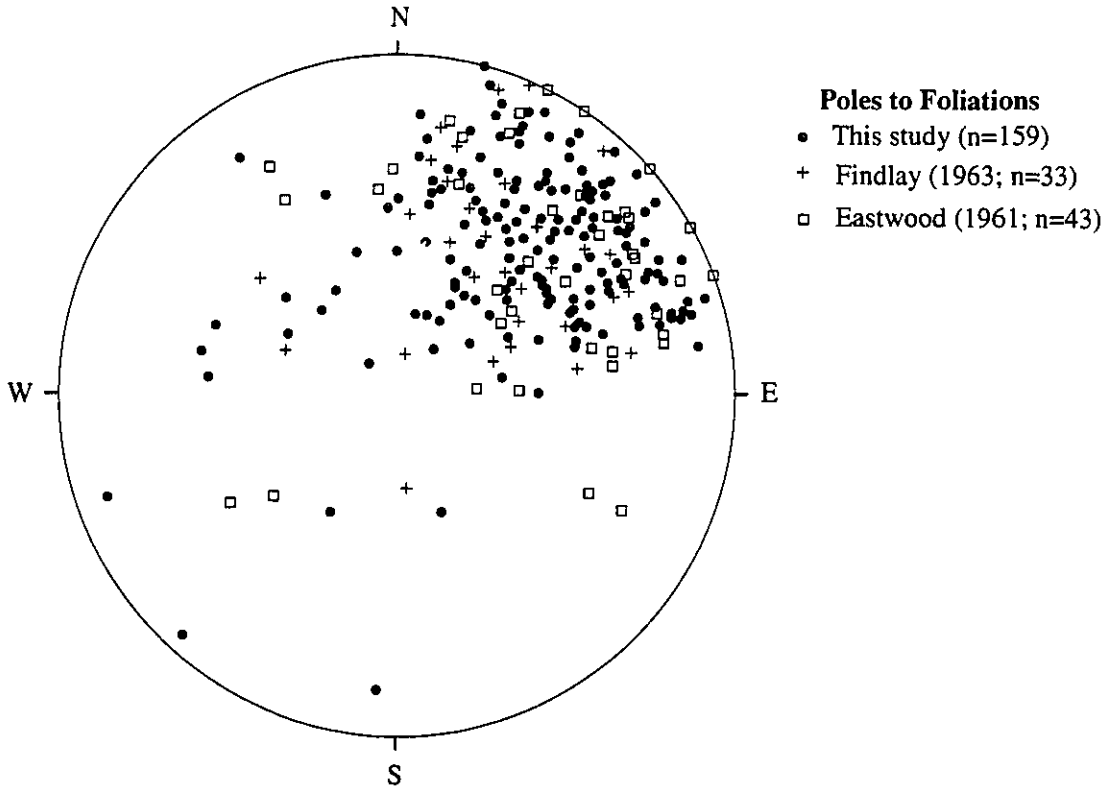

Figure 3.4. Poles to foliations measured in Nicola Group, schistose and Tulameen complex rocks.

Plate 3.5. Sketches (from thin sections) of kinematic indicators observed in structurally oriented (perpendicular to the foliation and parallel to the lineation) samples taken along the northwest striking, southwest dipping shear zones which bound and cut through the Tulameen complex. a) Broken and pulled apart diopside and plagioclase with asymmetric pressure shadows (samples 87-JR-16-04 and 87-JR-18-04). b) Pulled apart and flattened, sigmoidally shaped potassium feldspar and apatite in lithons between schistossity planes in L-S tectonites.

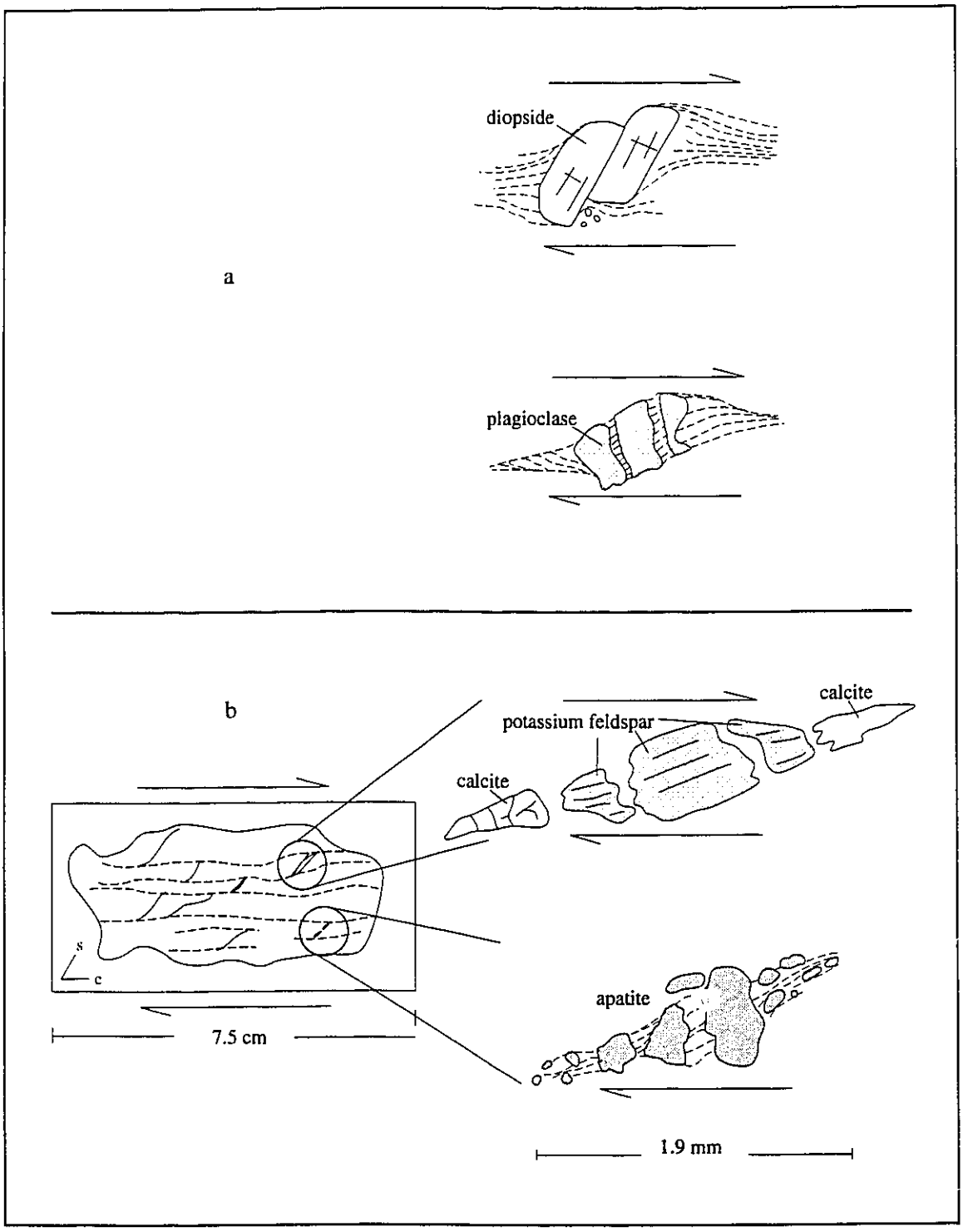
diopside
a
plagioclase
b
calcite
potassium feldspar
calcite
s
c
7.5 cm
apatite
1.9 mm

Figure 3.5

Plate 3.2. Field photographs of kinematic indicators observed along the northwest striking, southwest dipping ductile shear zones which bound and cut through the Tulameen complex. a) Dextral sense of shear is inferred from shear bands, asymmetric tails on rotated clasts and pulled apart fragments. Contact between syenodiorite and Nicola Group 1 km southwest of Olivine Creek. b) Dextral shear-sense indicators (pulled apart competent layers and z-shaped drag fold) in mylonitized syenodiorite and Nicola Group rocks at their contact in Newton Creek.

Plate 3.2a

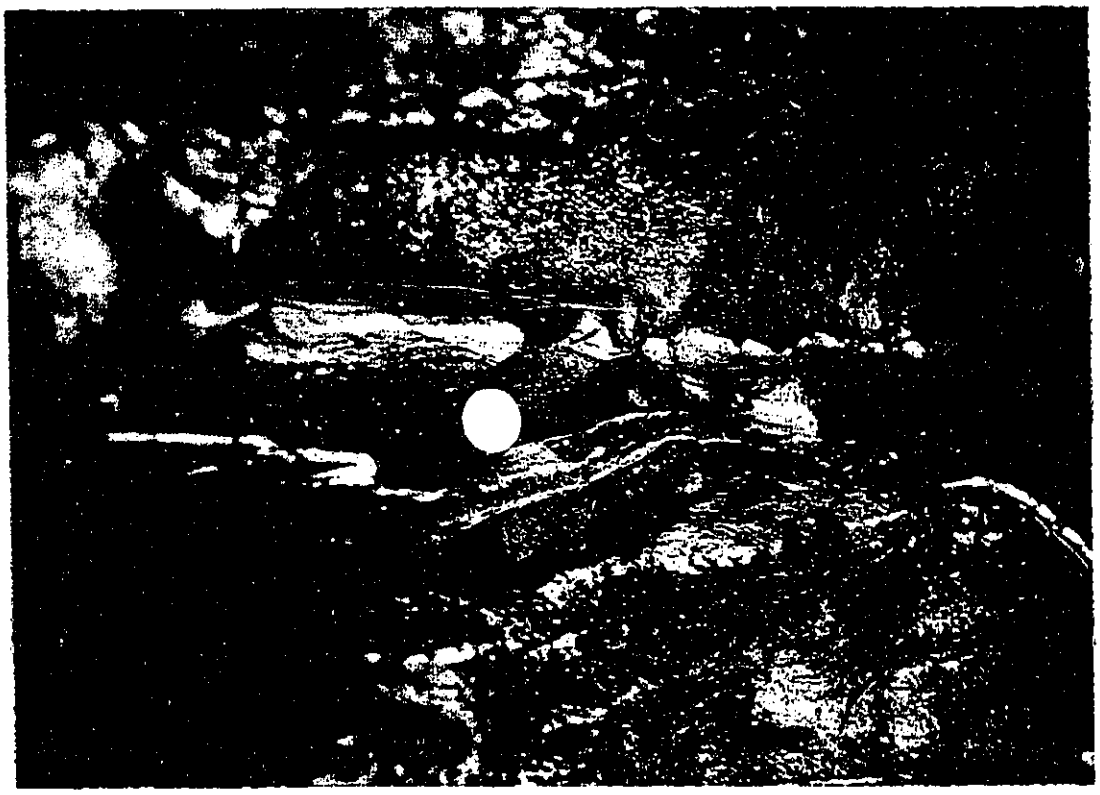

Plate 3.2b

c) Brittle structures

Tertiary brittle structures cut across and extensively disrupt all three structural domains in the Tulameen area. Although the stereonet projections of measured brittle structures (Fig. 3.6) exhibit a wide dispersal of the data, several prominent sets of joints and faults and associated quartz veins can be described and documented. The nature and orientation of these brittle structures are summarized in Table 3.1.

The most prominent set of brittle structures, and apparently the youngest, are the northeast-oriented faults which control much of the drainage of the area. The Tulameen River and Lawless, Olivine, Blakeburn, Newton and Arrastra creeks follow the trace of these northeast-trending faults and chop the Tulameen complex into several fault-bounded blocks. Two orientations of northeast-striking faults are discernable and are reflected in the gentle sigmoidal shape of the river and creeks—east-northeast (50-70°) and north-northeast (25-40°) with moderate (45-70°) dips to both the northwest and southeast. Movement along these northeast-trending faults is consistently dextral with a down dip extensional component; spectacular coarse fibrous tremolite and quartz slickenlines, up to 10 cm in length, are exposed along Lawless Creek and the northern contact of the Tulameen complex on the northeast flank of Grasshopper Mountain, indicate dextral oblique movement along these faults. This is in agreement with Eastwood (1959) who noted that northwest-trending lenses of magnetite were dextrally offset by northeast trending faults near the summit of Lodestone Mountain. Findlay (1963) mapped a parallel structure along Blakeburn Creek near its source, and noted a right-handed offset of approximately 650 m along it.

East-trending (85-100°) faults are frequently encountered in the central part of the Tulameen complex in the area west of Tanglewood Hill. Characteristically, these structures are steeply dipping crush, clay and chlorite gouge zones accompanied by quartz- and chlorite-filled

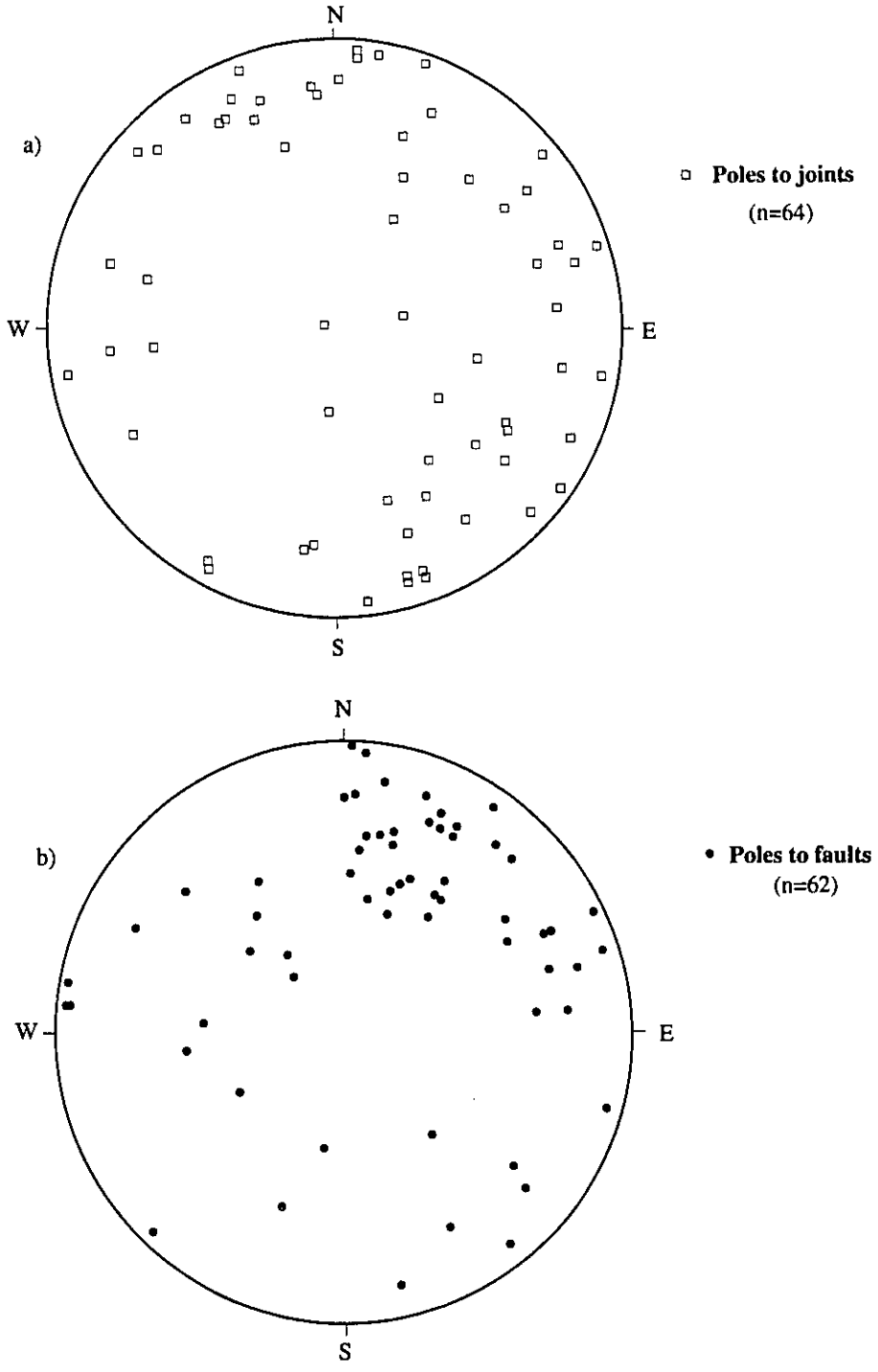

Figure 3.6. Stereoplot of poles to joints (a) and faults (b) measured in the Tulameen complex, and peripheral Nicola Group and schistose rocks.

Table 3.1

Orientation, nature and relative timing of brittle structures in the Tulameen River area.

Orientation	Character	Kinematics	Relative timing
50-70°/ 45-65° NW,SE (east-northeast striking)	Dilational and cataclastic -quartz cemeted wall rock breccia -crush, gouge zones	dextral with dip-slip movement	cut all other structures and Tertiary dykes -parallel to post-Eocene to early Miocene Coquihalla F.
25-40°/ 45-70° NW, SE (northeast striking)	Dilational and cataclastic -symmetrical crustiform chalcedony and calcite veins -comb-textured quartz veins	dextral with dip-slip movement -spectacular subhorizontal quartz-fibre slickenlines	-parallel to post-Eocene Murray Lake (Zoa) F.
85-100°/ steep to N and S (east striking)	Brittle -clay and gouge zones -quartz cemented breccias -quartz and chlorite filled tension gashes	dip-slip and strike-slip movement	-offset WNW brittle faults along southeastern contact
170-180°/ 55-70° W (north striking)	Brittle - Fe-stained carbonate zones -serpentine-lined joints -quartz and chlorite filled tension gashes	dextral (n. of Tulameen R.) sinistral (Skwum Cr.)	-parallels Pasayten F.
0-17°/ 80-90°W (north-northeast striking)	Brittle normal faults -associated axial planar jointing to Tertiary open folds	-dip-slip movement	

younger ↑ ↓ older

tension gashes. Both subhorizontal and subvertical slickensides occur on the fault planes.

Steeply-dipping, north-trending brittle faults, with dextral sense of movement were documented by Eastwood (1961) in the rocks of the Nicola Group north of the Tulameen River. Parallel (2 km to the west) breccia zones were observed on the northeast flank of Grasshopper Mountain and are believed to join up with the north-trending, heavily iron-carbonate altered faults exposed within the olivine pyroxenite in the Tulameen River. In the central part of the Tulameen complex, southeast of Olivine Creek, north-trending brittle structures overprint northwest-trending ductile fabrics. North-northeast (1-17°) trending joints, and axial planar to broad north trending Tertiary folds, offset the mylonitic foliation at the contact between the Tulameen complex and Nicola Group—exposed along the switchbacks southeast of Olivine Creek (Plate 3.3a). More spectacular however, is the disruption of the coal-bearing strata of the Eocene Allenby Formation of the Princeton Group (Goodharzi and Van der Flier-Keller, 1988) by north-trending faults within the Blakeburn open-cast mine, 1.5 km due east of Tanglewood Hill (Plate 3.3b). Large blocks in the hanging wall of the normal faults are rotated in such a way that the originally subhorizontal strata are now vertical. Near vertical, north-trending chlorite- and quartz- filled tension gashes occur within brecciated syenodiorite between Tanglewood Hill and Olivine Creek.

d) Dykes and vein sets

A characteristic feature of the Tulameen area is the conformity in attitudes of the planar structures (bedding, foliations, dykes and veins). Sills of foliated granodiorite intrude schistose rocks of the Nicola Group near the contact with the Eagle plutonic complex and parallel sets of steeply-dipping, unfoliated Tertiary hornblende basalt dykes—observed within the Tulameen complex at its northern and southern extremities—are consistently concordant with the foliation (Fig. 3.7). Exceptions to this uniform dyke orientation are variably-trending deformed Nicola feldspar porphyry and pyroxene basalt dykes, Tulameen clinopyroxenite

Plate 3.3 Field photographs showing Tertiary brittle structures. a) Mylonitic foliation and stretched clast within sheared Nicola Group pyroclastic breccia is offset by joints with dip-slip sense of movement (1 km southwest of Olivine Creek along the sheared contact with the Tulameen complex). b) Larger scale expression of a) is exposed in the Blakeburn open-cast mine (approximately 1.5 km east of a) location where the coal-bearing strata of the Eocene Allenby Formation are disrupted by normal faults.

Plate 3.3a

Plate 3.3b

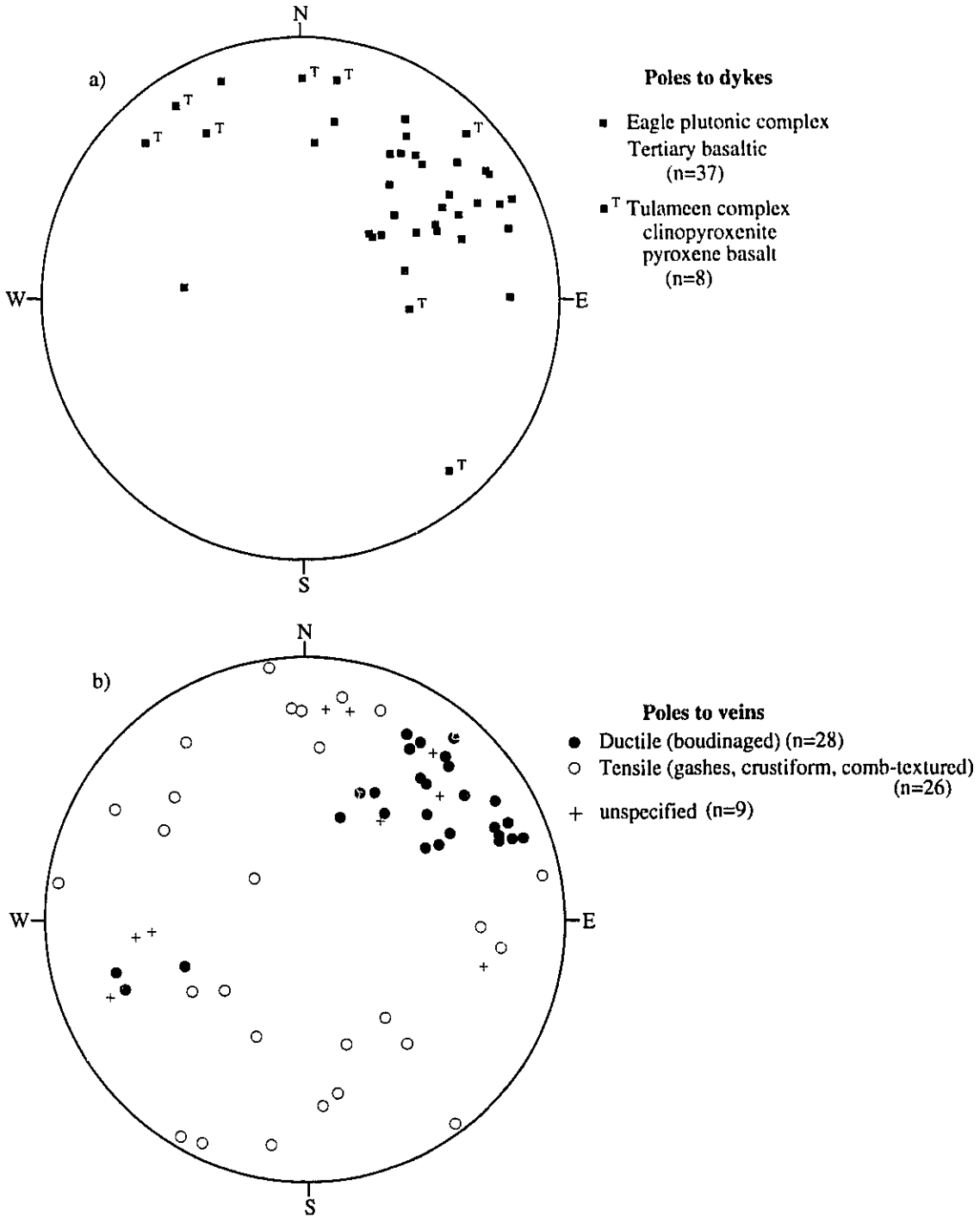

Figure 3.7. Stereoplot of poles to dykes (a) and quartz veins (b) measured in the Tulameen complex and peripheral Nicola Group and schistose rocks.

dykes and the unfoliated granitic dykes (presumably related to the Eocene Illal stock; Greig, 1989) which cross-cut the mylonitic fabric at the western contact between the Nicola Group and Tulameen complex exposed on the west flank of Grasshopper Mountain. The unfoliated Tertiary hornblende basaltic dykes are brecciated and truncated by the northeast- and east-trending brittle faults along the northern side of Grasshopper Mountain. However, highly sheared, northwest trending, southwest-dipping hornblende basalt dykes were noted along the western margin of the Tulameen complex as exposed in the Tulameen River and in the logging scar on the northwest side of Grasshopper Mountain.

Three vein sets are distinguished in the Tulameen area (Fig. 3.7b). The most prevalent are boudinaged, heavily iron stained, quartz-carbonate veins which are confined to the northwest-trending mylonitic shear zones. The second type consists of northeasterly trending comb-textured and symmetrically crustiform veins and discontinuous zones of hydrothermally altered breccia composed of quartz, chalcedony and calcite. These open-spaced filled veins trend northeast and dip moderately to the northwest and southeast. Both types of these fault-hosted veins may be either barren of visible sulphides or mineralized with disseminated pyrite, chalcopyrite, galena and sphalerite. The veins of the third type are east-trending, quartz-chlorite filled tension gashes which occur within the central part of the Tulameen complex, that is extensively disrupted by Tertiary normal faulting. These extensional veins are generally unmineralized, although coarse-grained pyrite and chalcopyrite have been observed within veinlets.

Folding

Evidence for folding within the Tulameen area is limited to local drag folds found in the Nicola Group and Tulameen complex rocks, within the mylonitized margins of the plutonic body and the broad open folds associated with the Tulameen Tertiary basin. The drag folds

have a northwest-trending, southwest-dipping axial planes with subhorizontal, northwest-plunging fold axes.

Discussion

The structural fabrics observed in the rocks of the Tulameen complex record a protracted deformational history. Extensive disruption of the original igneous layering within the ultramafic and feldspathic rocks is evidenced by the predominance of schlieren textures over laterally continuous igneous layering and sheared or brecciated lithologic contacts over gradational ones. As described in the previous chapter, the minerals themselves exhibit many characteristics of crystal deformation such as strained extinction, kink-banding and deformational twinning and lamellae. It is difficult to determine if this deformation of the cumulates was syn-intrusive (near magmatic, high temperature deformation synchronous with crystallization), post-intrusive (i.e. subsolidus deformation occurring after the consolidation of the cumulus minerals) or possibly a continuum. The conformity of northwest-trending, southwest-dipping zones of alteration—expressed as contours of serpentinization (Fig. 2.2), saussuritization of the marginal gabbros and post-cumulate hornblende-banding—with the northwest-trending structural fabric implies a genetic relationship between alteration and deformation. A strong argument for high temperature (syn-magmatic) deformation of the Tulameen complex is the Ar-Ar hornblende plateau age of 207.5 Ma (McDougall, 1974) obtained from a foliated outcrop of syenodiorite, approximately 100 m east of a major northwest-trending shear zone, separating the hornblende clinopyroxenite from the gabbro on the Lodestone Mountain road. The hornblende, itself pristine, appears to postdate the alteration of the gabbro pyroxenite as discussed in the previous chapter. The flat profile of the Ar-Ar age spectrum (Fig. 4.3) indicates that the hornblende has not lost any radiogenic Ar since its crystallization, and consequently has not undergone any thermal disturbance (i.e. above the closure temperature of argon in hornblende ~ 550° ± 50°C; McDougall and Harrison, 1988)

since its formation shortly after the crystallization of the syenodiorite (discussed in the following chapter).

The preservation of primary low temperature minerals within the highly strained Nicola Group pyroclastic breccias at the northeastern contact, exposed on the east flank of Grasshopper Mt., precludes a metamorphic aureole within the country rocks. The lack of Tulameen dykes within the Nicola Group rocks or inclusions of country rock at the margins of the plutonic body, as well as observance of faulted slivers of hornblendite within the Nicola Group indicates that the Tulameen complex was structurally emplaced into the Nicola Group rocks. The Ar-Ar hornblende age of 207.5 Ma (McDougall, 1974) implies that the Tulameen complex has not experienced any significant thermal disturbance (>500°) since the earliest Jurassic.

Greig et al. (1992) document widespread Cretaceous resetting of K-Ar hornblende data in the Eagle plutonic complex and the schistose belt of rocks which separates the Eagle and Tulameen complexes. This, in addition to the differences in the structural fabrics (i.e. northeasterly-verging contractional structures with west to southeast directed lineations in the Eagle shear zone versus consistent northwest directed stretching lineations within oblique-strike slip shear zones in the Tulameen complex; Fig. 3.3) implies that the western and central structural domains of the Tulameen area, represented by the Eagle shear zones and the Tulameen complex respectively, have experienced different structural and thermal histories prior to their post-Cretaceous juxtaposition.

On the basis of these observations, it is postulated that the formation of the northwest-trending ductile fabric in the Tulameen complex is genetically unrelated to the Middle Jurassic deformation associated with the Eagle shear zone, as proposed by Greig (1992). If deformation of the Tulameen complex is syn-intrusive—as suggested by the closed system behavior of the hornblendes for argon (McDougall, 1974)—the ductile fabric in the Tulameen

complex may be correlatable with post-Permian to pre-Middle Jurassic ductile deformation of the southwestern Intermontane belt recorded in the Mount Lytton complex and Nicola horst (Parrish and Monger, 1992; and Moore, 1989 respectively). Speculatively, the dextral shearing of the Tulameen complex may represents a deeper structural equivalent of the dextral faulting associated with the emplacement of the Guichon Creek batholith (Hollister et al., 1975).

Subsequent to this the Tulameen complex was deformed by brittle structures, presumably associated with Tertiary movements along the north-striking Murray Lake (Zoa; Greig, 1992), northeast-trending Coquihalla and northwest-trending Pasayten faults, and the extensional margins of the Tulameen basin.

Chapter 4

Isotope geochemistry of the Tulameen complex.

Introduction

Published isotopic data for the Tulameen complex indicate a range of K-Ar hornblende ages of 196-208 Ma (Roddick and Farrar, 1971), and a ^{40}Ar-^{39}Ar hornblende plateau age of 207.5 Ma (McDougall, 1974).

For a more precise age of crystallization, a U-Pb zircon age has been determined. Because of the unlikelihood of finding zircons in the ultramafic or mafic rocks, the more differentiated feldspar-bearing portion of the complex was sampled. The syenodiorite phase of the felsic suite of Tulameen complex was selected because it is a homogeneous and representative unit of the gabbro-syenogabbro-syenodiorite body. The outcrop from which the 10 kg sample was taken (Fig. 4.1) shows no observable compositional layering, inclusions or dykes. The medium-grained rock is made up of diopside (7%), biotite (5%), oligoclase (An_{30} 40%), orthoclase (45%), magnetite (2%) and apatite (2%). Alteration is evidenced by fibrous actinolite rims on stubby diopside prisms, saussuritization and albitization of the plagioclase, chloritization of the biotite and overgrowths of secondary microcline on the orthoclase. A mineral lineation (15° towards 320°) is defined by the alignment of the 1.0 cm laths of orthoclase.

Sample preparation and analysis

The sample was prepared at the University of Ottawa, Carleton University and the Geological Survey of Canada in Ottawa. Dr. R.R. Parrish and staff of the Geochronology Laboratory of the Lithosphere and Canadian Shield Division of the Geological Survey of Canada carried out the U-Pb chemistry and mass spectrometry.

Legend to sample location map (Fig. 4.1) on verso.

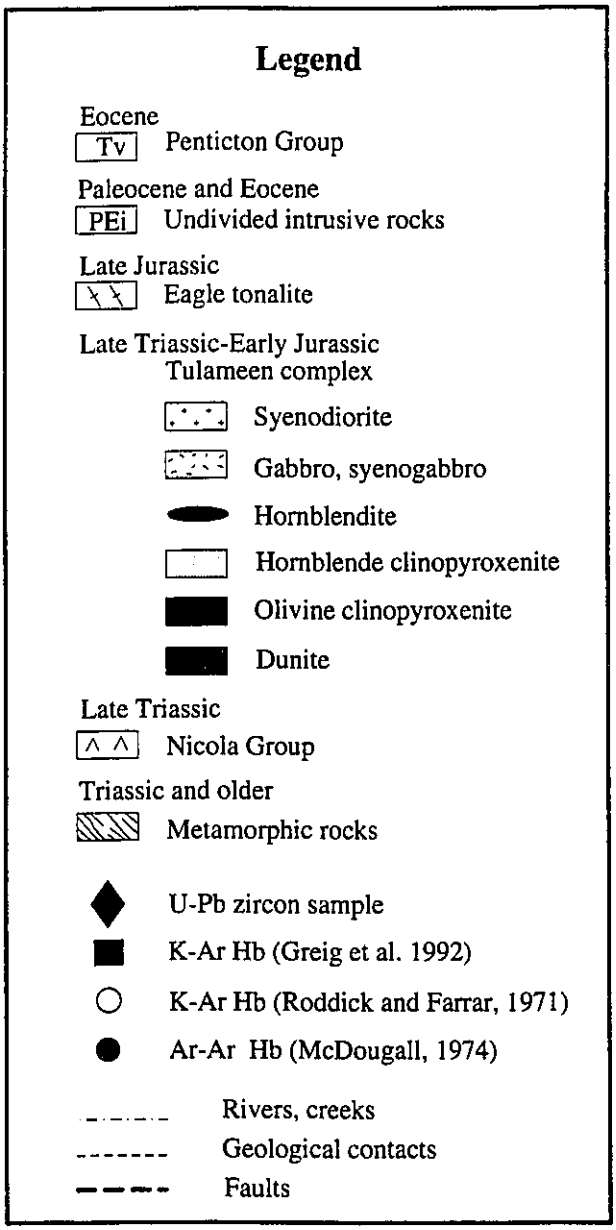
Legend
Eocene
Tv
Penticton Group
Paleocene and Eocene
PEi
Undivided intrusive rocks
Late Jurassic
Eagle tonalite
Late Triassic-Early Jurassic
Tulameen complex
Syenodiorite
Gabbro, syenogabbro
Hornblendite
Hornblende clinopyroxenite
Olivine clinopyroxenite
Dunite
Late Triassic
Nicola Group
Triassic and older
Metamorphic rocks
U-Pb zircon sample
K-Ar Hb (Greig et al. 1992)
K-Ar Hb (Roddick and Farrar, 1971)
Ar-Ar Hb (McDougall, 1974)
Rivers, creeks
Geological contacts
Faults

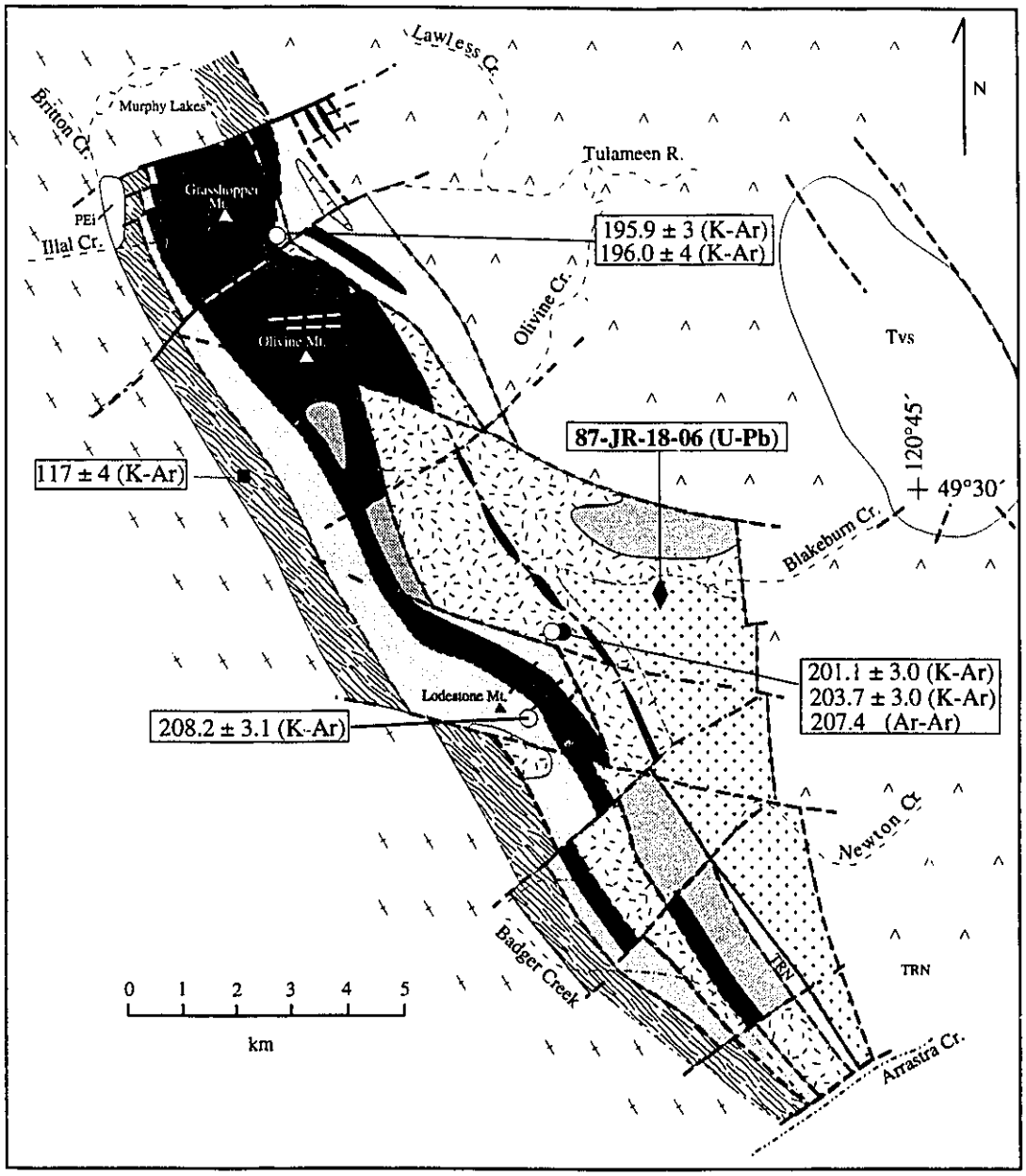

Figure 4.1. Location of U-Pb (zircon) sample 87-JR-18-06. Also shown are locations and ages obtained on published K-Ar hornblende (Roddick and Farrar, 1971; Greig et al., 1992) and Ar-Ar hornblende (McDougall, 1974) ages for Tulameen complex and schistose country rocks.

Approximately 8 of the original 10 kg of sample were crushed and milled to 250 μm size; from this a heavy mineral portion was separated with a Rogers wet shaking table, followed by further extraction using standard heavy liquid (methylene iodide) techniques. The zircon separate was purified magnetically with a Franz isodynamic separator. Four non-magnetic and two magnetic zircon fractions were hand picked on the basis of size, colour and presence or absence of inclusions and cracks. The hand-picked grains were colourless to light yellow broken fragments, characteristically 100-300 μm in length and 100-200 μm in width, with poorly faceted crystals and rare terminations. No cores were observed. None of the fractions was abraded (Krogh, 1982).

The following abridged procedure for the U-Pb chemistry and mass spectrometry is described in detail by Parrish et al. (1987). The six fractions were weighed, spiked with a small amount of mixed ^{205}Pb-^{233}U-^{235}U tracer and then dissolved in HF and HNO_3. U and Pb were separated by anion exchange colorimetry and loaded onto separate rhenium filaments. Isotopic compositions of the U and Pb were measured on a Finnigan 261 variable multi-collector mass spectrometer. Data were reduced and propagation of errors was determined according to the methods described by Parrish et al. (1987). Errors given in Table 4.1, and diagrammatically represented as error ellipses in Fig. 4.2, represent 2 standard deviations.

Results and interpretation

The six data points (Table 4.1) plot as an overlapping cluster off concordia between 203.5 and 205 Ma (Fig. 4.2). The $^{207}Pb/^{206}Pb$ ages for the six fractions (Table 4.1) range from 207.2 ± 2.2 Ma to 212.9 ± 1.6 Ma, with a mean of 209.9 ± 4.7 Ma.

The interpretations of the isotopic data which account for the differences in the measured $^{206}Pb/^{238}U$, $^{207}Pb/^{235}U$, and $^{207}Pb/^{206}Pb$ ages, are; 1) the age of crystallization of the syenodiorite is no older than $^{206}Pb/^{238}U$ ages of ~ 204 Ma and the older $^{207}Pb/^{206}Pb$ ages

Table 4.1

U-Pb data.

Fraction	Wt. (mg.)	U (ppm)	Pb (ppm) [a]	$^{206}Pb/^{204}Pb$ [b]	Pb [c] (pg) [c]	^{208}Pb (%) [d]
A= (NM 250-300μ clr a bk p n=12)	0.154	348	12	3338	33	14.9
B= (NM 100-200μ clr bk p n=27)	0.208	278	9	4122	28	13.1
C= (NM 100-200μ clr bk eq n=36)	0.166	198	7	2758	24	12.8
D= (NM >300μ clr r bk eq n=23)	0.329	286	10	5501	35	13.0
E= (M 150-300μ clr a bk p n=12)	0.374	225	8	4986	34	13.0
F= (M 200-250μ clr bk p n=10)	0.254	178	6	1775	52	13.2

	$^{206}Pb/^{238}U$ [e]	$^{207}Pb/^{235}U$ [e]	Correlation coefficient	$^{207}Pb/^{206}Pb$ [e]	$^{207}Pb/^{206}Pb$ age(Ma) [f]
A	0.03218 ± 0.09	0.2232 ± 0.11	0.91	0.05030 ± 0.05	209.3 ± 2.2
B	0.03213 ± 0.09	0.2229 ± 0.10	0.92	0.05031 ± 0.04	209.4 ± 2.0
C	0.03216 ± 0.09	0.2229 ± 0.11	0.93	0.05026 ± 0.04	207.2 ± 1.9
D	0.03220 ± 0.10	0.2234 ± 0.11	0.96	0.05033 ± 0.03	210.2 ± 1.5
E	0.03218 ± 0.10	0.2236 ± 0.11	0.96	0.05039 ± 0.03	212.9 ± 1.6
F	0.03211 ± 0.10	0.2228 ± 0.13	0.90	0.05033 ± 0.06	210.2 ± 2.6

NM, M = non-magnetic, magnetic
μ= zircon length in micrometres
a,r = amber, rose colored
bk = broken
p, eq = prismatic, equant
n = number of crystals

a Radiogenic Pb, corrected for spike, fractionation, blank, and common Pb.
b Measured ratio, corrected only for spike and fractionation.
c Total common Pb in analysis.
d Radiogenic 208 Pb, expressed as % of total radiogenic Pb.
e Uncertainties are 1 s.
f Uncertainties are 2 s in Ma.

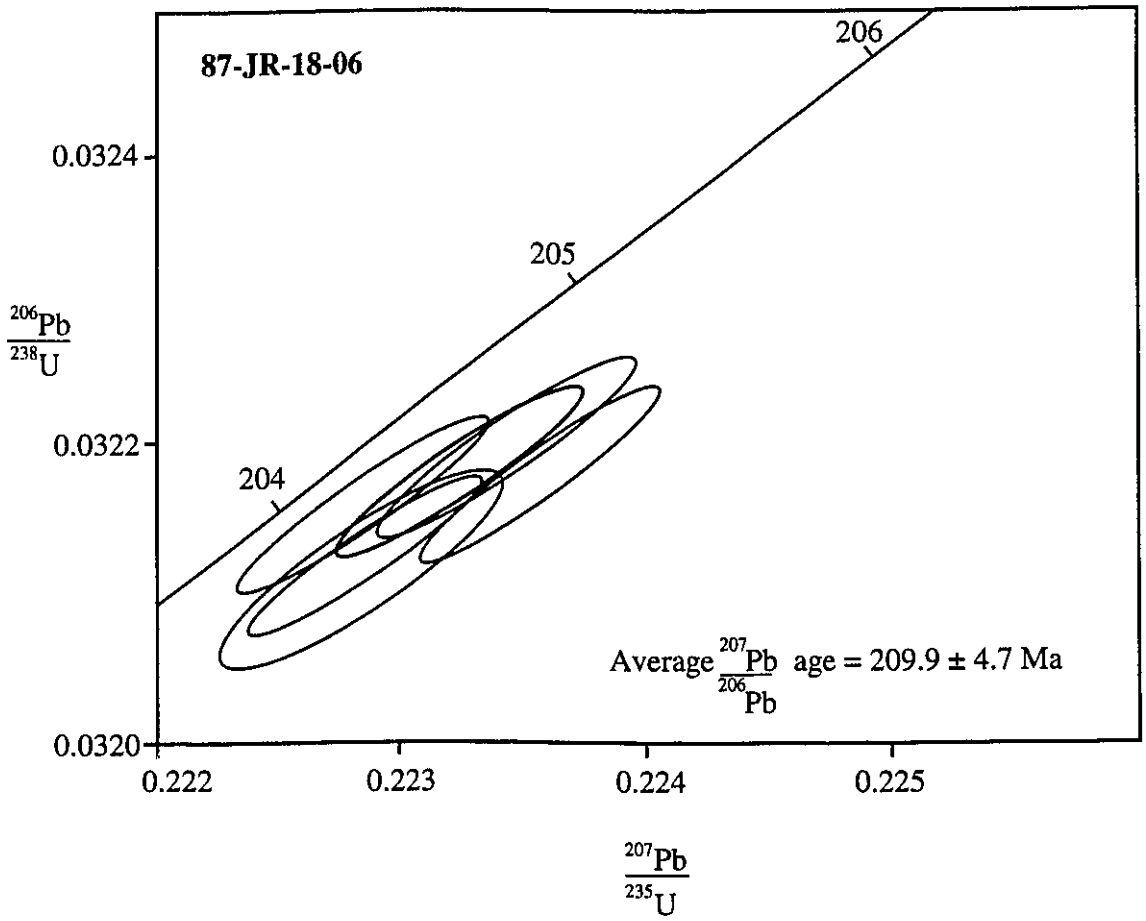

Figure 4.2. U-Pb concordia diagram.

reflect a small amount of inheritance of older zircon; (2) the $^{206}Pb/^{238}U$ ages of 203.5-205 Ma are the crystallization age and the older $^{207}Pb/^{206}Pb$ ages result from excess radiogenic ^{207}Pb (Mortensen et al., 1992); or 3) the mean of the $^{207}Pb/^{206}Pb$ ages, 209.9 ± 4.7 Ma, is the closest approximation of the crystallization age and the younger, discordant $^{207}U/^{235}Pb$ and $^{206}Pb/^{238}U$ ages are due to lead loss.

Because the inheritance of older zircon is considered unlikely due to the clear, coreless nature of the zircons as well as the coincidence of the $^{207}U/^{235}Pb$ and $^{206}Pb/^{238}U$ ages for the six fractions (Fig. 4.2), the first explanation of the data is rejected. In addition, no cases of inheritance were reported by Parrish and Monger (1992) during an extensive U-Pb dating project on this part of the Intermontane belt. Although excess radiogenic ^{207}Pb cannot be disproven with the available data, the mean of the $^{207}Pb/^{206}Pb$ ages, 209.9 ± 4.7 Ma, is considered the best interpretation of the crystallization age of the syenodiorite for the following reasons.

McDougall (1974) obtained an hornblende age of 207.5 Ma. (recalculated using new decay constants from Steiger and Jäger, 1977) from a foliated outcrop of syenogabbro, 1.5 km southeast from the U-Pb zircon sample site (Fig. 4.1). The ^{40}Ar-^{39}Ar age spectra diagram for the sample (Fig. 4.3) shows a flat plateau and according to McDougall (1974):

> "we can state with great confidence that this hornblende has not lost any radiogenic Ar subsequent to crystallization; indeed these data indicate that the simple model of crystallization with subsequent closed system behavior is correct."

This ^{40}Ar-^{39}Ar hornblende age is consistent with previously determined K-Ar hornblende ages of 196-208 Ma reported by Roddick and Farrar (1971; recalculated using new decay constants from Steiger and Jäger, 1977). Since hornblende is a post-cumulus mineral which replaces diopside in both the ultramafic and feldspathic rocks at their contacts, the older averaged

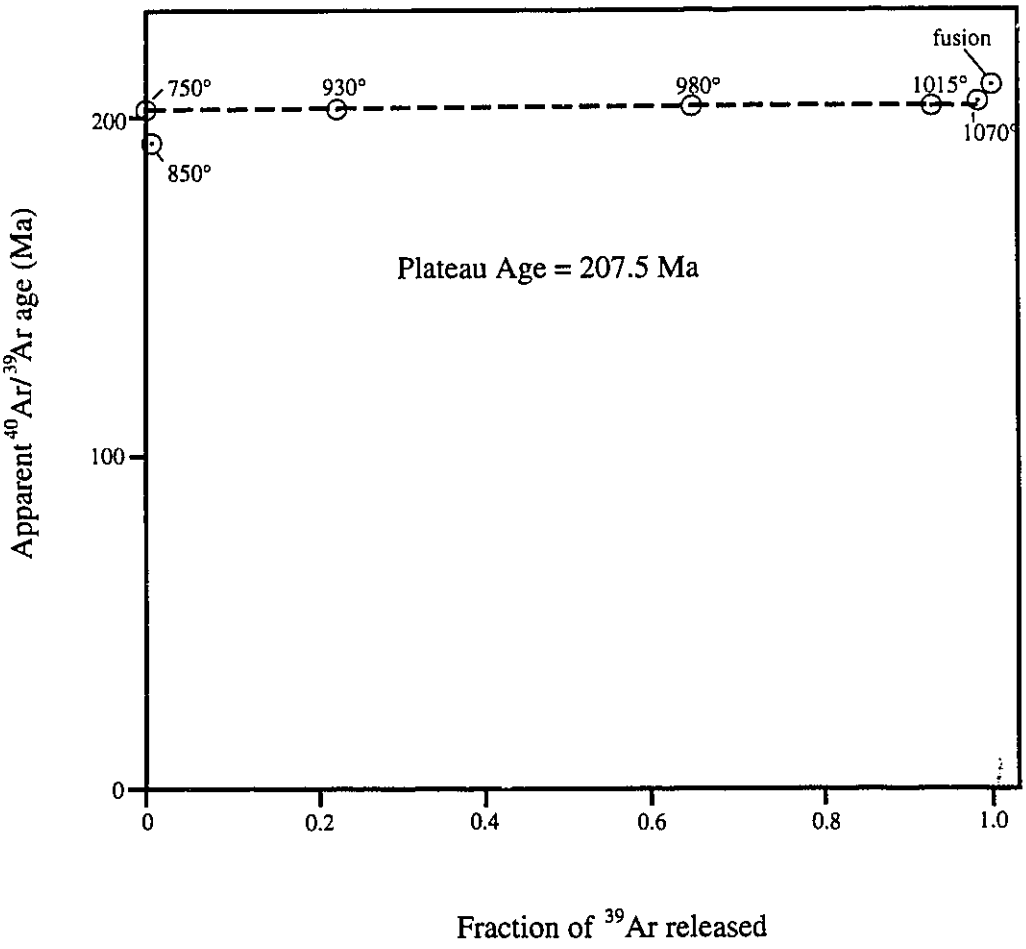

Figure 4.3. Plot of $^{40}Ar/^{39}Ar$ hornblende plateau from McDougall (1974).

$^{207}Pb/^{206}Pb$ age of 209.9 ± 4.7 Ma seems more reasonable, and the younger, discordant $^{207}U/^{235}Pb$ and $^{206}Pb/^{238}U$ ages are attributed to lead loss. The closed system behavior of the ^{40}Ar-^{39}Ar hornblende age spectrum precludes the loss of radiogenic lead due to a particular episode of thermal disturbance. Therefore, the loss of radiogenic Pb is proposed to have occurred continuously by diffusion. Supporting evidence for the acceptance of the mean of the $^{207}Pb/^{206}Pb$ ages, 209.9 ± 4.7, as the minimum crystallization age for the Tulameen are the latest Triassic U-Pb zircon ages from the related Guichon Creek batholith (210 ± 3 Ma; Mortimer et al., 1990) and Mount Lytton complex (212 ± 1 Ma; Parrish and Monger, 1992).

Prospective abrasion of the zircon fractions may determine if the discordance of the data is due to radiogenic Pb loss or excess radiogenic lead. If radiogenic Pb loss is the culprit, the effect of abrasion will be to move the data point toward concordia, as much of this type of discordance is associated with the outer layers of the crystals which are removed by abrasion (Krogh, 1982).

Discussion

The interpreted crystallization age of 209.9 ± 4.7 Ma for the syenodiorite is a minimum crystallization age for the Tulameen complex. The ^{40}Ar-^{39}Ar hornblende plateau age of 207.4 Ma (McDougall, 1974) indicates that the Tulameen complex was sheared in the ductile regime (as discussed in the previous chapter) and cooled below 550°C (the closure temperature of hornblende for argon; McDougall and Harrison, 1988) shortly after the crystallization of the syenodiorite.

Similarly, Hollister et al. (1975) documented that the Guichon Creek batholith (210 ± 3 Ma; Mortimer et al., 1990) differentiated during continuous and simultaneous movements along the dextral Lornex and Highland Valley faults. Sericites from structurally-controlled mineralized veins associated with the fault zones, yield 210-190 Ma K-Ar cooling ages (Mortimer et al., 1990).

These two latest Triassic to earliest Jurassic plutons, along with several other calc-alkaline to alkaline plutons (Fig. 4.4), are interpreted as representing the final culmination of Nicola-related magmatism (Mortimer, 1987). This intrusive suite is characterized by low initial $^{87}Sr/^{86}Sr$ ratios (0.7036-0.7039; Preto et al., 1979; Mortimer, 1987) and K-Ar and Rb-Sr isochron ages ranging from 205-220 Ma (Armstrong, 1988). Table 4.2 summarizes the age data for these and a suite of younger (Early Jurassic) plutons. Monger (1989), interprets the Late Permian (ca. 250-260 Ma; Friedman and van der Heyden, 1992), Early and late Late Triassic (225 ± 5 Ma, 212 ± 1 Ma; Parrish and Monger, 1992) gneisses and plutonic rocks of the Mount Lytton complex as basement to the Nicola arc.

The eastward transition of calc-alkaline to shoshonitic volcanism within the Nicola Group (Mortimer, 1987) is crudely paralleled in the intrusive suite by the distribution of the alkaline plutons (Iron Mask, Copper Mountain and Tulameen) east of the calc-alkaline plutons (Guichon Creek, Mount Lytton, Coldwater and Allison; Fig. 4.4). Although alkaline and calc-alkaline plutonism was contemporaneous, plutonism and volcanism was not (Fig. 4.5). This suggests that either; i) the calc-alkaline volcanic equivalents to the Guichon Creek, Allison and Coldwater bodies have been eroded and that the high K-suite of volcanic rocks in the eastern belt are equivalents of the Tulameen, Copper Mountain and Iron Mask bodies (a view presented by Parrish and Monger, 1992), or alternatively, ii) that during the waning stages of Nicola arc-related magmatism, plutonism was unaccompanied by volcanism and the intrusions were emplaced into an older cover of volcanic rocks. The answer to this may be recorded within the clastic rock record of the Jurassic to Cretaceous Methow terrane which O'Brien et al. (1992) have shown, by the presence of a 235 ± 10 Ma biotite quartz diorite clast (Mount Lytton equivalent) within the basal conglomerate of the Early Jurassic Boston Bar Formation, to be contiguous with Quesnel terrane in the Early Jurassic.

Table 4.2

Summary of age data for early Mesozoic plutons in the southwestern Intermontane belt

	Pluton	Lithology	Age	Method	Reference
Late Triassic-Early Jurassic (Nicola related)	Tulameen	dunite, pyroxenite gabbro-syenodiorite	209.9 207.4 197-212	U-Pb (zircon) Ar-Ar (hornblende) K-Ar (hornblende)	this study McDougall (1974) Roddick and Farrar (1971)
	Copper Mountain	clinopyroxenite, gabbro-syenodiorite	196-212	? (unpub. data)	Mortimer (1987)
	Iron Mask	gabbro-syenite	194 ± 6 209 ± 6	K-Ar (biotite) K-Ar (biotite)	Preto et al. (1979) Preto et al. (1979)
	Guichon	tonalite-granodiorite	210 ± 3 196-213	U-Pb (zircon) K-Ar (hornblende)	Mortimer et al., 1991 Preto et al. (1979)
	Coldwater	tonalite-granodiorite	215 ± 4 234 ± 9	K-Ar (hornblende) K-Ar (hornblende)	Preto et al. (1979) Preto et al. (1979)
	Allison	diorite-granodiorite	204 ± 7 207 ± 5	K-Ar (hornblende) K-Ar (hornblende)	Preto et al. (1979) Preto et al. (1979)
	Mount Lytton	granodiorite tonalite	212 ± 1 250 ± 5	U-Pb (zircon) U-Pb (zircon)	Parrish and Monger (1992) Friedman and van der Heyden (1992)
Early Jurassic	Wild Horse	granodiorite	196 ± 1	U-Pb (zircon)	Parrish and Monger (1992)
	Bromley	granodiorite	193 ± 1	U-Pb (zircon)	Parrish and Monger (1992)
	Pennask	granodiorite	194 ± 1	U-Pb (zircon)	Parrish and Monger (1992)

Legend for Fig. 4.4 on verso.

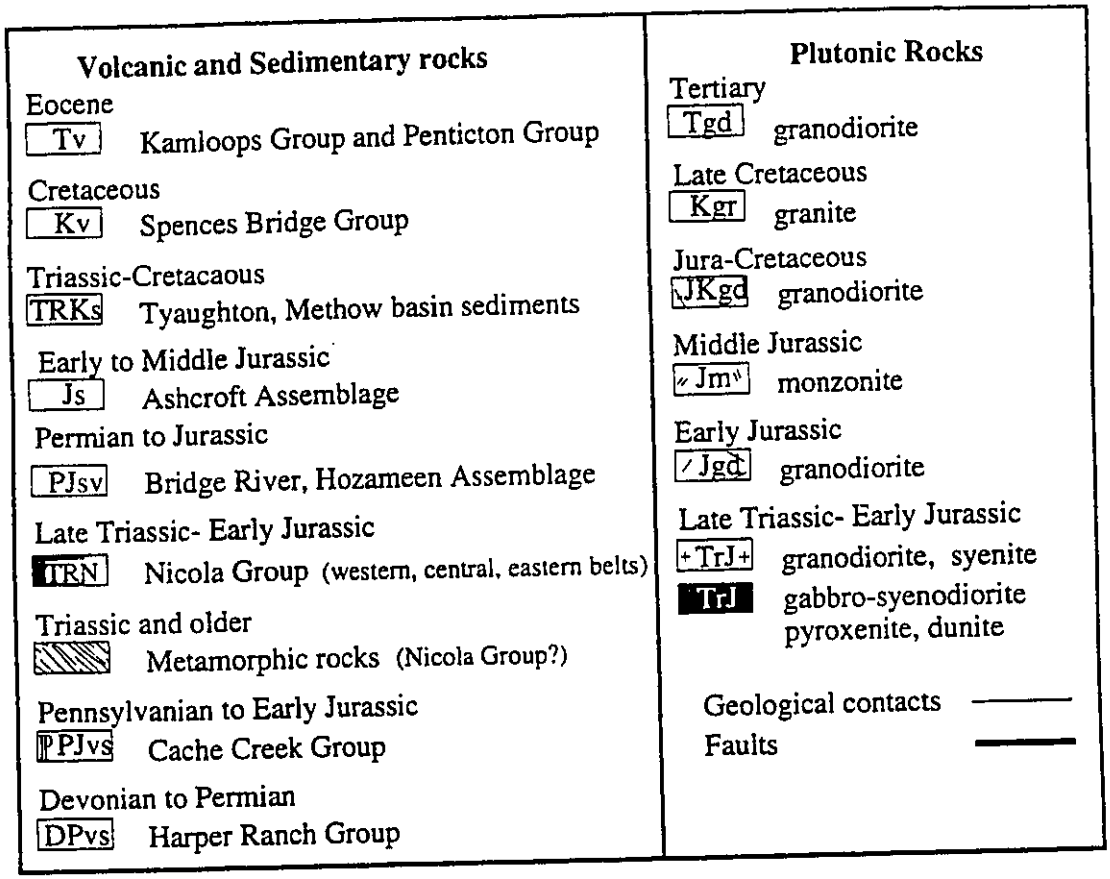
Volcanic and Sedimentary rocks
Eocene
Tv
Kamloops Group and Penticton Group
Cretaceous
Kv
Spences Bridge Group
Triassic-Cretacaous
TRKs
Tyaughton, Methow basin sediments
Early to Middle Jurassic
Js
Ashcroft Assemblage
Permian to Jurassic
PJsv
Bridge River, Hozameen Assemblage
Late Triassic- Early Jurassic
TRN
Nicola Group (western, central, eastern belts)
Triassic and older
Metamorphic rocks (Nicola Group?)
Pennsylvanian to Early Jurassic
PPJvs
Cache Creek Group
Devonian to Permian
DPvs
Harper Ranch Group
Plutonic Rocks
Tertiary
Tgd
granodiorite
Late Cretaceous
Kgr
granite
Jura-Cretaceous
JKgd
granodiorite
Middle Jurassic
Jm
monzonite
Early Jurassic
Jgd
granodiorite
Late Triassic- Early Jurassic
TrJ
granodiorite, syenite
TrJ
gabbro-syenodiorite
pyroxenite, dunite
Geological contacts
Faults

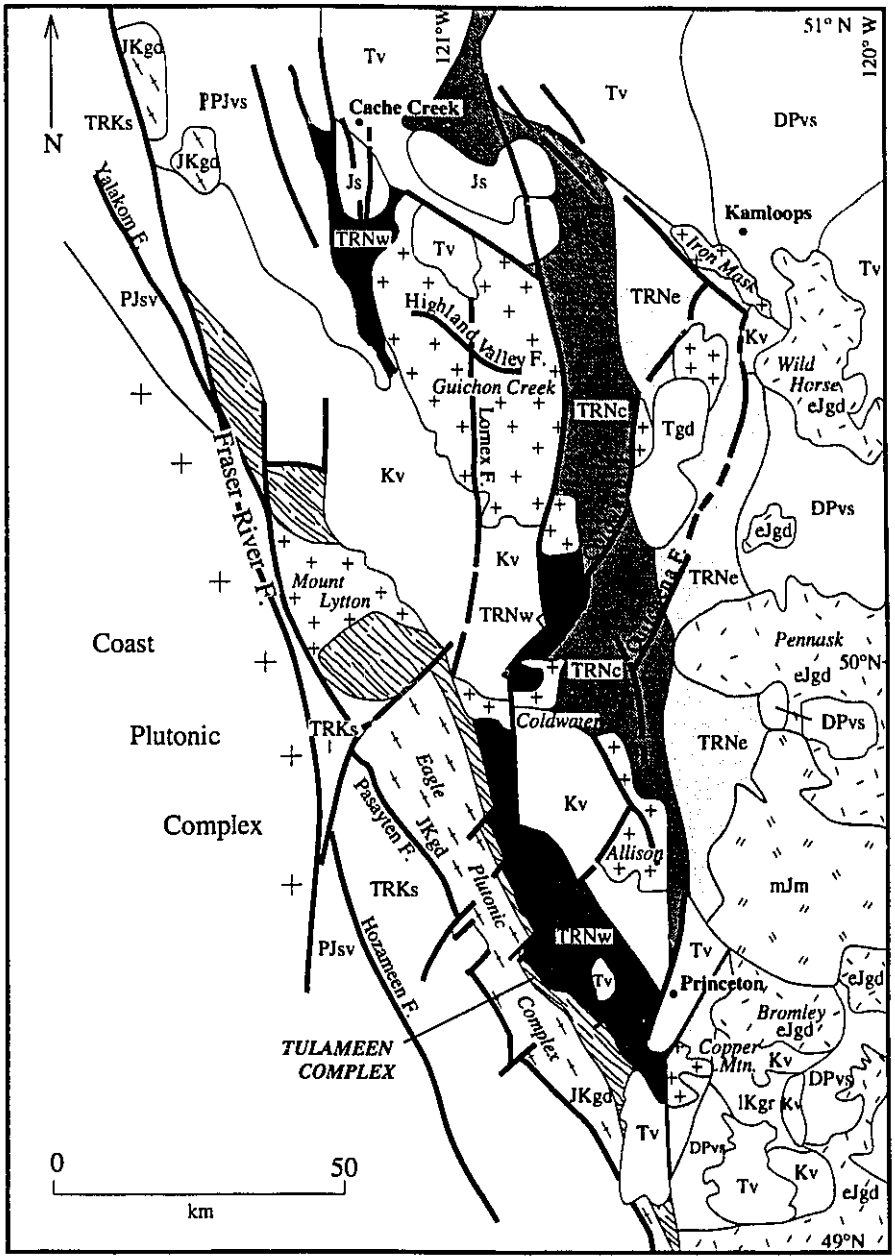

Figure 4.4. Simplified geological map of the southwestern Intermontane belt showing Late Triassic to Early Jurassic plutons and the western, central and eastern belts of the Late Triassic to Early Jurassic Nicola Group. Modified after Mortimer (1987), Parrish and Monger (1992) and Monger (1985).

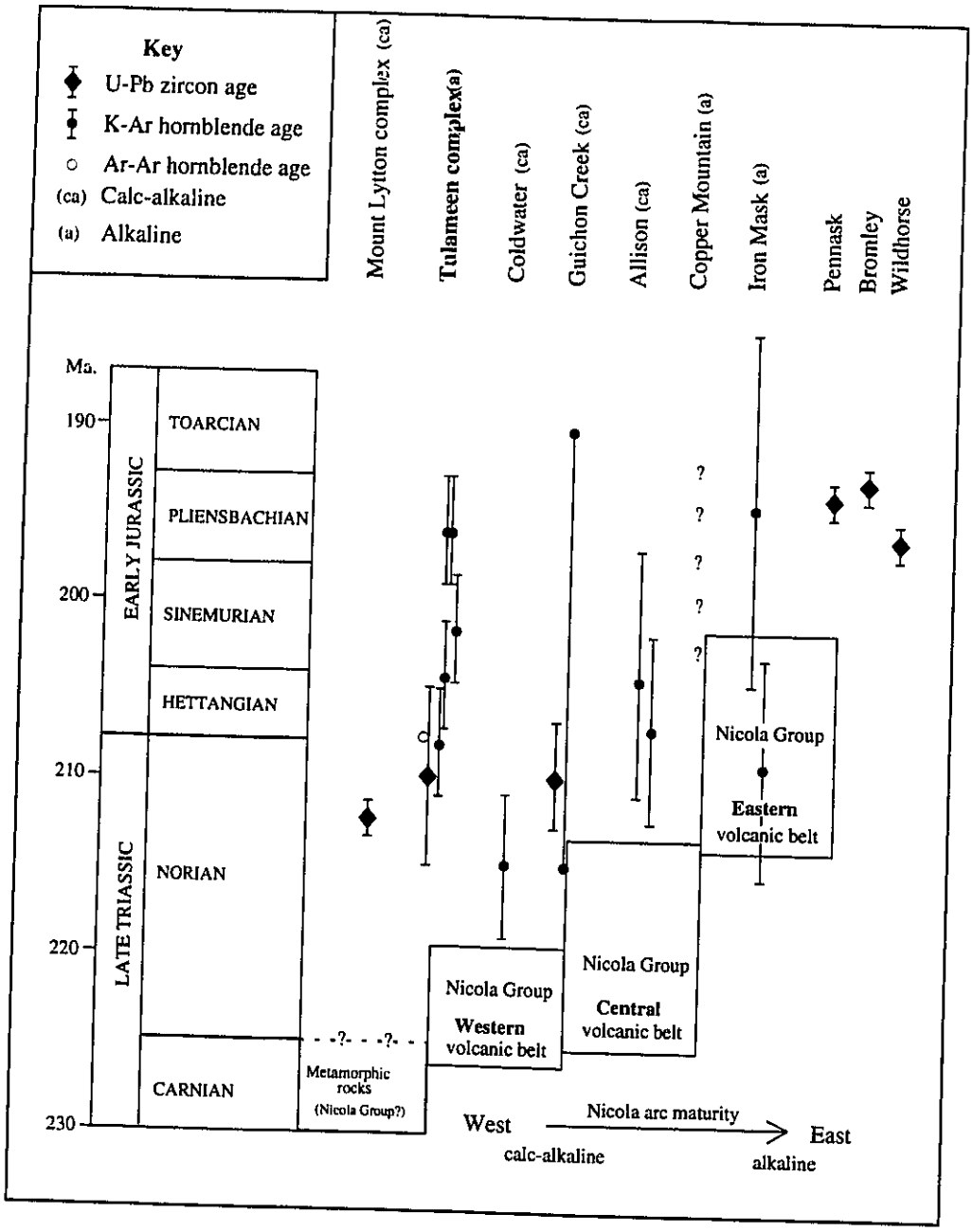

Figure 4.5. Diagram showing isotopic ages for Nicola-associated plutons and biostratigraphically determined age ranges for the three belts of the Nicola Group. Modified after Mortimer (1987) with time scale of Palmer (1983). Sources of data are provided in Table 4.2.

Chapter 5.

Chemical petrology and mineralogy.

Introduction

The results of whole rock and mineral analyses presented in this chapter add to the existing geochemical data base for the Tulameen complex. Previously published analyses include whole rock major element compositions (Camsell, 1913; and Findlay, 1969), whole rock PGE abundances (Camsell, 1913; Kemp, 1902; MacKenzie, 1920; O'Neill and Gunning, 1934; Findlay, 1969 and St. Louis et al., 1986), PGE phase microprobe analyses (Cabri et al., 1973; Cabri et al., 1973; Raceivic and Cabri, 1976; Nixon et al., 1990; and Talkington et al., 1986), chromite and magnetite analyses (O'Neill and Gunning, 1934; and Eastwood, 1959) as well as osmium isotopic determinations on selected platinum nuggets from the Tulameen area (Hattori and Hart, 1991).

In this investigation, the compositional variation of the Tulameen complex was studied by employing several analytical techniques for determining bulk rock and mineral compositions. Thirty-one representative rock samples were analyzed for major and trace element abundances, using the Philips PW 1410 X-ray spectrometer at the University of Ottawa. Five of these rock powders were submitted to École Polytechnique (Montreal) for rare earth element determination by instrumental neutron activation with the Slowpoke reactor. Locations of the samples selected for chemical analyses are shown in Fig. 5.1. Symbols for the various rock types used in the diagrams are listed in Table 5.2.

Whole rock chemistry

Major and trace element data for representative lithologic units of the Tulameen complex is summarized in Table 5.2 and Fig. 5.2 and 5.3. This data includes compositions for: 4 dunite, 1 wehrlite, 4 olivine clinopyroxenite, 1 clinopyroxenite, 4 hornblende clinopyroxenite,

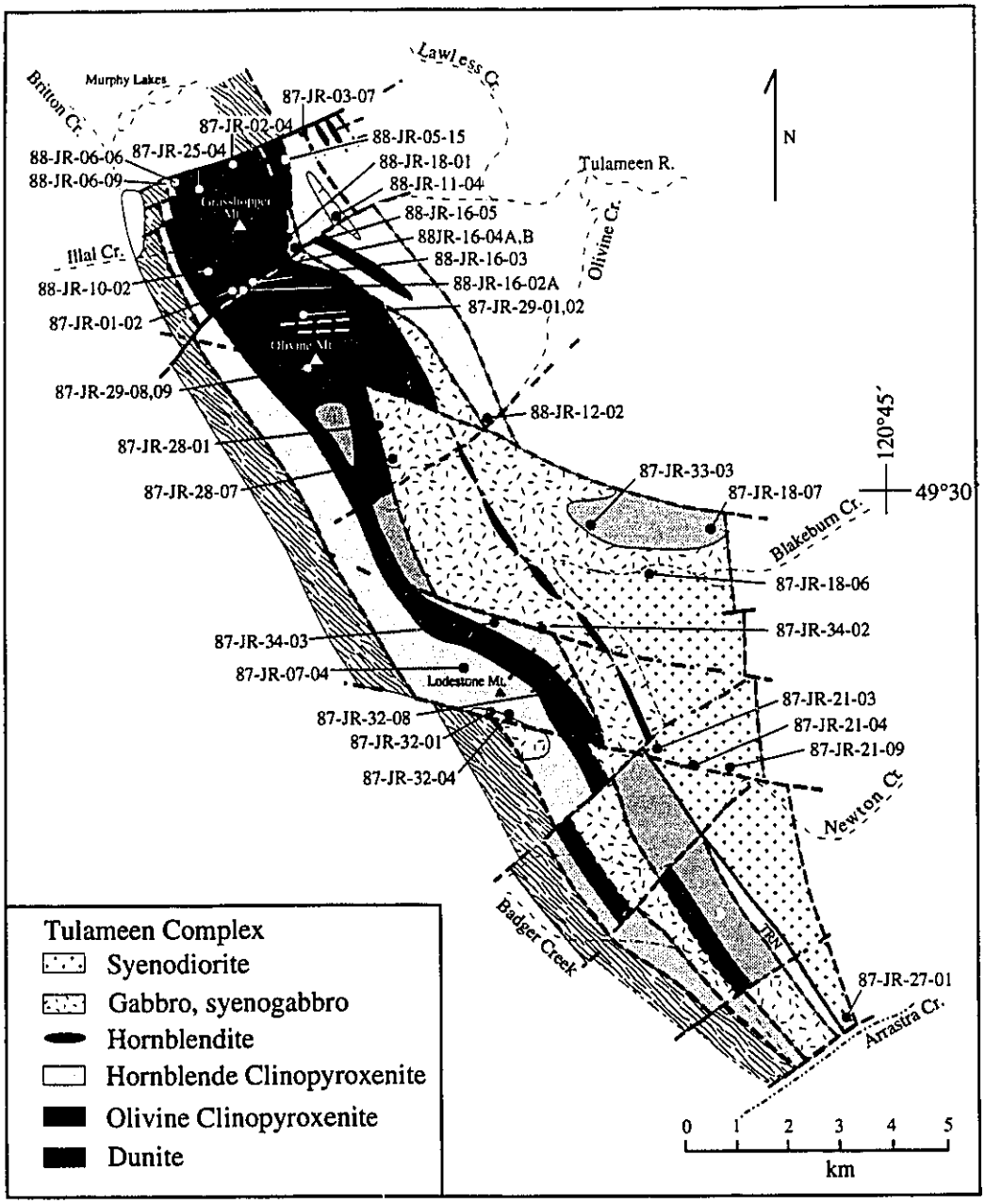

Figure 5.1. Sample location map. The type of chemical analysis employed for each sample is indicated in Table 5.1 .

Table 5.1.

Symbols used for the various rock-types of the Tulameen complex.

Symbol	Lithologies	Sample numbers	Chemical analyses
○	Hb dioritic dykes	88-JR-04-01E	XRF
		87-JR-03-07	XRF
+	Hb diorite	87-JR-27-01	XRF
△	Syenogabbro-syenodiorite	87-JR-18-01	Probe (Px)
		87-JR-21-09	XRF
		88-JR-18-06	XRF
		87-JR-21-03	XRF Probe (Px)
		87-JR-21-04	XRF
×	Px Gabbro	88-JR-11-04	XRF
⧗	(prism sector)	87-JR-28-01	XRF INAA Probe (Ol, Px)
⋈	(basal sector)	88-JR-16-05	XRF Probe (Px)
		88-JR-08-05	XRF
●	Px basalt dyke	88-JR-16-04B	XRF Probe (Px)
■	Hb gabbro	88-JR-16-04A	XRF INAA Probe (Am)
■	Ultramafic-feldspathic contact rocks ↑	87-JR-32-01	XRF Probe (Px, Am)
		88-JR-18-01	Probe (Px, Am)
		87-JR-32-04	INAA
	Hornblendite	88-JR-06-09	XRF
		87-JR-18-07	XRF
		87-JR-07-04	XRF
□	Hornblende Clinopyroxenite	87-JR-33-03	XRF
		88-JR-12-02	XRF
		87-JR-34-02	XRF Probe (Px, Am)
		87-JR-34-03	Probe (Px, Am)
⊕	Magnetite clinopyroxenite	88-JR-05-15	Probe (Px)
○	Clinopyroxenite dyke	88-JR-10-02	XRF
	Clinopyroxenite	88-JR-06-06	XRF
⊙	Olivine clinopyroxenite	88-JR-08-09	XRF
		87-JR-32-08	XRF INAA Probe (Ol, Px)
		87-JR-29-09	XRF Probe (Ol, Px)
		87-JR-29-02	XRF
		88-JR-16-2A	XRF INAA Probe (Ol, Px)
◐	Wehrlite	87-JR-29-08	Probe (Px)
		87-JR-29-01	Probe (Ol, Px)
●	Dunite	87-JR-01-01	Probe (Ol)
		87-JR-01-02	XRF
		87-JR-02-04	XRF
		87-JR-25-04	XRF
		88-JR-16-03	XRF

Table 5.2

Whole rock major and minor element abundances.

Sample	87-JR-01-02	87-JR-02-04	87-JR-25-04	88-JR-16-03	87-JR-29-02	88-JR-08-09	87-JR-32-08	87-JR-29-09
Lithology	dunite	dunite	dunite	dunite incl. in pxt	wehrlite	olpxt	ol-cpxt	ol-cpxt
Oxides (wt. %)								
SiO_2	34.5	33.5	36.6	37.8	34.2	51.4	50.4	51.7
TiO_2	0.02	0.02	0.01	0.01	0.01	0.14	0.12	0.13
Al_2O_3	0.18	0.17	0.14	0.05	0.13	1.70	1.18	1.24
Fe_2O_3	6.7	7.1	3.8	4.9	6.9	0.6	2.0	0.8
FeO	3.40	3.13	5.31	8.15	2.30	4.01	3.46	3.29
MnO	0.19	0.20	0.20	0.22	0.19	0.13	0.12	0.11
MgO	41.8	39.9	43.2	39.6	41.4	18.0	22.3	20.2
CaO	0.3	0.95	0.39	0.29	0.32	19.2	19.3	21.2
Na_2O	0.13	0.31	0.19	0.07	0.06	0.34	0.12	0.30
K_2O	0.01	b.d.	0.01	0.01	b.d.	0.12	0.01	0.01
P_2O_5	0.03	b.d.	b.d.	0.02	0.02	b.d.	b.d.	b.d.
Loss on Ignition	12.9	13.8	6.49	6.54	14.5	1.55	1.27	1.31
Sum	100.3	99.1	96.4	97.7	94.9	97.2	100.23	100.2
Trace elements (ppm)								
Ba	50	77	60	55	58	80	35	61
Cr	5020	4230	2990	220	4380	1660	1330	2470
Zr	<10	<10	<10	<10	<10	<10	<10	<10
Sr	<10	<10	<10	<10	<10	140	94	120
Rb	<10	<10	<10	<10	<10	<10	<10	<10
Y	<10	<10	<10	<10	<10	<10	<10	<10
Nb	<10	<10	<10	<10	<10	<10	<10	<10
Zn	76	77	73	100	53	110	<10	30
Ni	900	840	970	940	850	140	220	130
V	<10	<10	<10	<10	<10	67	25	46

Table 5.2

Whole rock major and minor element abundances.

Sample	88-JR-16-2A	88-JR-06-06	88-JR-10-02	88-JR-12-02	87-JR-32-04	87-JR-07-04	88-JR-06-09
Lithology	ol-cpxt	cpxt	cpxt dyke	pxt-hbt-gabbro contact rock	pxt-hbt-gabbro contact rock	pxt-hbt-gabbro contact rock	hbt
Oxides (wt. %)							
SiO_2	50.7	50.6	50.3	37.6	33.9	42.7	40.2
TiO_2	0.14	0.21	0.54	1.43	1.88	1.31	1.84
Al_2O_3	1.43	1.71	4.75	7.48	9.48	8.21	12.4
Fe_2O_3	1.4	1.3	3.7	12.1	11.4	6.5	7.2
FeO	3.83	5.05	6.20	8.11	9.04	8.61	8.93
MnO	0.12	0.12	0.20	0.23	0.21	0.18	0.16
MgO	19.9	17.1	15.3	11.6	11.1	13.3	13.9
CaO	19.8	21.8	15.7	15.4	13.3	14.6	10.6
Na_2O	0.43	0.39	0.68	0.77	1.04	1.11	1.53
K_2O	0.01	0.01	0.38	0.51	0.99	0.90	2.00
P_2O_5	b.d.	b.d.	b.d.	0.90	1.77	b.d.	0.01
Loss on Ignition	0.70	0.58	2.06	2.01	1.98	0.84	1.34
Sum	98.5	99	98.5	97.1	96.1	98.3	99.8
Trace elements (ppm)							
Ba	56	90	130	120	190	310	690
Cr	1960	830	290	<10	<10	37	<10
Zr	<10	<10	<10	27	31	18	27
Sr	140	100	260	320	580	200	260
Rb	<10	<10	<10	<10	<10	<10	27
Y	<10	<10	<10	19	29	18	21
Nb	<10	11	<10	<10	<10	<10	<10
Zn	50	74	95	140	80	68	150
Ni	210	110	88	11	<10	100	190
V	50	89	300	870	880	670	660

Table 5.2

Whole rock major and minor element abundances.

	87-JR-18-07	87-JR-33-03	87-JR-28-01	88-JR-16-05	88-JR-08-05	88-JR-11-04	88-JR-16-4A	87-JR-28-07
Lithology	hbt	hb-pxt	gabbro	gabbro	gabbro	gabbro	hb gabbro	syenogabbro
Oxides (wt. %)								
SiO_2	40.0	35.0	49.0	47.2	49.4	41.3	41.2	50.6
TiO_2	1.54	1.92	0.65	0.80	0.76	1.20	0.83	0.62
Al_2O_3	10.2	8.23	12.6	14.8	15.2	15.7	14.1	16.2
Fe_2O_3	8.4	13.4	7.3	6.4	3.9	7.2	3.0	5.9
FeO	7.92	9.30	4.26	4.42	5.82	7.44	9.37	2.06
MnO	0.20	0.24	0.21	0.23	0.18	0.25	0.23	0.20
MgO	13.2	10.7	7.30	5.91	6.39	8.45	12.1	4.28
CaO	13.0	14.3	11.1	12.1	10.0	13.9	14.4	8.14
Na_2O	1.50	0.69	2.50	2.67	3.67	1.31	0.47	2.88
K_2O	1.35	0.72	3.64	1.58	1.20	0.56	0.18	4.26
P_2O_5	b.d.	1.72	0.47	0.44	0.40	0.41	0.09	0.47
Loss on Ignition	1.49	1.29	0.55	1.41	2.59	2.21	4.73	1.31
Sum	98.9	97.4	99.7	97.1	97.6	98.3	95.9	98.5
Trace elements (ppm)								
Ba	360	530	1290	580	730	280	50	1370
Cr	21	10	110	36	62	29	710	12
Zr	30	31	87	61	37	39	64	74
Sr	490	460	1780	1870	1300	720	860	1670
Rb	<10	<10	69	22	21	<10	<10	81
Y	21	31	17	26	18	28	12	14
Nb	<10	<10	<10	<10	<10	<10	<10	<10
Zn	88	90	81	99	290	120	220	140
Ni	<10	<10	31	<10	20	<10	200	<10
V	670	920	370	400	340	560	250	320

Table 5.2

Whole rock major and minor element abundances.

Sample Lithology	**87-JR-18-06** syenodiorite	**87-JR-21-03** syenodiorite	**87-JR-21-04** syenodiorite	**87-JR-21-09** syenodiorite	**87-JR-27-01** hb-monzonite	**88-JR-04-01E** sydr-dyke	**87-JR-03-07** sydr dike	**88-JR-16-4B** px bslitic dyke
Oxides (wt. %)								
SiO_2	51.2	53.9	50.0	53.4	52.6	50.1	48.9	47.5
TiO_2	0.61	0.56	0.62	0.63	1.30	0.76	0.81	1.26
Al_2O_3	16.5	17.1	15.6	18.3	17.3	17.1	17.3	14.4
Fe_2O_3	6.2	4.9	6.1	4.7	2.0	4.2	3.2	3.5
FeO	3.10	3.09	3.70	2.68	5.53	4.47	6.71	6.38
MnO	0.20	0.18	0.21	0.16	0.12	0.15	0.20	0.16
MgO	4.39	3.83	4.81	3.24	5.26	5.87	5.48	10.4
CaO	8.12	7.49	9.08	7.45	6.43	11.9	10.6	8.70
Na_2O	3.02	3.57	3.15	4.16	4.26	3.40	3.38	3.44
K_2O	4.29	3.66	4.30	2.82	1.68	0.73	1.00	0.61
P_2O_5	0.56	0.51	0.50	0.37	0.36	0.17	0.23	0.28
Loss on Ignition	1.18	0.93	0.83	1.83	2.56	2.08	3.82	2.50
Sum	99.4	99.7	98.5	99.8	99.4	98.4	98.6	97.4
Trace elements (ppm)								
Ba	1410	1230	1240	1170	460	230	430	140
Cr	13	25	12	29	74	87	53	580
Zr	91	60	89	67	130	57	64	84
Sr	1660	1420	1710	1200	690	1470	790	730
Rb	79	60	86	46	31	<10	<10	<10
Y	20	22	20	19	22	20	21	18
Nb	<10	<10	<10	<10	<10	<10	<10	<10
Zn	92	71	120	69	68	110	140	110
Ni	<10	<10	<10	<10	<10	14	<10	200
V	350	300	330	260	200	410	320	250

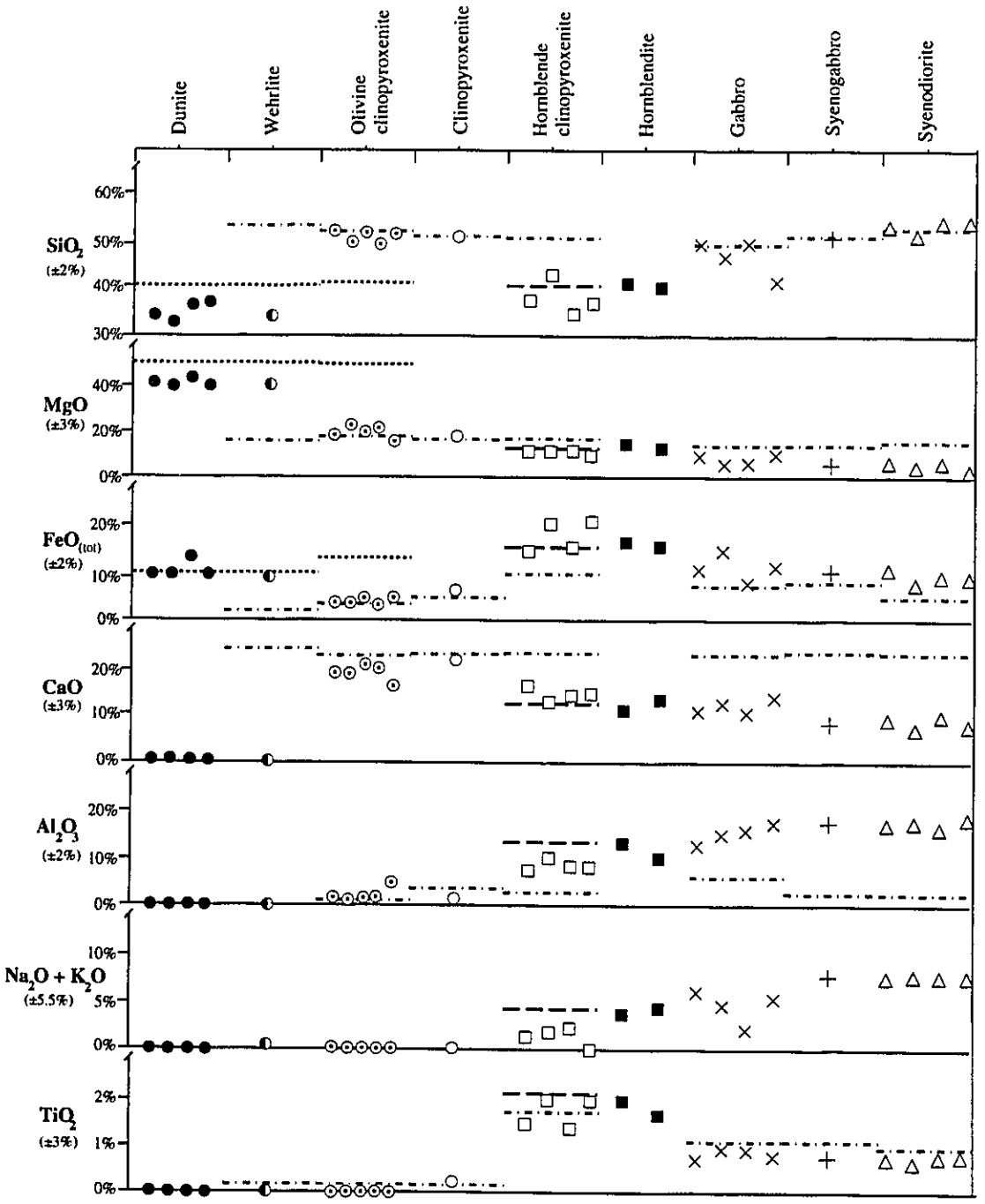

Figure 5.2. Diagram showing the variation in major elements in representative rocks of the Tulameen complex. For comparison, averaged olivine (dot), clinopyroxene (dot-dash) and hornblende (dash) microprobe compositions are shown.

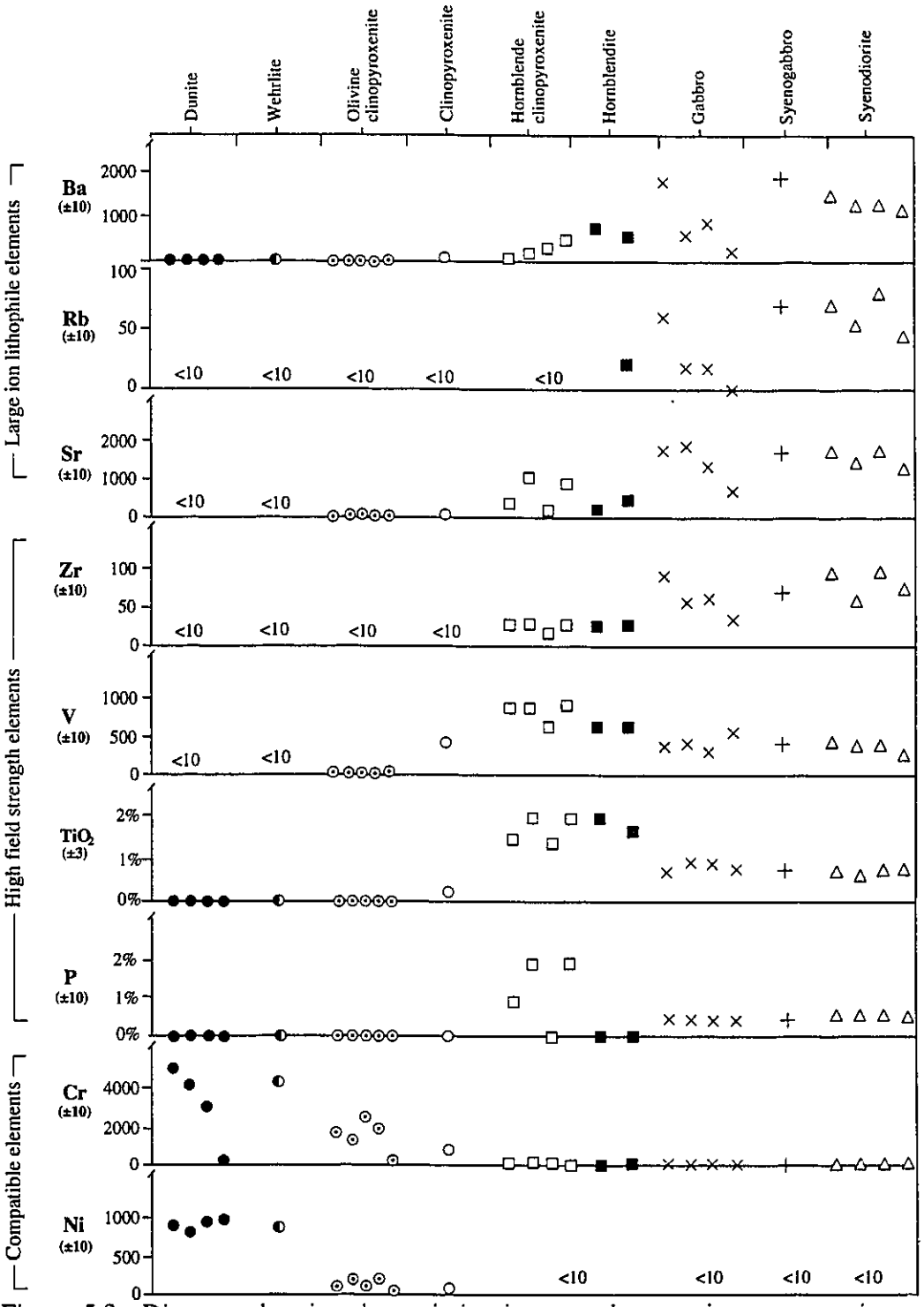

Figure 5.3. Diagram showing the variation in trace elements in representative rocks of the Tulameen complex.

2 hornblendite, 4 clinopyroxene gabbro, 1 hornblende gabbro, 1 syenogabbro, 1 hornblende syenodiorite and 4 clinopyroxene syenodiorite. Dyke rocks of clinopyroxenite, basaltic and syenodiorite composition were also analyzed.

Accuracy and precision of the whole rock XRF data are as follows (MacLellan and Taylor, 1989): SiO_2, Al_2O_3, Fe_2O_3 and K_2O, ± 2%; MgO, TiO_2, and CaO, ± 3%; Na_2O, ± 3.5%; MnO, P_2O_5, and S, ± 10%; Cr, V, Ni, Zn, Rb, Sr, Y, Zr, Nb, and Ba, ±10%. Accuracy and precision for elements determined by neutron activation are: Sc, La, Ce, Sm, Eu, Tb, Yb, Hf, Ta and Th ± 5%, and Cs, Nd, Dy, Ho and Lu ± 10%. FeO was determined by dichromate titration, and Fe_2O_3 by difference from total iron measured.

The olivine and pyroxene-rich samples are cumulate rocks, which by definition (Irvine, 1982), characterizes them as a framework of touching mineral grains or crystals formed through fractional crystallization of their parental magma. Post-cumulus phases—minerals which crystallized from the intercumulus liquid in the pores or interstices of the cumulus framework—are a minor (< 7 vol %) component of these rocks and further distinguish them as adcumulates (Irvine, 1982). The bulk chemical composition of adcumulate dunite, wehrlite, olivine clinopyroxenite and clinopyroxenite reflects the chemical characteristics of the fractionated phases rather than the parental magma from which they crystallized. Because of this, variation diagrams such as Figs. 5.2 and 5.3, which illustrate the concentrations of particular elements in the rocks do not represent the liquid line of descent of the parental magma. The strong chemical imprint of the cumulus mineral on the composition of the rock is indicated by the correspondence between rock and mineral chemistry and the mineral/matrix partition coefficients of the major and trace elements for the silicate and oxide minerals (Fig. 5.4).

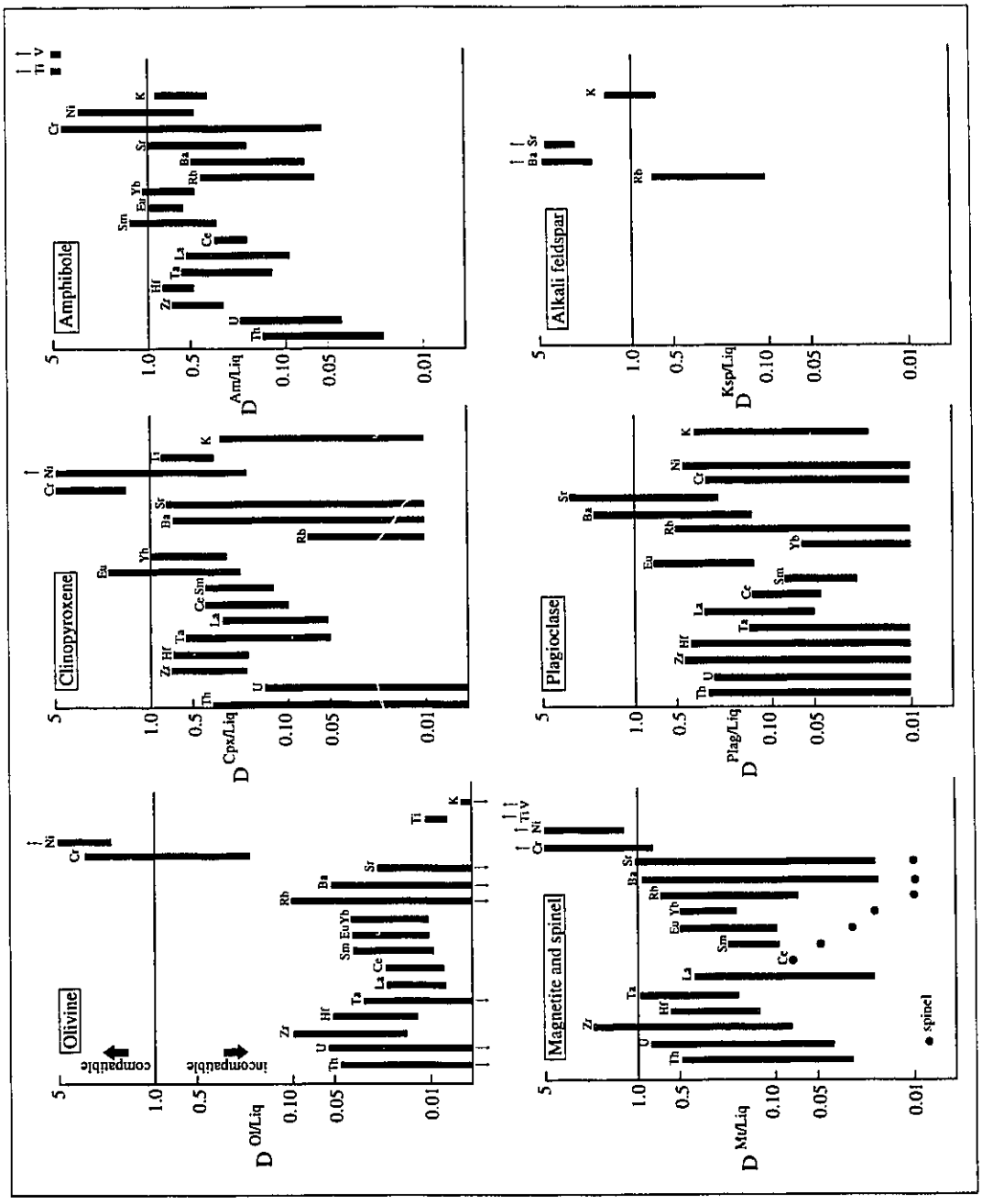

Figure 5.4. Diagram showing partition coefficients of trace elements in silicate and oxide minerals. Modified after Wilson (1989) with Ti and V data from Shervais (1982).

i) Major element chemistry

Given the cumulus nature of the ultramafic rocks, it is not unexpected that the distribution of SiO_2, MgO, CaO in dunite, wehrlite, olivine clinopyroxenite and clinopyroxenite can be accounted for by forsterite and diopside (Fig. 5.2). The variation of SiO_2 and FeO_t in dunite is attributed to variable modal amounts of silica-poor, iron-rich chromite. The dunites are serpentinized, but according to Coleman and Keith (1971), no appreciable change in the relative amounts of SiO_2, MgO, Fe_t, Al_2O_3, Cr, or Ni occurs during serpentinization of dunite or peridotite. The whole rock chemistry of olivine clinopyroxenite and clinopyroxenite parallels that of diopside, with high SiO_2 and CaO contents (50-52% and 19-23% respectively). The effect on the bulk chemical composition of clinopyroxenites with the appearance of hornblende (formed at the expense of diopside as documented in chapter 2; Plate 2.2) and magnetite is observed as decreased concentrations of SiO_2, CaO and enhanced FeO_t, TiO_2, MnO, alkalies (Na_2O+K_2O) and Al_2O_3 in hornblende clinopyroxenite and hornblendite (Fig. 5.2). Crystallization of feldspars in the gabbro, syenogabbro and syenodiorite is evident by the higher (relative to the ultramafic cumulate rocks) concentrations of Al_2O_3 and alkalies. Extensive sericitization of orthoclase and saussuritization of plagioclase is held responsible for the scattering of the more mobile elements (K, Na) in Fig. 5.2.

ii) Trace element chemistry

Figure 5.3 illustrates the distribution of trace elements in the analyzed rock suite of the Tulameen complex. Large ion lithophile elements (LILE), Ba, Rb and Sr are concentrated in the feldspar-bearing rocks, and have low abundances in the hornblende rocks. This distribution, as well as that of Na and K, reflects the compatibility of LILE in the feldspars (Fig. 5.4). The scatter of values is attributed to extensive sericitization and saussuritization of potassium feldspar and plagioclase, reactions which would bring about a mobility of these incompatible elements. High field strength elements, Ti, V and P show a parallel behavior in

their concentration in the hornblende, magnetite and apatite-rich rocks. Ti and V are highly compatible in magnetite and amphibole (Fig. 5.4), and closely follow Fe during magmatic crystallization (Mielke, 1979; Gill, 1981). Phosphorus tends to follow Ti not because of chemical similarity but because of the simultaneous crystallization of apatite and Fe-Ti oxides (Mielke, 1979). Although Zr is a high field strength element and shares chemical characteristic with Ti, V and P, it behaves differently by its progressive enrichment with increasing silica in the feldspathic rocks. The compatible elements, Cr and Ni—which have high partition coefficients in iron-magnesium silicates and oxides (Fig. 5.4)—exhibit parallel patterns of high values in dunite and wehrlite. Decreased abundances through clinopyroxenite to the feldspar-bearing rocks is attributed to the olivine, clinopyroxene and spinel fractionation of the earlier formed cumulates.

Rare earth element analyses for five samples from the Tulameen complex are displayed as chondrite normalized arrays in Figure 5.5a and are listed in Table 5.3. As a suite, the REE data, which represents olivine clinopyroxenite, hornblende-rich contact rocks, hornblende gabbro and pyroxene gabbro, is characterized as a stack of relatively flat and parallel (with the exception of 87-JR-28-01) arrays with increasing (1.5x, 2x, 10x, 15x and 20x) enrichment of these elements relative to chondrite abundances. Total REE abundances (Table 5.3) are lowest in the olivine-clinopyroxene cumulates (4.0 and 7.8 ppm respectively) and highest in the apatite-rich contact rocks (78.4 ppm): the hornblende gabbro and pyroxene gabbro have intermediate REE totals of 39.0 and 58.6 ppm respectively. Enrichment of the LREE over HREE from the olivine clinopyroxenites to the pyroxene gabbro is evidenced by the increase in $(La/Yb)_{CN}$ and accompanying steepening of the REE patterns (Fig. 5.5a).

The increase in the slope of the REE arrays (LREE>HREE) from olivine clinopyroxenite to gabbro, in the rocks of the Tulameen complex (Fig. 5.5a), is interpreted as indicating the fractional crystallization of Ca-pyroxene. In experimental cpx/melt partitioning

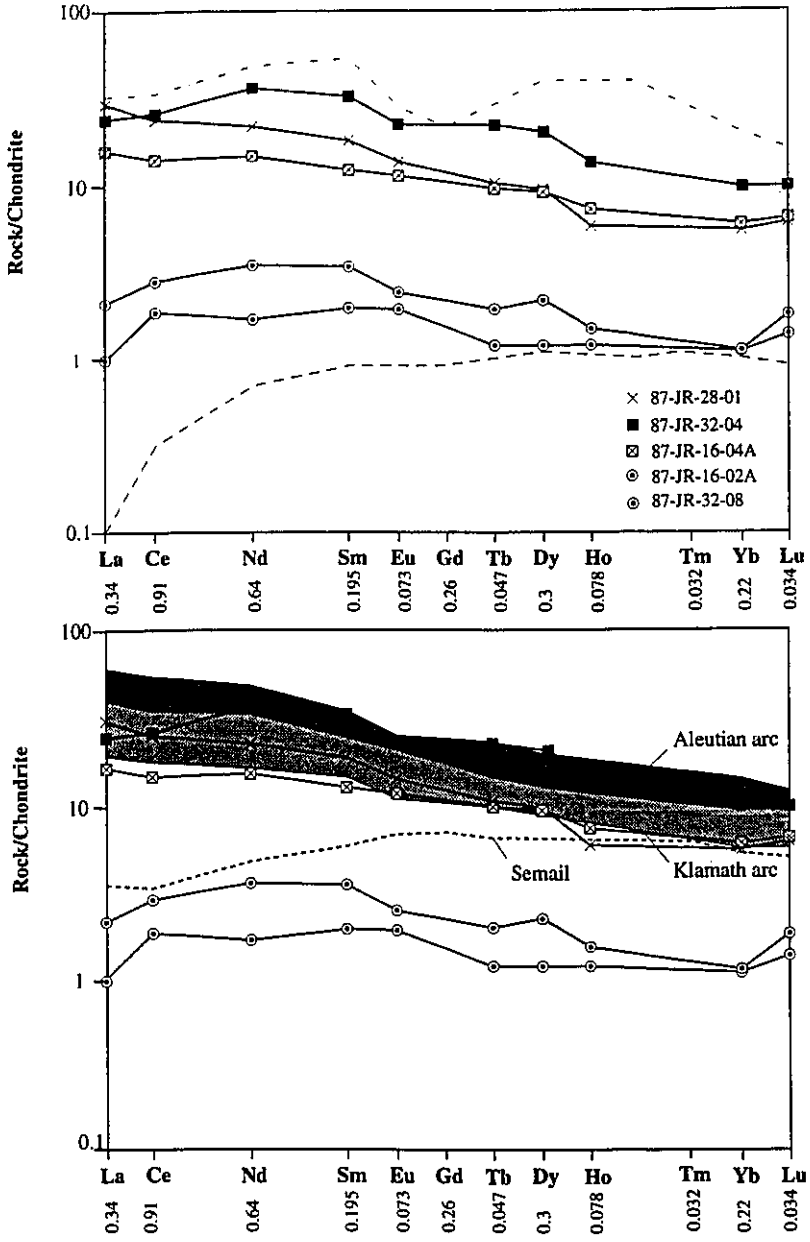

Figure 5.5. Chondrite normalized (Wakita et al., 1971) rare earth element arrays for five rocks from the Tulameen complex. a) REE patterns for the Tulameen complex. Included are patterns for clinopyroxene (dashed) and apatite (dot-dash; Henderson, 1984). b) Comparison with differentiated (SiO_2 = 47-52%) plutonic rocks from the Aleutian (Kay et al., 1990) and Klamath (Snoke et al., 1981) arcs and Semail (Lippard et al. 1986) ophiolite.

Table 5.3.
Whole rock trace element abundances determined by INAA.

Sample	87-JR-32-08	88-JR-16-02A	87-JR-32-04	88-JR-16-04A	87-JR-28-01
Lithology	ol-cpxt	ol-cpxt	hb-apt contact-rock	hb-gabbro	px-gabbro
Sc	67	62	95	35	35
Co	53	45	60	46	45
Hf	b.d.	b.d.	1.01	1.50	1.49
Ta	0.56	0.38	0.40	0.25	0.77
Th	b.d.	b.d.	0.31	0.45	2.45
U	b.d.	b.d.	0.12	0.20	1.30
REE (ppm)					
La	0.33	0.72	8.9	5.6	10.7
Ce	1.7	2.6	24.8	14.1	23.3
Nd	1.1	2.3	25.3	10.4	14.6
Sm	0.38	0.69	6.88	2.65	3.60
Eu	0.14	0.18	1.71	0.96	1.10
Tb	0.06	0.09	1.04	0.46	0.52
Dy	0.38	0.65	6.13	2.71	2.86
Ho	0.10	0.12	1.13	0.57	0.46
Yb	0.25	0.26	2.19	1.34	1.24
Lu	<0.05	0.06	0.34	0.22	0.21
Total	4.5	7.7	78.4	39.0	58.6
$(La/Yb)_{CN}$	0.85	1.79	2.6	2.7	5.6

Table 5.4.
Cpx-melt partition coefficients determined by Hart and Dunn (1993).

Element	D Cpx/melt	2 sigma %
La	0.0536	6.1
Ce	0.0858	6.1
Nd	0.1873	6.1
Sm	0.291	4.6
Dy	0.442	8.4
Yb	0.430	4.3
Lu	0.433	5.2

of 24 trace elements, Hart and Dunn (1993) determined that the distribution coefficients for the HREE are higher than those for the LREE (Table 5.4). From this it follows that fractional crystallization of Ca-pyroxene from a magma enhances LREE in the melt relative to HREE, and as a consequence the more evolved rocks will have higher LREE/HREE. Olivine crystallization has little effect on the partitioning of the REE as Ol/melt partition coefficients for the REE are all quite low (Henderson, 1984). Kay and Senechal (1976) proposed that the REE contribution of the various components of a mafic cumulate suite would be: olivine < plagioclase < orthopyroxene < clinopyroxene < interstitial magma. REE totals shown in Table 5.3a are higher in the more differentiated gabbros than the olivine-clinopyroxene cumulates. High REE content of the contact rocks (87-JR-32-04) is attributed to apatite (a repository for REE) which is present in modal abundances in excess of 2%.

The relatively flat form and degree (~15-30x) of rare earth element enrichment compared to chondrite of the differentiated Tulameen samples (87-JR-28-01 and 88-JR-16-4A) is similar to rare earth element patterns for differentiated (gabbro to diorite; SiO_2 = 47-52 %) plutonic rocks from volcanic arcs complexes (Fig. 5.5b). Chondrite normalized REE trends from volcanic arc-derived rocks are flat (tholeiitic) to LREE enriched (calc-alkaline to high-K shoshonitic). The hydrous conditions of the arc magmatism inhibits early crystallization of plagioclase and as a partial consequence, REE trends from arc environments characteristically lack Eu anomalies (Wilson, 1989; Bau and Knittel, 1993). The flat portion of the REE pattern for the HREE indicates that the source region that underwent partial melting in the mantle did not contain garnet, a phase which has high partition coefficients for the HREE (Wilson, 1989). Figure 5.5b compares and contrasts the Tulameen REE arrays with those from mafic (SiO_2= 47-52%) plutonic rocks from island arcs and ocean ridge settings. REE patterns for gabbros and diorites from the Aleutian (Kay et al., 1990) and Klamath (Snoke et al., 1981) volcanic arcs are similar both in shape and concentration to those of the Tulameen gabbros. In

comparison, REE trends for rocks generated by continental and ocean island (within plate) magmatism exhibit enrichment (>100x chondrite) in both LREE and HREE (Wilson, 1989). Differentiated ocean ridge rocks (i.e. Semail ophiolite) are LREE depleted relative to chondrite, and exhibit significant Eu anomalies due to early crystallization of plagioclase (Lippard et al., 1986). Additionally, total content of rare earth elements is low in comparison to arc rocks of similar composition (Fig. 5.5b).

An alternate means to examine the chemical characteristics of the Tulameen complex is by displaying the trace element data on a Coryelle-Matsuda diagram, more commonly referred to as a spiderdiagram (Thompson et al., 1984; Fig. 5.6). This diagram combines several trace elements which are arranged on the abscissa on the basis of their relative mobility in aqueous fluids (Pearce, 1982). The more mobile elements (LILE) are arranged on the left with the immobile elements (HFS and REE) to the right: incompatibility of both mobile and immobile elements increase from the outer margins towards the centre of the diagram. Normalizing the data to MORB values (Pearce, 1982), highlights the subduction-zone component of arc magmas and partially unveils the nature of the mantle source, with the assumption it was derived by the partial melting of a MORB-like (i.e. depleted upper mantle) source.

Figure 5.6 shows the array of trace element data for the Tulameen data as a spiked pattern created by excesses in LILE, Ce, P and Sm, and deficiencies in the HFS, relative to MORB. It is important to note that in many of the samples, the abundance of Rb and Nb was below the detection limit of the XRF (10 ppm). The degree of LILE enrichment relative to MORB increases from olivine clinopyroxenite to syenodiorite. In the samples for which there is a full spectrum of elements (87-JR-28-01, 88-JR-16-04A, 87-JR-32-04), there is a progressive increase in the ratio of incompatible to compatible immobile elements with differentiation.

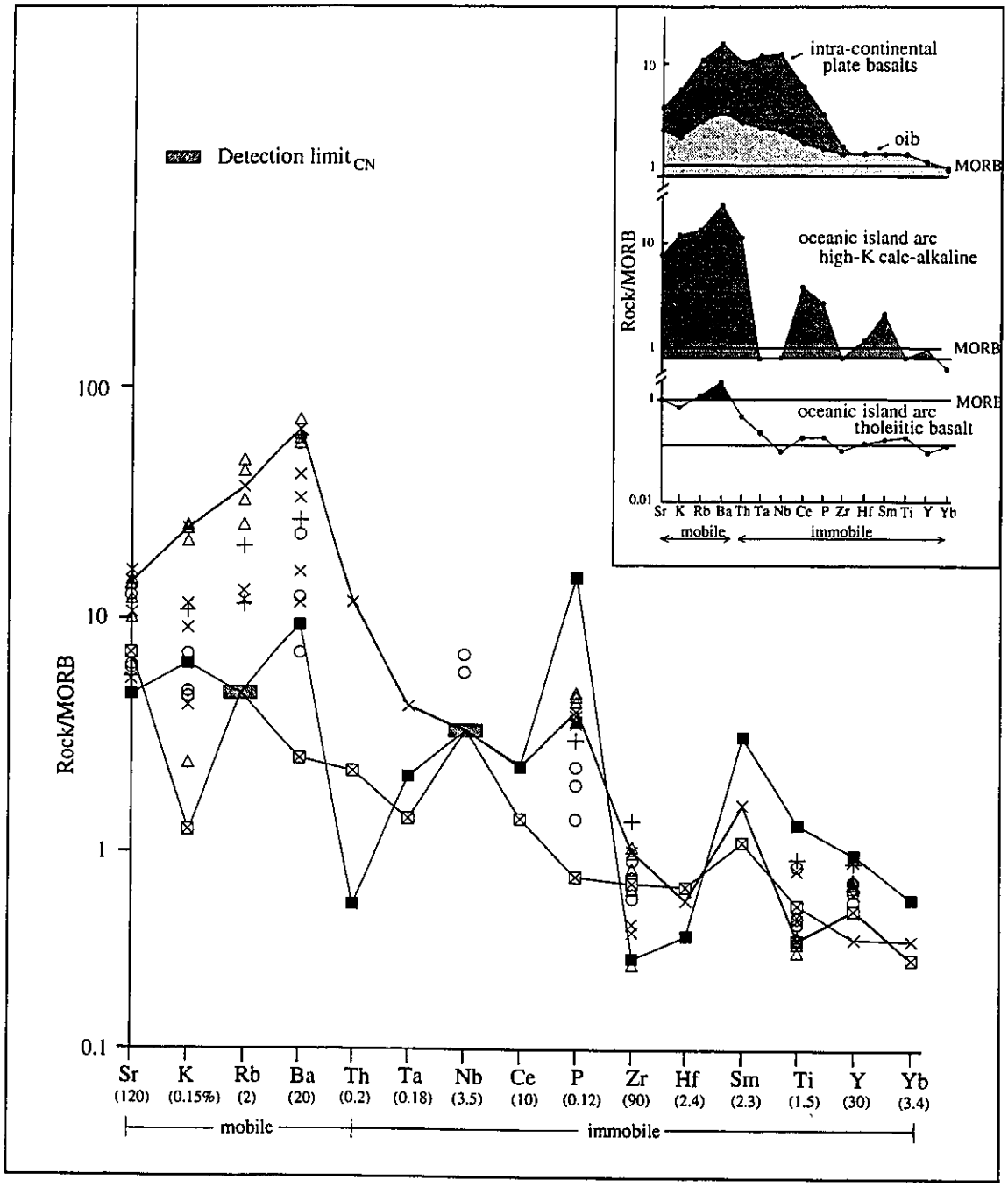

Figure 5.6. Spiderdiagram for rocks of the Tulameen complex. Data is normalized to MORB values of Pearce (1983). Inset shows MORB normalized arrays for within plate and arc rocks (modified after Wilson, 1989).

The pattern of enriched LILE, Ce, Sm and P and depleted HFSE with reference to MORB abundances observed in the samples from the Tulameen complex, is a chemical signature of subduction-related magmatism (Thompson et al., 1984). In addition, Ce, Sm and P peaks distinguish calc-alkaline and high-K calc-alkaline island arc basalts (IAB) from tholeiitic basalts (Wilson, 1989). Barium, Sr, K and Rb—sourced in the subducted sediments—are transported via aqueous fluids (Tatsumi et al., 1986; Tatsumi, 1989) or a combination of aqueous fluids and small degree partial melts (Bau and Knittel, 1993) from the descending and dehydrating slab into the overlying mantle wedge at P and T conditions which induce partial melting of the mantle lithosphere. Experimental work by Tatsumi et al. (1986) determined that during the formation of secondary minerals in the dehydrating slab, LILE and LREE are distributed along the grain boundaries of these phases. HREE, on the other hand, are preferentially incorporated into the crystal lattice of secondary Mg minerals such as serpentine (Morgan and Wandless, 1980). The slab-derived fluid phase generated by the prograde metamorphism of the subducted oceanic crust and associated pelagic sediments, is enriched in both LILE and LREE (Bau and Knittel, 1993) and infiltrates the partially melted mantle wedge. Cerium, P and Sm are more likely to be transported in a partial melt than an aqueous fluid (Wilson, 1989) which may substantiate the proposal put forth by Bau and Knittel (1993) that both slab-derived aqueous fluids and partial melt are involved in the process of element transfer between the slab and wedge.

The lithospheric mantle contributes the HFSE (Ta, Nb, Hf, Zr, Ti, Y and Yb; McCulloch and Gamble, 1990). Their distinctive low abundances in volcanic arc-related rocks compared to back-arc (Woodhead et al., 1993) and ocean floor (Thompson et al., 1984) basalts has been attributed to several different processes such as: 1) the presence of a residual Nb-TiO_2-bearing phases (rutile, titanite, ilmenite or perovskite) which retain the HFSE in the source region during partial melting (Saunders et al., 1980), 2) interaction between depleted

peridotite wall rock in the wedge with fertile, partially melted mantle (Kelemen et al., 1990) and 3) partial melting of an arc-source region depleted in HFSE by a melting episode prior to the arc-magma genesis (McCulloch and Gamble, 1990; Woodhead et al., 1993).

Mineral Chemistry

The compositions of olivine, clinopyroxene and amphibole were determined by electron microprobe analyses of 15 representative samples of the Tulameen complex. These mineral analyses were obtained at McGill University (Montreal) using a wavelength dispersive Camebax microprobe. Operating conditions included counting times of 30 seconds for the elements analyzed, an accelerating voltage of 15 kV and a beam intensity of 7 nA. Natural and synthetic minerals of known compositions were used as standards. Matrix corrections were performed with the ONQUANT software package of Cameca.

The classification and nomenclature used for olivine, pyroxene and amphibole follows that suggested by Deer et al. (1978a), Morimoto (1988) and Rock and Leake (1984) respectively.

i) Olivine

The composition of olivine in the ultramafic and mafic rocks of the Tulameen complex is summarized in Table 5.5 and illustrated in Figs. 5.7 and 5.8. This data represents the averages of several spot determinations for a particular sample; core to rim traverses within olivine grains did not detect any compositional zoning. Appendix 1 includes the individual analyses of the grains probed. Totals of the six oxides measured (SiO_2, MgO, FeO, MnO, CaO and NiO) range from 99.1 to 101.4%. Structural formulae were calculated on the basis of three cations.

Table 5.5. Composition of olivine determined by electron microprobe.

	Sample	87-JR-01-01	87-JR-29-01	87-JR-29-09	87-JR-32-08	88-JR-16-2a	87-JR-28-01
	Lithology	dunite	wehrlite	ol. cpxt.	ol. cpxt.	ol. cpxt.	gb
	Number of targets	(n=3)	(n=2)	(n=3)	(n=4)	(n=4)	(n=3)
Weight %	SiO_2	41.1	41.3	40.2	40.2	40.2	38.3
	FeO^*	10.2	9.20	12.3	13.6	13.7	22.6
	MnO	0.23	0.20	0.23	0.23	0.25	1.16
	MgO	49.2	49.6	47.1	46.8	46.4	38.7
	NiO	0.12	0.07	0.11	0.12	0.12	0.04
	CaO	0.22	0.13	0.02	0.02	0.02	0.06
			Number of cations based on 3 cations.				
Molecular proportions	Si^{4+}	0.9983	1.0053	0.9965	0.9912	0.9953	0.9905
	Fe^{2+}	0.2075	0.1875	0.2554	0.2808	0.2841	0.4895
	Mn^{2+}	0.0047	0.0041	0.0048	0.0048	0.0052	0.0254
	Mg^{2+}	1.7814	1.7997	1.7405	1.7202	1.7125	1.4920
	Ni^{2+}	0.0023	0.0022	0.0022	0.0024	0.0024	0.0008
	Ca^{2+}	0.0057	0.0034	0.0005	0.0005	0.0005	0.0017
	100Mg/(Mg+Fe)=	89	90	87	86	86	74

FeO^*= all Fe as FeO

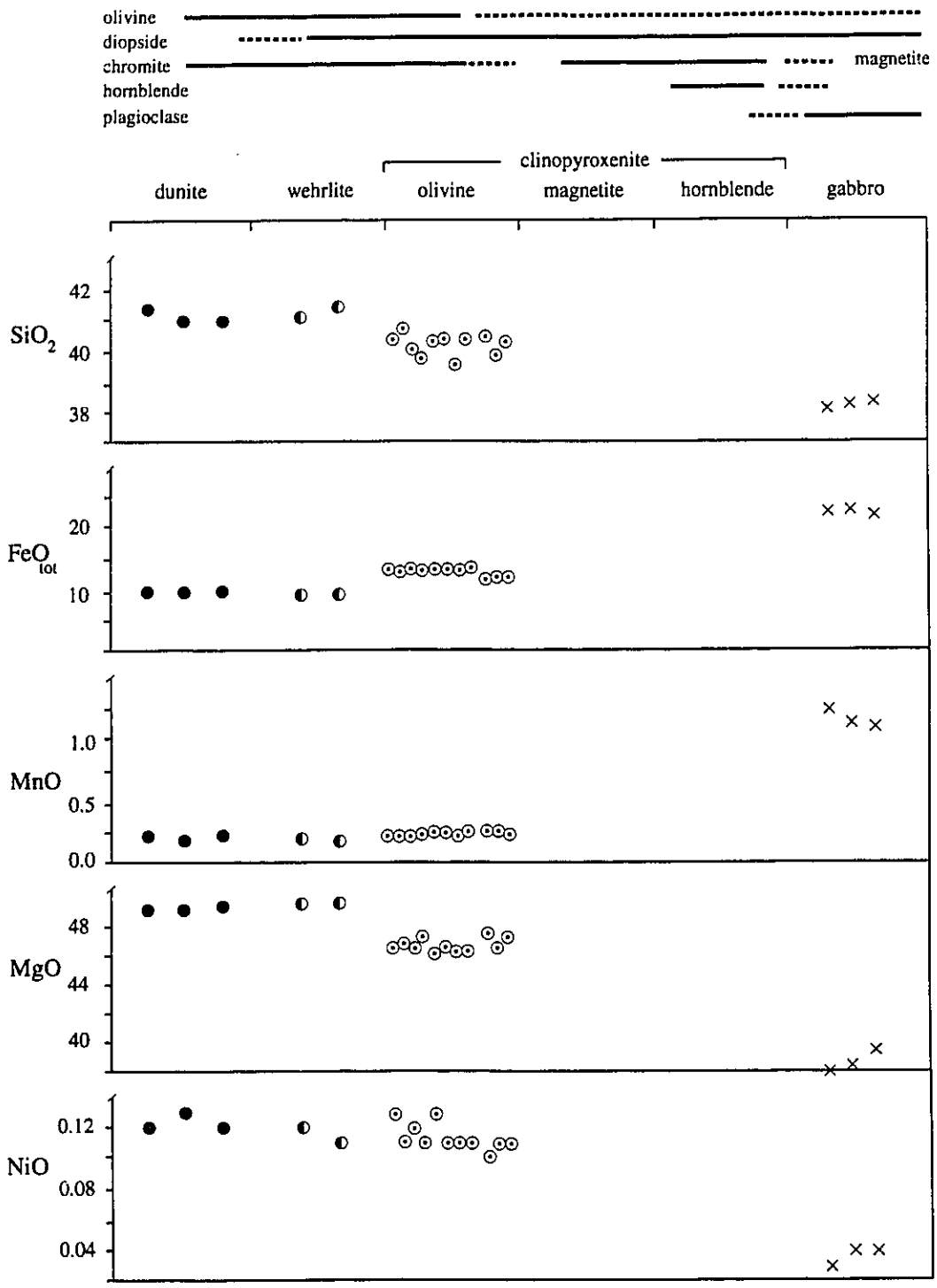

Figure 5.7. Diagram illustrating the composition of olivine in representative rocks from the Tulameen complex.

Olivines analyzed from the ultramafic and mafic rocks are Mg-rich and exhibit a limited enrichment in Fe through the suite. Forsterite contents range from Fo_{90-91} in dunite and wehrlite, to Fo_{87-86} in olivine clinopyroxenite and Fo_{74} in the gabbro. The compositional break between olivine pyroxenite and gabbro is attributed to insufficient sampling as Findlay (1963) documented forsterite contents of Fo_{81} to Fo_{88} in olivine clinopyroxenite, Fo_{74} and Fo_{84} in hornblende clinopyroxenite.

The major element trends in olivine from dunite to gabbro, as revealed in Fig. 5.7, are characterized by decreasing SiO_2 (41.1 to 38.3%), MgO (49.2 to 38.9%) and increasing FeO_t (10.2 to 22.5%). CaO, MnO and NiO, present in trace abundances, exhibit less well-developed trends. CaO levels are comparatively high (0.13-0.22%) in the dunites and wehrlites and low (0.02-0.06%) in the olivine clinopyroxenites and gabbros; calcium oxide abundances of 0.22% were similarly reported by Nixon et al. (1990) in dunite olivines. MnO contents are much higher in olivines from gabbro (1.16%) than in the ultramafic rocks (0.20-0.23 wt. %). NiO contents are low, in the range 0.04-0.12 wt. %. Findlay (1963) noted high alumina contents (1.23-2.04%) in olivines from dunite that were chemically analyzed. Repeat analyses by emission spectrographic techniques (Findlay, 1969) yielded high, but not identical values (1.8-2.3%). Alumina was not determined in the microprobe analyses presented here.

a) Interpretation of olivine data.

Figure 5.8 is a compilation of all available olivine data from the Tulameen complex including those previously published. Included are 29 microprobe analyses presented here, 20 microprobe analyses determined by Nixon et al. (1990), and 80 XRF measurements reported by Findlay (1969). The analyses of Findlay's are included because they are in agreement with the microprobe data and their addition greatly supplements the limited number of microprobe analyses. Figure 5.8, shows that there is an overall trend of decreasing 100Mg/(Mg+Fe) with lithology from dunite (Fo_{92}) to gabbro (Fo_{74}). This range in olivine composition through the

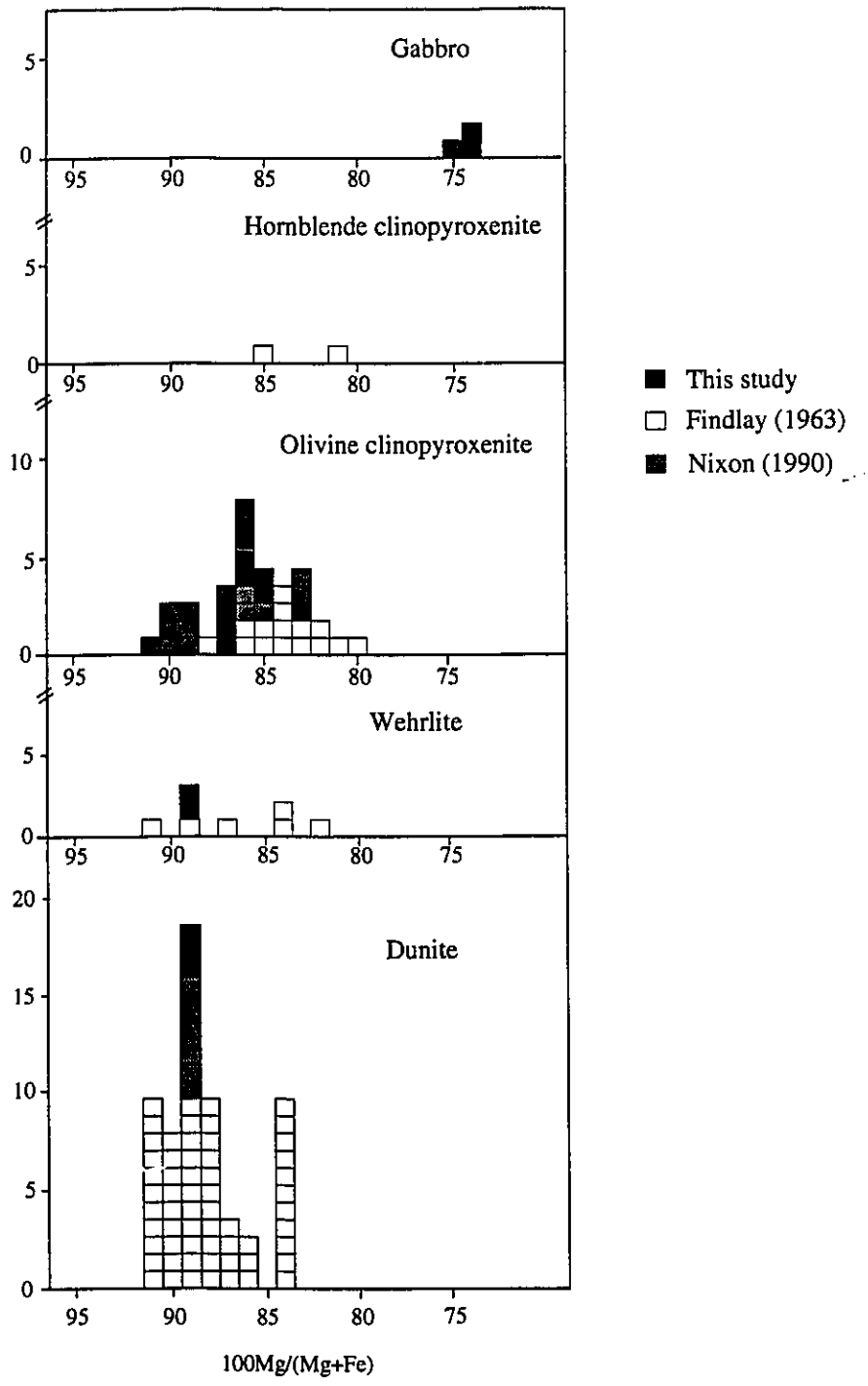

Figure 5.8. Compilation of olivine data from the Tulameen complex.

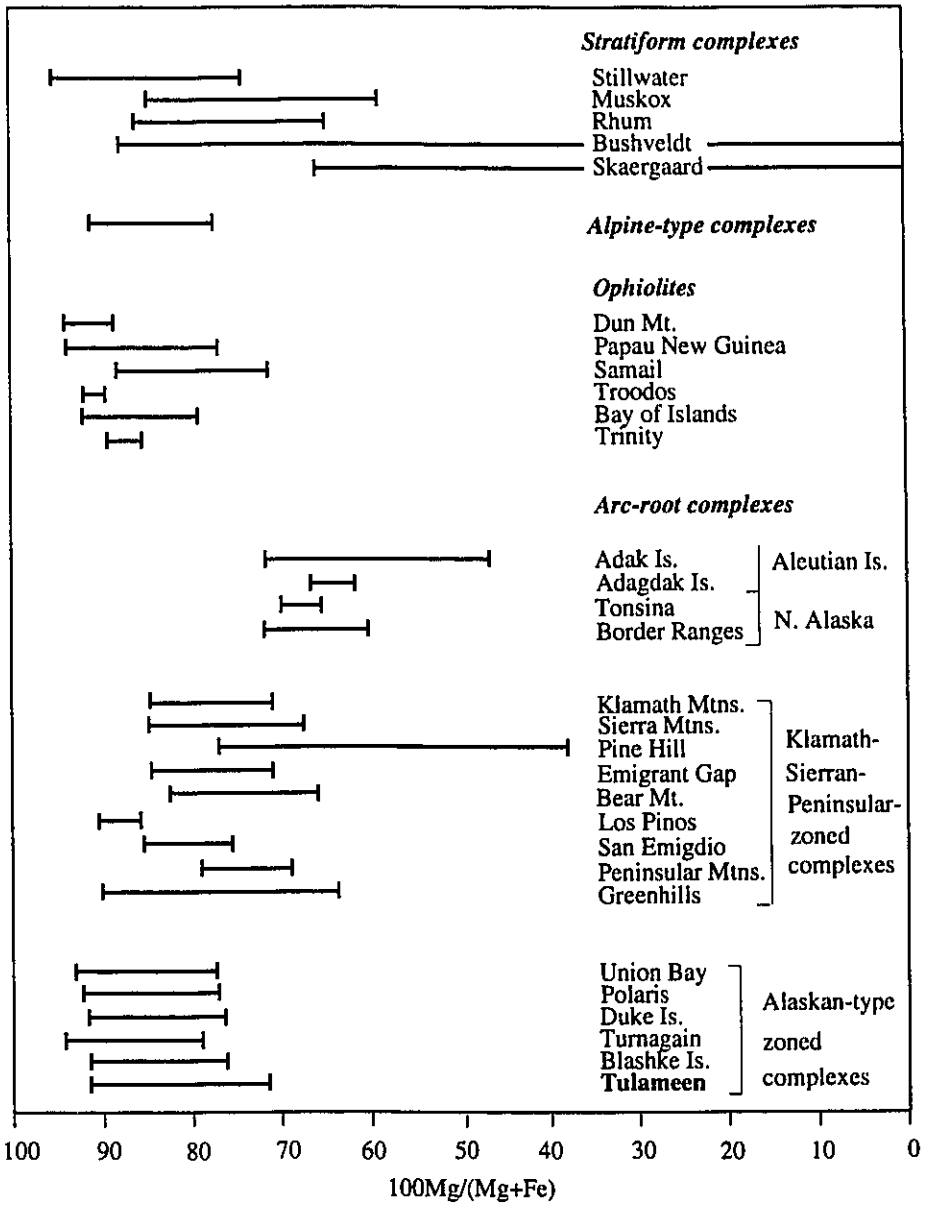

Figure 5.9. Comparison of magnesium proportions in olivines from ultramafic complexes representing various igneous environments. Sources: Wager and Brown (1968), Deer et al. (1978a), Coleman (1977), Conrad and Kay (1984), Debari et al. (1987), Debari and Coleman (1989), Burns (1985), Gray et al. (1986), Snoke et al. (1981), Snoke et al. (1982), Springer (1989), James (1971), Walawender and Smith (1979), Reitz (1986), Mossman (1973), Irvine (1974, 1976), Clark (1980), Smith et al. (1983) and Himmelberg et al. (1986).

ultramafic to mafic suite of rocks in the Tulameen complex is comparable to that observed in arc-related ultramafic-mafic complexes, ophiolites and alpine-type ultramafic bodies (Fig. 5.9). Olivines from stratiform complexes, exemplified by the Bushveld, Stillwater, Muskox and Skaergaard intrusions, are less magnesian and display extreme iron enrichment to fayalite. The lower nickel content in the olivines of the Tulameen complex distinguishes it from alpine and ophiolitic bodies which are characterized by high NiO values (0.27-0.40%; Coleman, 1977)

The CaO contents of olivines in the dunites (0.22 wt.. %) and wehrlite (0.12 and 0.14%) are high, compared to the 0.1% CaO maximum for olivines from plutonic rocks and ultramafic inclusions in lavas, put forward by Simkin and Smith (1970). Calcium solubility in equilibrated natural magmatic olivine—surprising in view of the large size of Ca relative to Mg, Fe and Mn (Simkins and Smith, 1970)—has been associated with both the composition of the melt and the pressure of crystallization. Stormer (1972; 1973) and Ferguson (1978) correlated calcium contents in olivine with alkalinity and silica undersaturation of the magma by demonstrating that olivine crystals from strongly alkaline feldspathoidal rocks are more enriched in CaO than those from tholeiitic and more siliceous lavas. High CaO contents, however are also documented in olivines from dunites and wehrlites within Alaskan-type zoned ultramafic complexes (0.21-0.46%; Himmelberg et al., 1986; 1 to 1.7%, Irvine 1974; and 0.12-0.15%; Clark, 1980) and ultramafic inclusions within island arc volcanic rocks (0.49%; Conrad and Kay, 1984; Takahashi, 1986). According to Gill (1980) the elevated water activity in subduction-generated magmas decreases the activity of silica in the melt and as a result, the stability field of olivine increases over that of Ca-rich pyroxene:.

$$(2CaMgSi_2O_6)Di = (Ca_2SiO_4)Lrn + (Mg_2SiO_4)Fo + (2SiO_2)liq \text{ (Stormer, 1972)}$$

The lower the a_{SiO2} in the liquid, the higher the monticellite component ($CaMgSiO_4$) as long as olivine is coexisting with liquid and Ca-rich pyroxene.

$$(CaMgSi_2O_6)Cpx = (CaMgSiO_4)Mtc + (SiO_2)liq \text{ (Sato et al., 1991)}$$

The identification of primary hydrous silicate phases such as magnesian phlogopite and ferroan pargasitic hornblende as inclusions within chromite by Talkington et al. (1986) and Nixon et al. (1990), suggests that the melt from which the olivines crystallized may have been enriched in both alkalies and water. The analyzed olivines are from adcumulate rocks, which by their nature imply very slow cooling (Irvine, 1982). Simkin and Smith (1970) report that calcium contents are lowest in slowly cooled olivines from plutonic rocks. Brown (1982) indicates that the solubility of calcium decreases with increasing pressure and consequently calcium contents in olivines from hypabyssal and extrusive rocks are higher than those formed at deeper structural levels. Therefore, the effect of pressure on calcium enrichment in olivines is not considered to be a significant factor with respect to the Tulameen complex.

MnO contents of the olivines in the ultramafic and gabbroic rocks of the Tulameen complex exceed those assigned by Deer et al. (1978a) for olivines of the corresponding compositions. According to Deer et al. (1978a) basic plutonic rocks contain 0.13 wt. % MnO for olivines in the compositional range Fo_{100-80}, and 0.24 wt. % MnO for Fo_{80-70}. MnO values for olivines from the Tulameen complex with the compositional range of Fo_{90-86}, yield between 0.19-0.26 wt. % MnO and 1.1-1.2 wt % MnO for Fo_{74-75}. Explanations for manganese enrichment in olivines include high a_{Fe} (Simkin and Smith, 1970), and silica undersaturated melt composition (Brown, 1982; Best, 1975; and Simkin and Smith, 1970). The high manganese contents in the olivines in the Tulameen complex are interpreted as being more indicative of low $aSiO_2$ than high a_{Fe}, considering the magnesium numbers of the olivines. This interpretation is consistent with conclusions drawn from the calcium chemistry of the olivines.

ii) Clinopyroxene

The composition of clinopyroxenes from the ultramafic to syenodiorite rocks of the Tulameen complex is presented in Table 5.6. Averaged compositions are given of several

Table 5.6

Composition of clinopyroxene determined by electron microprobe.

	Sample	87-JR-29-01	87-JR-29-09	87-JR-32-08	88-JR-16-2A	87-JR-29-08	88-JR-5-15	87-JR-34-02
	Lithology	wehrlite	ol-cpxt	ol-cpxt	ol-cpxt	ol-cpxt	mt-cpxt	pxt/gb contact
	Number of targets	2	3	4	4	2	2	4
Weight %	SiO_2	53.2	52.5	52.3	51.5	52.2	50.8	50.5
	TiO_2	0.02	0.13	0.18	0.16	0.28	0.46	0.32
	Al_2O_3	0.77	1.24	1.35	1.60	2.06	3.46	2.78
	Fe_2O_3	0.62	0.94	0.97	1.34	1.21	2.95	4.12
	FeO	1.51	2.31	2.77	2.69	2.94	3.13	4.35
	MnO	0.02	0.09	0.06	0.12	0.12	0.20	0.29
	MgO	17.3	17.2	17.0	17.2	16.0	15.2	13.1
	CaO	24.7	23.6	23.5	22.7	23.0	23.1	23.4
	Na_2O	0.35	0.25	0.26	0.30	0.32	0.26	0.51
Molecular proportions	Si^{4+}	1.9560	1.9408	1.9321	1.9176	1.9433	1.8783	1.8946
	Ti^{4+}	0.0006	0.0036	0.0050	0.0045	0.0078	0.0128	0.0090
	$^{(iv)}Al^{3+}$	0.0334	0.0545	0.0593	0.0708	0.0567	0.1217	0.1054
	$^{(vi)}Al^{3+}$	0.0000	0.0000	0.0000	0.0000	0.0345	0.0304	0.0186
	$^{(iv)}Fe^{3+}$	0.0106	0.0047	0.0086	0.0116	0.0000	0.0000	0.0000
	$^{(vi)}Fe^{3+}$	0.0066	0.0215	0.0184	0.0260	0.0339	0.0821	0.1163
	Fe^{2+}	0.0465	0.0714	0.0856	0.0838	0.0915	0.0968	0.1365
	Mn^{2+}	0.0006	0.0028	0.0019	0.0038	0.0038	0.0063	0.0092
	Mg^{2+}	0.9481	0.9479	0.9362	0.9547	0.8879	0.8378	0.7326
	Ca^{2+}	0.9730	0.9348	0.9302	0.9057	0.9175	0.9152	0.9406
	Na^{+}	0.0249	0.0179	0.0186	0.0217	0.0231	0.0186	0.0371
	100Mg/(Mg+Fe)	94	90	89	88	87	82	74
	Fe^{2+}/Fe^{3+}	3.00	0.71	0.76	0.69	0.68	0.54	0.54
Wo (%)	Ca/(Ca+Mg+Fe+Mn)	49	47	47	46	47	47	49
En (%)	Mg/(Ca+Mg+Fe+Mn)	48	48	47	48	46	43	38
Fs (%)	Fe/(Ca+Mg+Fe+Mn)	3	5	6	6	5	10	13
Assigned end members (%)	$NaFeSi_2O_6$ (Agt)	2	2	2	2	2	2	4
	$CaTiAl_2O_6$ (CaTiTs)	0	0	1	1	2	3	2
	$CaFe(AlSi)_2O_6$ (Es)	0	3	0	0	1	6	4
	$CaAl(Al,Si)_2O_6$ (AlCaTs)	2	0	3	3	3	3	5
	$Ca_2Si_2O_6$ (Wo)	47	45	44	44	43	40	42
	$Mg_2Si_2O_6$ (En)	47	47	46	46	44	41	36
	$Fe_2Si_2O_6$ (Fs)	2	3	4	4	5	5	7

Table 5.6

Composition of clinopyroxene determined by electron microprobe.

	Sample	87-JR-34-03	88-JR-18-01	88-JR-16-05	87-JR-28-01	87-JR-28-01	87-JR-28-01
	Lithology	pxt/gb contact	pxt/dior contact	gb	gb	gb	gb
	Number of targets	3	2	3	14	3	5
					unzoned px	basal sector	prism sector
Weight %	SiO_2	50.2	51.2	48.7	49.5	50.8	49.4
	TiO_2	0.31	0.14	0.59	0.58	0.42	0.66
	Al_2O_3	2.14	1.04	5.03	4.73	3.23	5.10
	Fe_2O_3	4.47	4.71	3.79	3.85	3.68	3.89
	FeO	4.73	4.98	3.41	3.47	3.32	3.51
	MnO	0.28	0.40	0.25	0.27	0.25	0.27
	MgO	12.7	12.9	13.5	13.6	14.5	13.3
	CaO	22.0	23.1	21.7	21.8	22.1	21.6
	Na_2O	0.52	0.45	1.08	1.08	0.84	1.14
Molecular proportions	Si^{4+}	1.9299	1.9423	1.8289	1.8450	1.8878	1.8427
	Ti^{4+}	0.0090	0.0040	0.0167	0.0163	0.0117	0.0185
	$^{(iv)}Al^{3+}$	0.0701	0.0469	0.1777	0.1550	0.1112	0.1573
	$^{(vi)}Al^{3+}$	0.0277	0.0000	0.0535	0.0547	0.0315	0.0689
	$^{(iv)}Fe^{3+}$	0.0000	0.0108	0.0000	0.0000	0.0000	0.0000
	$^{(vi)}Fe^{3+}$	0.1293	0.1237	0.1071	0.1080	0.1029	0.1092
	Fe^{2+}	0.1521	0.1579	0.1071	0.1082	0.1032	0.1095
	Mn^{2+}	0.0091	0.0129	0.0080	0.0085	0.0079	0.0085
	Mg^{2+}	0.7278	0.7295	0.7558	0.7557	0.8032	0.7395
	Ca^{2+}	0.9062	0.9390	0.8732	0.8707	0.8800	0.8633
	Na^{+}	0.0388	0.0331	0.0786	0.0784	0.0605	0.0825
	100Mg/(Mg+Fe)	71	70	77	77	79	76
	Fe^{2+}/Fe^{3+}	0.54	0.54	0.50	0.50	0.50	0.50
Wo (%)	Ca/(Ca+Mg+Fe+Mn)	47	48	47	47	46	47
En (%)	Mg/(Ca+Mg+Fe+Mn)	38	37	41	41	42	40
Fs (%)	Fe/(Ca+Mg+Fe+Mn)	15	15	12	12	12	13
Assigned end members (%)	$NaFeSi_2O_6$ (Act)	4	3	8	7	6	8
	$CaTiAl_2O_6$ (CaTiTs)	2	1	3	3	2	3
	$CaFe(AlSi)_2O_6$ (Es)	7	7	4	4	5	3
	$CaAl(Al,Si)_2O_6$ (AlCaTs)	2	0	7	7	4	8
	$Ca_2Si_2O_6$ (Wo)	40	43	36	36	38	36
	$Mg_2Si_2O_6$ (En)	36	36	36	37	40	36
	$Fe_2Si_2O_6$ (Fs)	8	9	6	6	5	6

Table 5.6

Composition of clinopyroxene determined by electron microprobe.

	Sample	**87-JR-18-01**	**87-JR-21-03**	**88-JR-16-4B**	**88-JR-16-4B**	**88-JR-16-4B**
	Lithology	syenogabbro	syenodiorite	andesite dike	andesite dike	andesite dike
	Number of targets	3	2	6	3	3
				avg comp.	end (111) sector	prism sector
Weight %	SiO_2	51.5	52.0	49.5	51.2	47.9
	TiO_2	0.33	0.34	0.59	0.36	0.83
	Al_2O_3	1.83	2.10	4.03	2.72	5.33
	Fe_2O_3	4.40	3.72	2.87	2.02	3.38
	FeO	3.97	3.35	3.36	3.71	3.32
	MnO	0.56	0.54	0.13	0.13	0.13
	MgO	14.2	15.2	15.3	16.4	14.1
	CaO	22.4	21.7	21.8	21.5	22.1
	Na_2O	0.48	0.56	0.22	0.20	0.24
Molecular proportions	Si^{4+}	1.9229	1.9294	1.8607	1.9085	1.8168
	Ti^{4+}	0.0093	0.0095	0.0167	0.0101	0.0237
	$^{(iv)}Al^{3+}$	0.0771	0.0706	0.1393	0.0915	0.1832
	$^{(vi)}Al^{3+}$	0.0042	0.0221	0.0408	0.0290	0.0572
	$^{(iv)}Fe^{3+}$	0.0000	0.0000	0.0000	0.0000	0.0000
	$^{(vi)}Fe^{3+}$	0.1286	0.1039	0.0812	0.0567	0.0965
	Fe^{2+}	0.1238	0.1380	0.1058	0.1157	0.1055
	Mn^{2+}	0.0177	0.0170	0.0041	0.0041	0.0042
	Mg^{2+}	0.7904	0.8407	0.8573	0.9113	0.7972
	Ca^{2+}	0.8962	0.8627	0.8780	0.8587	0.8982
	Na^{+}	0.0348	0.0403	0.0160	0.0145	0.0177
	100Mg/(Mg+Fe)	75	76	82	84	79
	Fe^{2+}/Fe^{3+}	0.50	0.50	0.43	0.33	0.48
Wo (%)	Ca/(Ca+Mg+Fe+Mn)	46	44	46	44	47
En (%)	Mg/(Ca+Mg+Fe+Mn)	40	43	45	47	42
Fs (%)	Fe/(Ca+Mg+Fe+Mn)	14	13	11	9	11
Assigned end members (%)	$NaFeSi_2O_6$ (Act)	4	4	2	1	1..8
	$CaTiAl_2O_6$ (CaTiTs)	2	2	3	2	5
	$CaFe(AlSi)_2O_6$ (Es)	8	5	7	4	8
	$CaAl(Al,Si)_2O_6$ (AlCaTs)	0	2	4	3	6
	$Ca_2Si_2O_6$ (Wo)	40	38	37	45	36
	$Mg_2Si_2O_6$ (En)	39	41	42	38	39
	$Fe_2Si_2O_6$ (Fs)	7	8	6	6	6

analyses of samples where no compositional zoning was detected in core to rim traverses. The exception to this is in sector zoned pyroxenes which are shown with averaged analyses for the basal and prism sectors. Individual analyses are provided in appendix 1 along with sketches of the targets. Oxide totals range from 97.8 to 99.6 wt. %. The structural formulae of the pyroxenes, Table 5.6, have been calculated on the basis of 4 cations. Cations were assigned to the T, M_1 amd M_2 structural sites in the order Si^{4+}, Al^{3+}, Fe^{3+}, Ti^{4+}, Mg^{2+}, Fe^{2+}, Mn^{2+}, Ca^{2+} and Na^{+}, assuming ideal site occupancy (Morimoto, 1988). Of the 55 determinations made, 13 are considered "superior" analyses by the criteria outlined by Cameron and Papike (1981) for assessing the quality of individual pyroxene analyses. By this convention, a pyroxene analysis, with an oxide wt. % sum between 99-100%, is judged "superior" if: (1) the sum of the tetrahedral site cations ($Si + {}^{iv}Al$) equal 2.00 ± 0.02 atoms per six oxygens, (2) the sum of the octahedral cations (Mn, Fe^{2+}, Fe^{3+}, Mg, Ti, Cr, ${}^{vi}Al$) is >0.98 atoms per six cations, (3) the sum of the cations (Na, Ca, Mn, Fe^{2+}, Mg) in the M_2 site=1.00+/-0.02, and (4) the charge balance equation (${}^{vi}Al+{}^{vi}Fe^{3+}+{}^{vi}Cr^{3+}+2{}^{vi}Ti^{4+} = {}^{iv}Al+M_2Na$) is balanced to +/- 0.03 of a charge. The remaining 42 analyses have oxide totals less than 99%. According to Deer et al. (1974), if the iron is treated entirely as ferrous iron, the sum of the calculated oxide wt. % and numbers of cations will be low.

The pyroxenes from the sampled lithologies of the Tulameen complex are characterized by high CaO and MgO, low TiO_2 and variable SiO_2 and Al_2O_3. The proportion of magnesium (100Mg/(Mg+Fe) of the pyroxenes from the Tulameen suite range from 94 in the wehrlite to 70 in the hornblende-rich contact rocks; the more differentiated syenodiorites have intermediate values of 75-76. According to the chemical grouping of pyroxenes proposed by Morimoto (1988), all analyses are Ca-Mg-Fe pyroxenes which can be classified on a pyroxene quadrilateral diagram (Fig. 5.10). This ternary diagram also expresses the variation of the major elements, Ca, Mg and Fe within the data array. The pyroxenes plot within an elongate

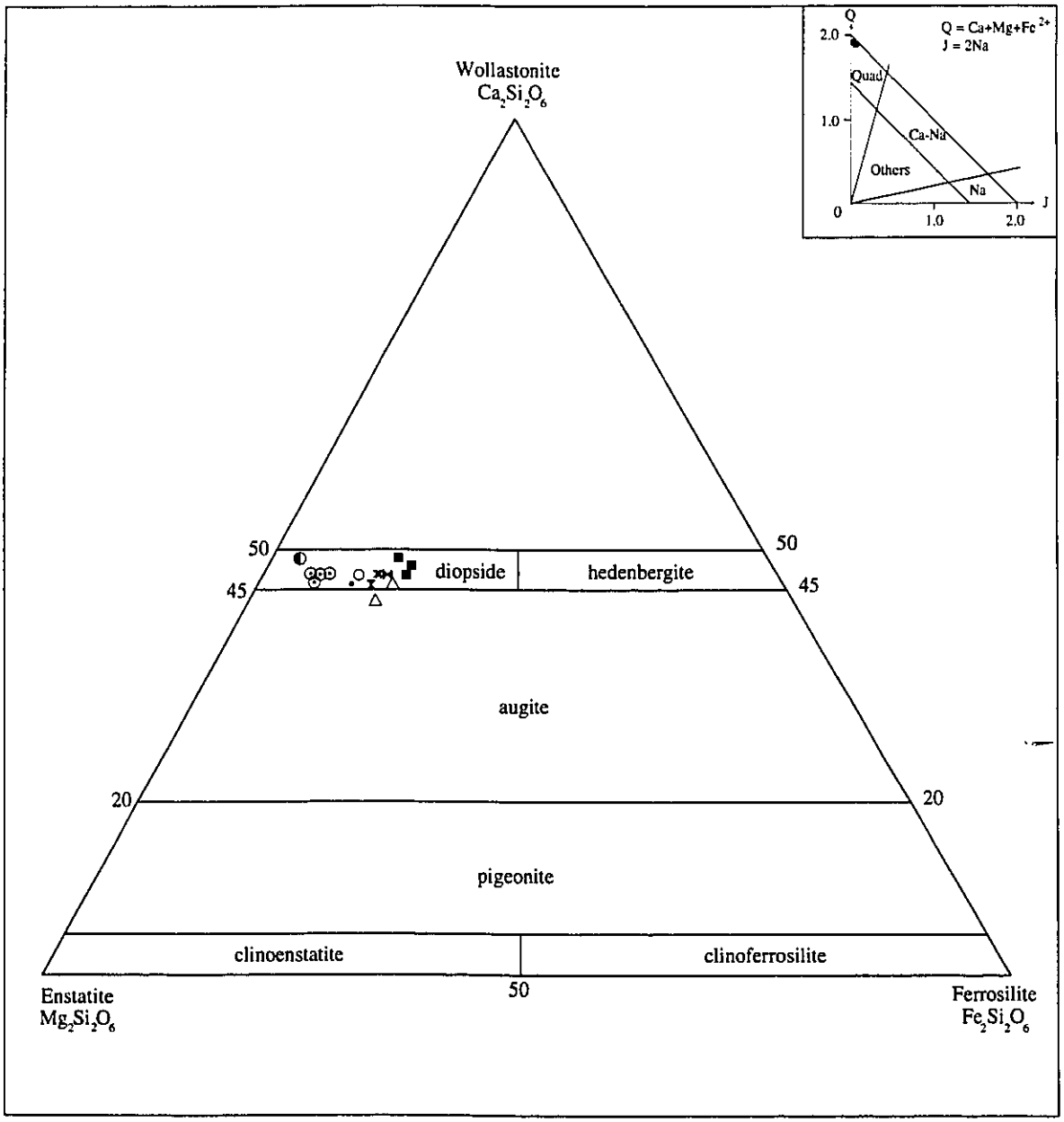

Figure 5.10. Classification diagram for Ca-Mg-Fe pyroxenes (modified after Morimoto 1988). Inset shows all pyroxenes analyzed fall within the quadrilateral (Ca-Mg-Fe) field of Morimoto (1988).

cluster which parallels the diopside-hedenbergite tie-line. All but one of the samples (87-JR-21-03 syenodiorite) plot within the diopside field of Morimoto (1988). The suite exhibits a limited iron enrichment, and magnesium decreases systematically at a relatively constant calcium content (47%). Silica decreases in content from 53.2 to 50.2 wt. % in wehrlite through to the hornblende-rich contact rocks, and increases to 52 wt. % in the syenodiorites.

The concentrations of the minor elements, Al, Ti, Mn and Na, show an irregular but overall increase in concentration through the data suite. There is a progressive enrichment of Al from 0.77% in wehrlite to 5.1% in gabbro. Diopsides from the hornblende-rich contact rocks and syenodiorites have lower Al abundances in the range of 1.0-2.1% and 1.8-2.1% respectively. The calculated structural formulae (Table 5.6) indicate that most of the aluminum is allocated to the tetrahedral site. TiO_2 similarly increases in abundance from 0.02% to 0.59% in pyroxenes from wehrlite to gabbro, with lower values (0.33-0.34%) in the syenodiorites. MnO systematically increases to 0.56% through the suite. The highest values of Al_2O_3, TiO_2 and Na_2O are measured within the prism sectors of the zoned pyroxenes in the gabbro and basaltic dykes.

The chemical variation within the sector (also referred to as "hourglass") zoned clinopyroxenes is summarized in Figure 5.11. Plate 2.4b reveals the sector zoning under polarized light. Analyses are provided in appendix 1. SiO_2, Al_2O_3, TiO_2, MgO and Na_2O show the greatest variation, whereas the concentration of FeO_{tot}, CaO and MnO remain relatively constant between the sectors. This type of partitioning of the minor elements (Al_2O_3, TiO_2, MnO and Fe_{tot}) to the prism sectors is characteristic of sector zoned pyroxenes reported from alkaline volcanic rocks (Leung, 1974; Dowty, 1976; Strong, 1969; Duncan, 1974; Downes, 1974; Duda and Schmincke, 1987; Thompson, 1972; Mortimer, 1987; Wass, 1973; Hollister and Gancarz, 1971), pegmatitic bodies within tholeiitic diabases (Smith and Lindslay, 1971; Harkins and Hollister, 1977; Nakamura and Coombs, 1973; Preston, 1966), peralkaline

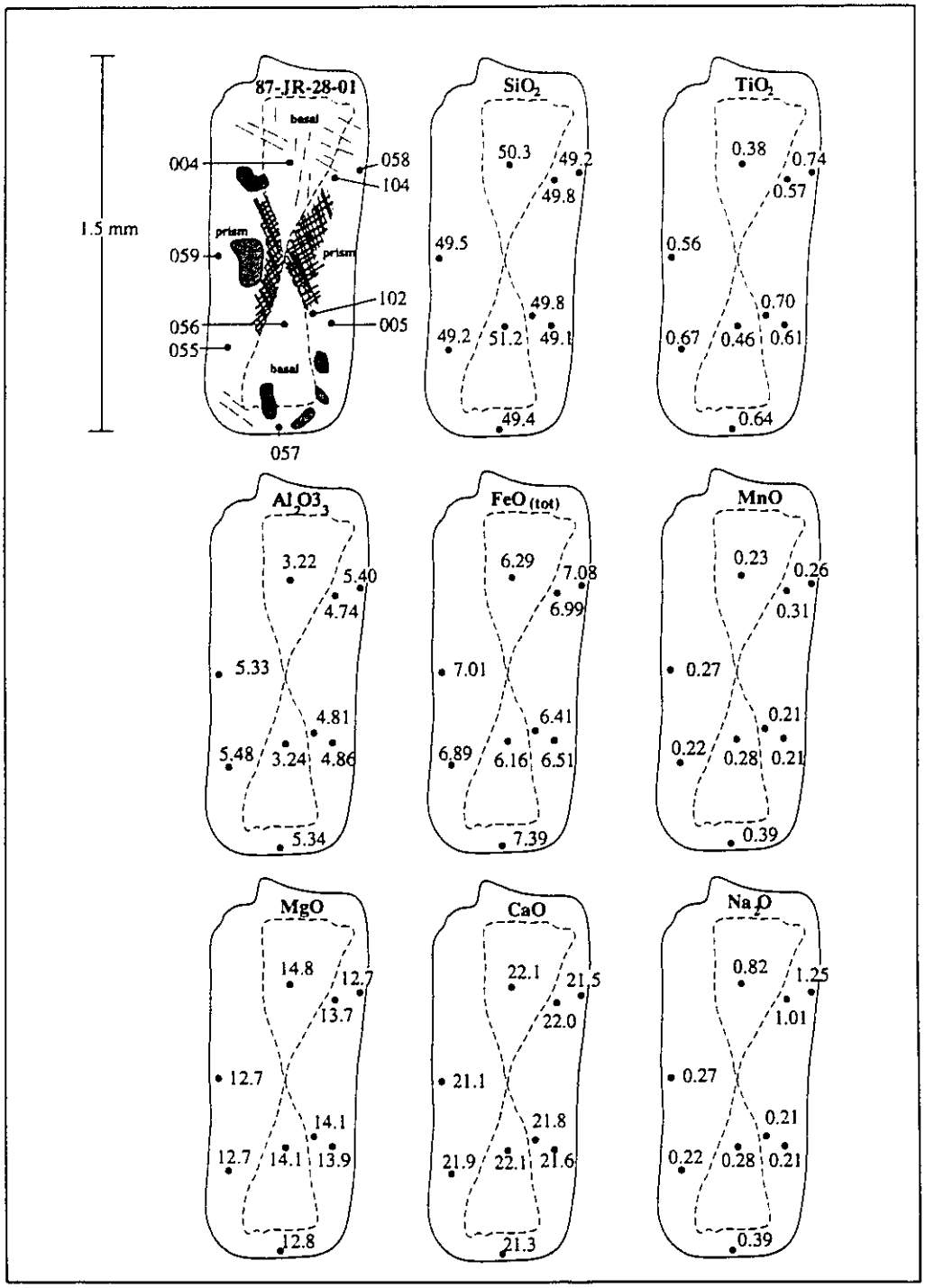

Figure 5.11. Chemical variation within basal and prism sectors of zoned diopside (plate 2.4).

plutonic rocks (Larson, 1976, 1981; Rock, 1982) and lunar rocks (Hargraves et al., 1970; Bence et al., 1970; Hollister and Hargraves, 1970; Ferguson, 1973; Fleet, 1975).

Probe analyses of acicular needles and blebs of oxides included within the pyroxene and in the gabbros and syenodiorites, indicate they are principly magnetite with lesser amounts of titanium (appendix 1, sample 87-JR-28-01, target 8, spot 103). Chromium was not measured.

The substitution mechanism by which Al^{3+}, Fe^{3+}, Ti^{4+} and Na^{+} were incorporated into the pyroxenes during differentiation of the Tulameen complex, was estimated by calculating the end-member compositions for the non-quadrilateral components, as proposed by Morimoto (1988). The results, which are shown in Table 5.6, indicate the predominance of the Tschermak ($^{vi}R^{3+}$—^{iv}Al; where R^{3+}=Fe^{3+}, Al^{3+}) and acmite (R^{+}—$^{vi}R^{3+}$; where R^{+}=Na^{+} and R^{3+}= Fe^{3+}) substitution couples. The percentages of non-quadrilateral components increases from 4% in wehrlite to a maximum of 22% in the minor-element enriched prism sectors of the zoned pyroxenes in the gabbros.

a) Interpretation of pyroxene data:

The trends of major and minor element partitioning in the pyroxenes of the Tulameen complex are studied as an aid to determining what the condition of crystallization were and to discover the chemical and structural characteristics of the magma. The Tulameen pyroxene suite is marked by high MgO and CaO bearing pyroxenes, with limited iron enrichment, low TiO_2, and increasing Al_2O_3 and 100Mg/(Mg+Fe).

The pyroxene array for the Tulameen complex is compared with fractionation trends for pyroxenes from various mafic plutonic suites, in Fig. 5.12. The concentration of analyses towards the diopside corner of the quadrilateral overlaps with the restricted ranges of clinopyroxenes from island arc and ocean ridge cumulate rocks. These short fractionation trends are distinct from the iron enriched, two-pyroxene, augite-ferroaugite trends observed in

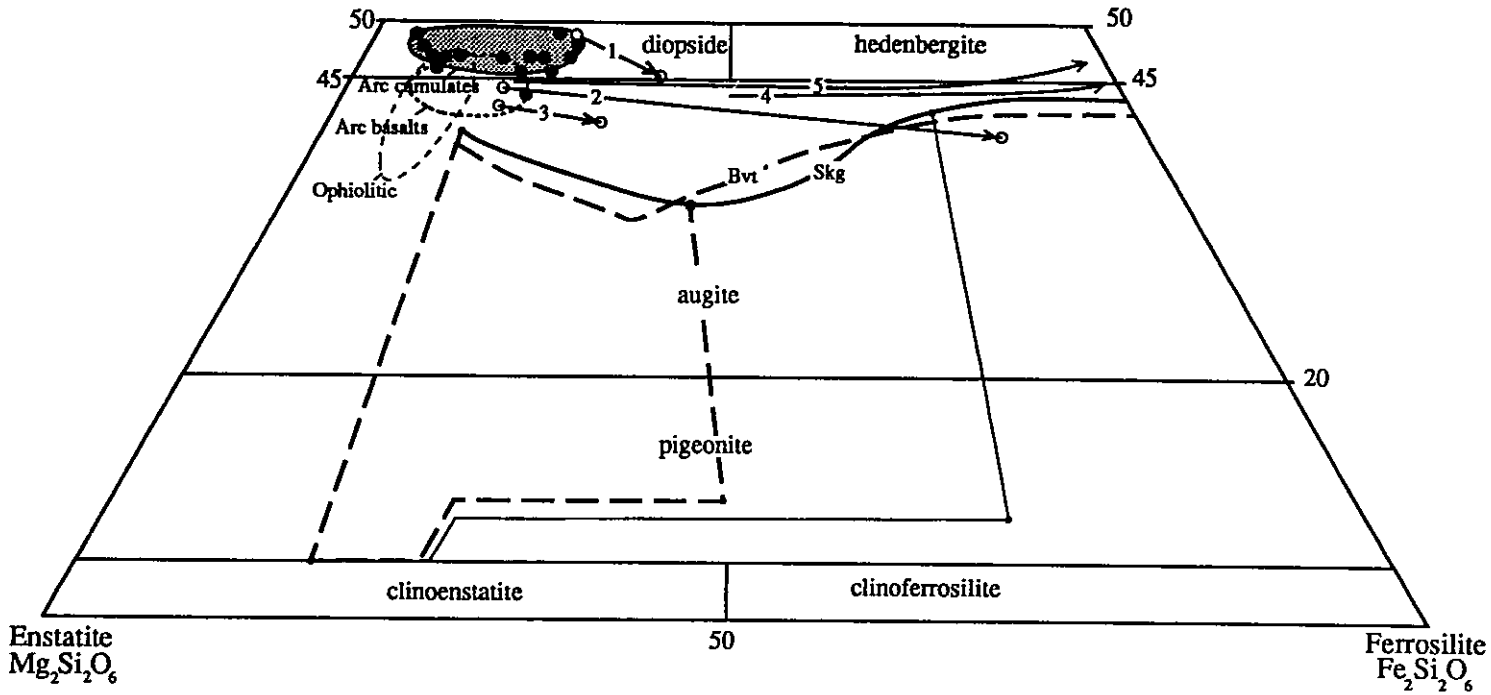

Figure 5.12. Pyroxene trends from mildly alkaline (1=Black Jack sill, 2=Alkali basalt-trachyte series, Japan, 3=Gough Is.), strongly alkaline (4=Kungnat syenites, 5=Shiant Isles sill), tholeiitic (Bvt=Bushveldt, Skg=Skaergaard), ophiolitic and arc suites. Sources: Gill (1981), Coleman (1977), Conrad and Kay (1984) and Gibb (1973).

tholeiitic stratiform complexes and the flat calcic-augite-hedenbergite arrays for differentiated alkaline intrusive suites. Limited Fe-enrichment in pyroxenes at spreading ocean ridges is attributed to open system fractionation where continuous replenishment of primitive melt opposes the effects of differentiation (Hopson et al, 1981). The confined trend of iron enrichment in arc-related cumulate rocks is due to crystallization in a more oxidizing environment. High water contents in the melt, characteristic of subduction-zone magmatism (Wyllie, 1979), promote oxidation of iron and induces early crystallization of ferric iron-rich oxides resulting in removal of iron from the melt. It is significant to note that high ferric iron contents, in the early-crystallized chrome spinels, are characteristic of arc cumulates and differentiate them from stratiform intrusions, alpine peridotites and ophiolites (Irvine, 1967).

The progressive enrichment of aluminum in pyroxene, noted in the pyroxene of the Tulameen complex, has been documented in silica undersaturated rocks (Kushiro, 1960; Le Bas, 1962; Leterrier et al., 1982) and island arc cumulate rocks (Murray, 1972; Irvine, 1974; Conrad and Kay, 1980; Debari and Coleman, 1989; Loucks, 1990 and Loney and Himmelberg, 1992). Kushiro (1960) and LeBas (1962) correlated the distribution of aluminum in pyroxene with the $aSiO_2$ of the melt. They observed that in silica saturated tholeiitic suites (i.e. high $aSiO_2$ in melt) Al_2O_3/SiO_2 in pyroxene decreases with differentiation as aluminum is preferentially partitioned into plagioclase. In strongly silica undersaturated alkaline to peralkaline magmas (low $aSiO_2$), pyroxenes are increasingly enriched in aluminum (in the tetrahedral sites) as Al_2O_3/SiO_2 increases with fractionation (LeBas, 1962). Titanium, present in significant amounts in strongly undersaturated magmas (Verhoogen, 1962; Kushiro, 1960) substitutes into the octahedral site, and charge balances the pyroxene by the coupled substitution $^{iv}Mg^{iv}Si_2$-$^{vi}Ti^{iv}Al_2$ in the molecule $CaTiAl_2O_6$ (Loucks, 1990).

Patterns of increasing aluminum with fractionation in pyroxenes from convergent plate margins is attributed to the hydrous nature of subduction zone magmatism. The $aSiO_2$ of these

melts is also low due to the abundant dissolution of water, which depolymerizes the melt by reacting with the bridging oxygens that join the $(Si,Al)O_4$ tetrahedra in the silicate framework:

$$H_2O_{(melt)} + Si_2O^{4-}{}_{6(melt)} = SiO(OH)_{2(melt)} + SiO^{4-}{}_6 \quad \text{(Loucks, 1990)}$$

The activity of the aluminous component in pyroxene and in the melt, is increased as the OH-groups in the melt bond strongly to tetrahedral Si^{4+} and not to tetrahedral Al^{3+} (Loucks, 1990). With this decrease of $aSiO_2$, and increase of aAl_2O_3 the stability fields of olivine and diopside are expanded at the expense of enstatite and plagioclase. The following reactions at elevated PH_2O, presented by Loucks (1990), show that with this decrease in $aSiO_2$, the crystallization of olivine, diopside, aluminous and ferric-Tschermakite components (es, ts) is favored over anorthite and enstatite.

$$3H_2O_{(melt)} + CaAl_2Si_2O_{8(melt)} + Mg_2Si_2O_{6(melt)} = CaMgSi_2O_{6(di)} + 0.5\ Mg_2SiO_{4\ (fo)} + Al_2O_{3(melt)} + 1.5\ Si(OH)_{4(melt)}$$

and

$$2H_2O + CaAl_2Si_2O_{8(melt)} + 0.5Fe_2O_{3(melt)} = CaFe^{3+}AlSiO_{6(es)} + 0.5Al_2O_{3(melt)} + Si(OH)_{4(melt)}$$

and

$$CaAl_2Si_2O_{8(melt)} + 2H_2O_{(melt)} = CaAlAlSiO_{6(ts)} + Si(OH)_{4(melt)}$$

This crystallization assemblage (olivine, diopside) is consistent with the mineralogy observed in Alaskan-type ultramafic complexes and mafic to ultramafic assemblages in the Aleutian arc, which are characterized by olivine and diopside-rich cumulates lacking orthopyroxene and plagioclase. These reactions also indicate the predominance of the

Tschermakite (CaMg-Al,Fe^{3+}Al) substitution couple which is the dominant non-quadrilateral pyroxene component in island arc-suites (Papike, 1980) and within Tulameen pyroxene (Table 5.6).

Loucks (1990) refined the aluminum versus titanium discriminant diagram of Le Bas (1962) to distinguish ophiolitic from arc-related mafic and ultramafic cumulate rocks. Clinopyroxene arrays from arc plutonic complexes exhibit steeper $^{iv}Al/TiO_2$ trends than those of ophiolites and alkalic gabbros from anorogenic settings. The data points for the pyroxenes from the Tulameen complex, plot along the steep trend of arc-cumulates (Fig. 5.13), which show a greater rate of increase in ^{iv}Al relative to TiO_2 than in clinopyroxenes from alkaline suites. Extreme enrichment of Al_2O_3 in clinopyroxene (up to 9%) with differentiation of arc cumulates has been documented by Debari and Coleman (1989) in the Tonsina assemblage of southern Alaska.

The assignment of cations to the structural sites (Table 5.6) suggests that a greater proportion of aluminum resides in the tetrahedral sites than octahedral sites in Tulameen pyroxene. The distribution of aluminum between these two structural sites is depicted in Fig. 5.14, which also shows the fields for various crustal levels (Aoki and Kushiro, 1968) defined by the predominance of octahedral (favored in high pressure domains) or tetrahedral sites. In the pyroxenes with higher aluminum contents, the $^{iv}Al/^{vi}Al$ remains relatively constant with differentiation, which suggests that the Tulameen may be interpreted as a single body which fractionated at middle to upper crustal levels.

The partitioning of the minor elements (Al, Ti) into the pyroxene lattice is also rate dependent, as shown by Grove and Bence (1977). Fast cooling rates, favor the entry of Ca, Fe, Al and Ti into the pyroxene lattice. An example of this is in the sector-zoned pyroxenes from the gabbros, where Al, Ti and Na are strongly partitioned into the slower growing prism faces. The elongated prismatic habit of sector zoned pyroxenes is evidence of this differential

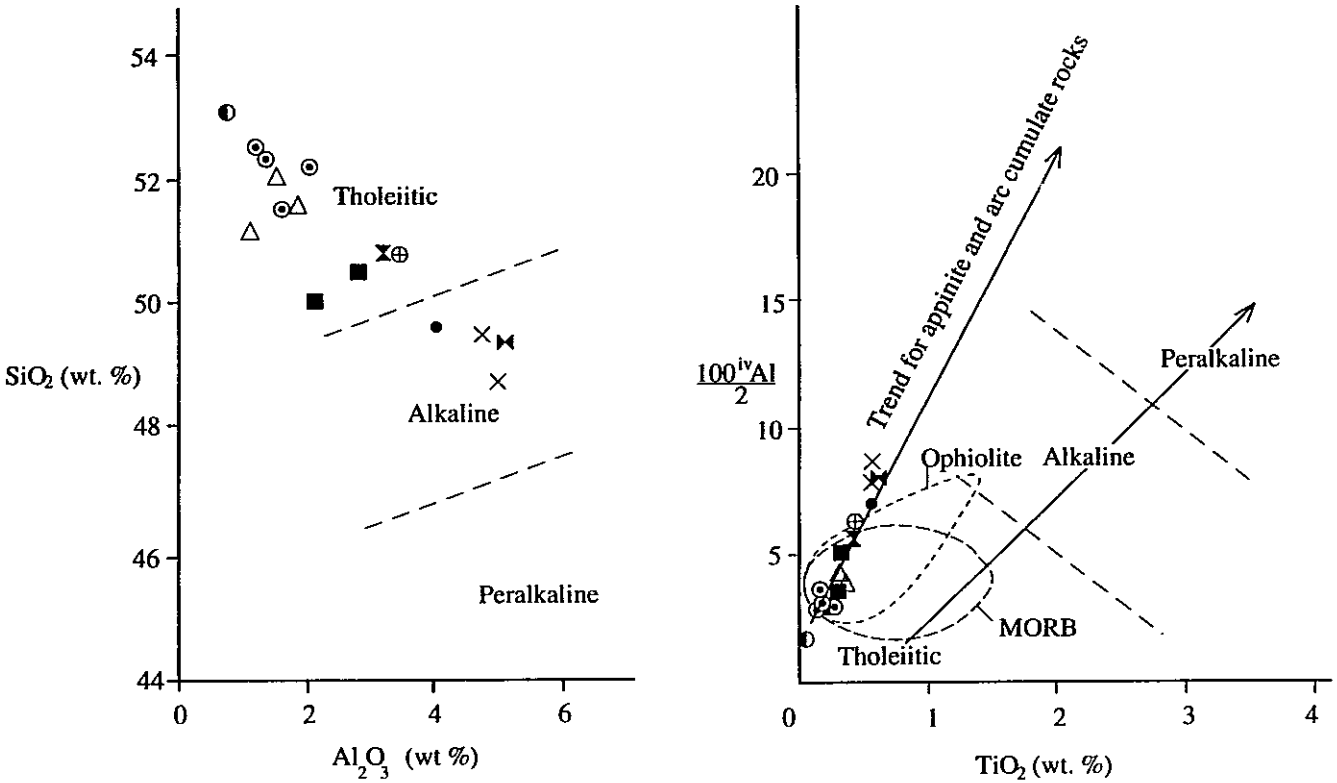

Figure 5.13. Aluminum trends in clinopyroxenes from the Tulameen complex. a) Al increases as Si decreases through the suite (modified after LeBas, 1962). b) The steep slope of the pyroxene array on this plot of (100 ^{iv}Al)/2 vs TiO_2 is characteristic of pyroxenes from magmas generated in the hydrous environments of subduction zones (modified after Loucks, 1990).

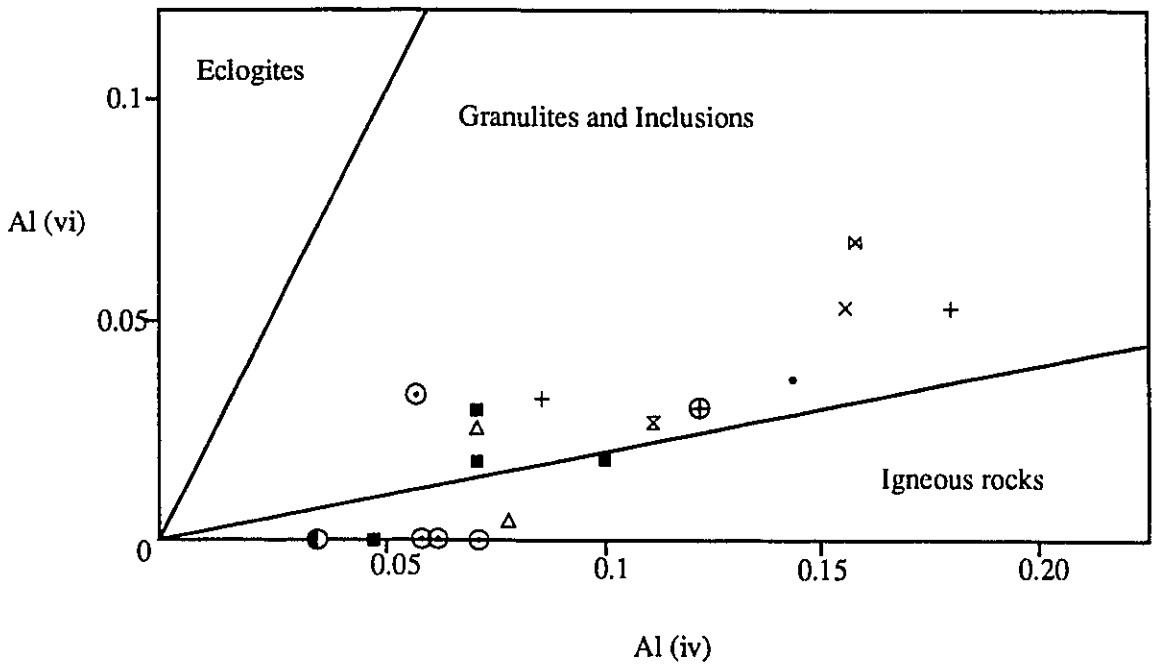

Figure 5.14. Plot of the partitioning of Al between the tetrahedral and octahedral sites in the pyroxene structure (modified after Aoki and Kushiro, 1968). The relatively constant $^{iv}Al/^{vi}Al$ with differentiation suggests that the Tulameen complex is a singular pluton which fractionated at middle to upper crustal levels.

rate of growth and uptake of elements with respect to the various crystallographic directions (Downes, 1974; Ferguson, 1973 and Strong, 1969; Fig. 5.11). This disequilibrium growth of the pyroxene may be related to such factors as: to rapid cooling in volcanic rocks (Dowty, 1976; Deer et al., 1978b and Wass, 1973) and removal of heat of vaporization in pegmatitic environments (Smith and Lindslay, 1971; Larson, 1976 and Nakamura and Coombs, 1973). The reason for this disequilibrium feature in the gabbros of the Tulameen may be related to some quench conditions, such as an abrupt decrease in temperature with the appearance of a new mineral phase, such as plagioclase or hornblende. Alternatively, the sector-zoned pyroxenes may reflect rapid cooling of the gabbroic margin of the feldspathic host against an older, cooler ultramafic body. It is significant to note that the gabbros are much finer grained than the pyroxenites or the syenogabbros.

Highly oxidizing conditions in the magma, at the time of pyroxene crystallization is suggested by ubiquity of platey iron oxides which are observed as an orthogonal grid of needles in the pyroxenes of the olivine pyroxenites, or concentrated in discrete clusters along with apatite in concentric zones and at the boundaries between sectors in the sector-zoned pyroxenes in the gabbros (plate 2.4). The exsolution of iron oxides from the pyroxenes in the olivine pyroxenite is similar to that described by Eldson (1971) in clinopyroxenes from the Upper Layered Series of the Kap Edvard Holm complex, in east Greenland. Eldson (1971) concludes that the chemistry of the clinopyroxenes is consistent with crystallization from a water-rich magma and the oxide inclusions were formed by the oxidation of the enstatite component at subsolidus temperatures. The oxide inclusions in the sector zoned pyroxenes are interpreted as being of primary origin, as their concentration with apatite inclusions along the surfaces of the faster growing faces suggests their incorporation as impurities during the rapid crystal growth (Downes, 1974 and Dowty, 1976). The Fe^{3+}/Fe^{2+} values of the pyroxene (Table 5.6), and hornblende (Table 5.7) of the gabbro and contact rocks are substantially

higher than those in the pyroxenes of the olivine pyroxenite, which supports the suggestion that the fO_2 increased during crystallization. The pyroxene in the syenodiorite lacks the oxide needles, but is more Mg-rich than the pyroxene of the gabbro.

Figure 5.15, which is a representation of the fractionation sequence of the Tulameen complex and which summarizes the variation in concentration of elements within pyroxenes, with differentiation from wehrlite to syenodiorite, and summarizes the factors which influence the composition of pyroxene in the complex. The effect of the composition and structure of the melt, at the time the pyroxene crystallized, is evident by the olivine and pyroxene fractionation in the absence of plagioclase and orthopyroxene (due to high water contents and consequently low $aSiO_2$) from wehrlite to gabbro. The aluminum content in pyroxene increases from 0.77% to 5%. Titanium and iron which balance the charge of aluminum in the tetrahedral site, increase in response. With the appearance of new aluminum-bearing phases, plagioclase and hornblende, and titanium-bearing oxides (magnetite) in the gabbro and contact rocks, aluminum and titanium contents of the pyroxene decrease. The unzoned nature of most of the pyroxene, as well as its consistency in composition within the various lithologies, suggests that the Tulameen complex cooled slowly under equilibrium conditions during most of its differentiation. Sector zoning in diopside is observed only in the gabbro (87-JR-28-01) and a basaltic dyke (88-JR-16-04B) and is interpreted as reflecting localized disequilibrium crystallization due to rapid cooling. The "salite trend" (Murray, 1972; Conrad and Kay, 1984) of the suite, characterized by high magnesium and calcium, low titanium, increasing aluminum contents and high calculated Fe^{3+} content, is interpreted as reflecting crystallization of pyroxene from progressively more hydrous melts. Platey oxide inclusions within the pyroxenes, in the olivine pyroxenite and gabbro, suggests magmatic oxidation of the magma due to increasing fO_2 during differentiation.

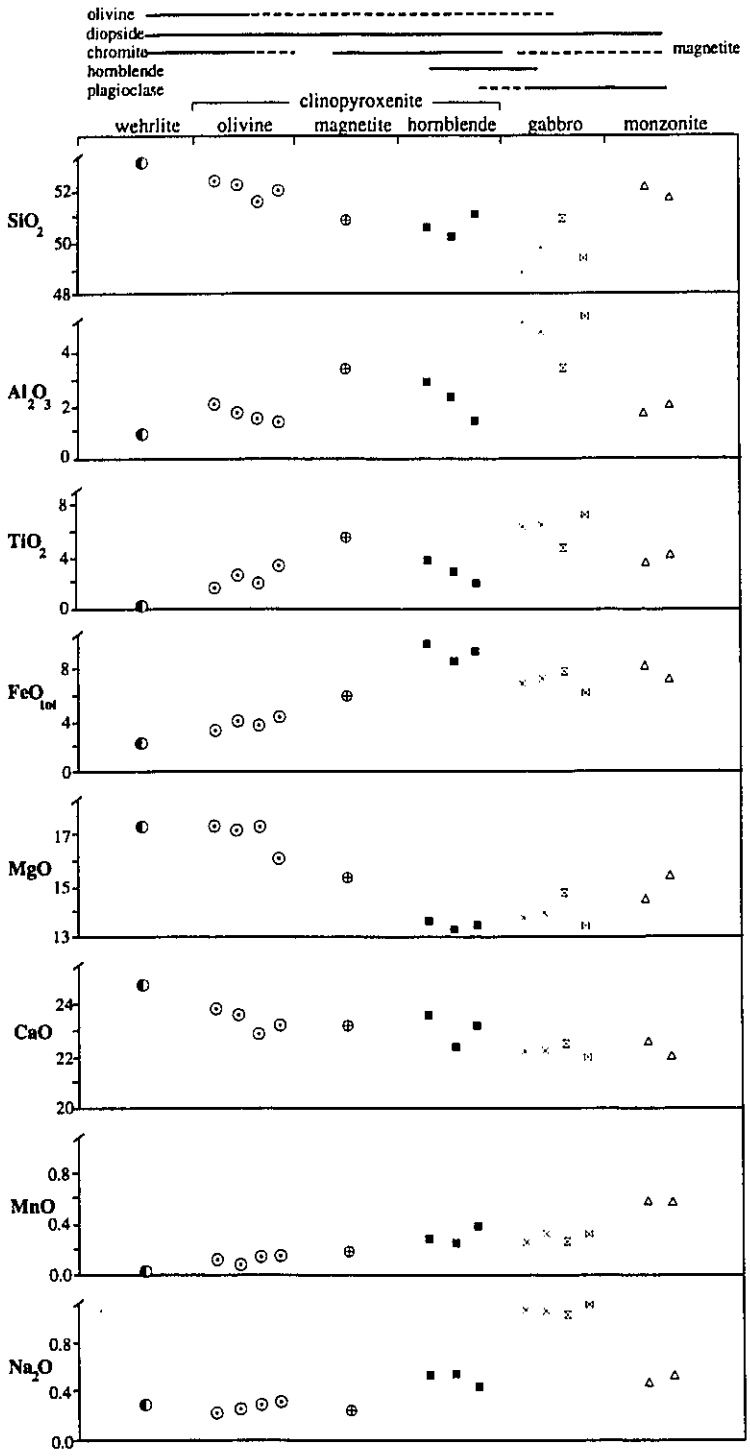

Figure 5.15. Diagram illustrating the composition of clinopyroxene in representative rocks from the Tulameen complex.

iii) Amphibole

The composition of amphibole from selected rocks of the Tulameen complex is presented in Table 5.7. This data represents individual analyses. Oxide totals range from 96.4 to 98.3 wt. %. The structural formulae of the amphibole, Table 5.7, were calculated on the basis of 23 oxygens. Cations were assigned to the T (tetrahedral), C (M1+M2+M3), B (M4) and A sites, in the order Si^{4+}, Al^{3+}, Fe^{3+}, Ti^{4+}, Mg^{2+}, Fe^{2+}, Mn^{2+}, Ca^{2+}, Na^{+} and K^{+}, using the method proposed by Leake (1978). Values for FeO determined by volumetric titration on three hornblende separates (87-34-03, 87-32-01 and 88-JR-16-4A) were applied to the analyses as a means of allocating Fe_2O_3 and FeO. The FeO content of the secondary (actinolite) amphiboles was not determined.

The four types of amphiboles, distinguished by field occurrence and petrography are: i) post-cumulus to sub-solidus hornblende, which replaces diopside in the pyroxenitic and syenodioritic rocks at their contact, ii) bladed to pegmatitic amphibole occurring in veins at this contact zone, iii) acicular hornblende in modally-layered hornblende gabbros and, iv) actinolitic fringes on altered diopside. All four types are monoclinic calcic amphiboles (Fig. 5.16)—according to the terminology used by Rock and Leake (1984)—distinguished by $(Ca+Na)_B \geq 1.34$ and $Na_B < 0.67$.

a) Replacement amphibole:

The amphibole that occurs at the contact between the ultramafic rocks with the gabbro to syenodiorite, is a green-tan pleochroic hornblende which appears to replace diopside along fractures, cleavages and grain boundaries and as tiny, optically continuous patchy grains within the interior of the pyroxene (plate 2.2). These amphiboles are characterized by low SiO_2 (39.2-42.8 %), moderate TiO_2 (1.83-2.25%), high Al_2O_3 (11.4-13.9) and CaO (11.6-12.1%)

Table 5.7

Composition of amphibole determined by electron microprobe.

	Sample	87-34-02	87-34-2	87-34-02	87-34-03	87-34-3	87-32-01	87-34-03	87-34-03
	Lithology type	pxt/gb contact replacement	pxt/gb contact replacement	pxt/gb contact replacement	pxt/gb contact replacement	pxt/gb contact replacement	pxt/gb contact replacement	pxt/gb contact replacement	pxt/gb contact replacement
	Target no.	109	110	111	112	113	125	118	115
Weight %	SiO_2	39.8	40.4	39.8	39.2	40.3	42.8	40.2	40.7
	TiO_2	2.17	1.83	1.91	2.08	2.13	2.07	2.20	2.15
	Al_2O_3	12.7	12.1	13.1	13.9	12.8	11.8	12.8	11.8
	Fe_2O_3	7.9	8.8	7.9	8.1	8.1	4.3	8.5	8.6
	FeO	7.5	8.3	7.4	7.7	7.7	7.6	8.0	8.1
	MnO	0.17	0.20	0.26	0.30	0.26	0.24	0.28	0.25
	MgO	11.7	11.0	12.0	11.5	11.4	13.4	10.9	11.1
	CaO	12.1	11.7	12.1	11.7	11.8	11.9	11.6	11.8
	Na_2O	2.02	1.95	2.02	2.23	1.97	2.04	2.03	2.07
	K_2O	1.32	1.36	1.26	1.40	1.41	0.91	1.33	1.35
Total		96.7	97.2	97.3	97.7	97.1	96.8	97.2	97.2
100Mg/(Mg+Fe)		59	54	59	57	57	67	55	55
Molecular proportions	Si^{4+}	5.949	6.046	5.922	5.829	5.992	6.299	5.99	6.071
	$^{iv}Al^{3+}$	2.051	1.954	2.078	2.171	2.008	1.701	2.01	1.929
	T site =	**8**	**8**	**8**	**8**	**8**	**8**	**8**	**8**
	$^{vi}Al^{3+}$	0.187	0.181	0.22	0.266	0.236	0.346	0.238	0.146
	$^{vi}Fe^{3+}$	0.889	0.992	0.885	0.907	0.907	0.477	0.954	0.96
	Ti^{4+}	0.244	0.206	0.214	0.233	0.238	0.229	0.247	0.241
	Mg^{2+}	2.607	2.454	2.662	2.549	2.527	2.94	2.421	2.468
	Fe^{2+}	0.938	1.039	0.921	0.958	0.958	0.935	0.997	1.01
	Mn^{2+}	0.0215	0.025	0.033	0.038	0.033	0.03	0.035	0.316
	Ca^{2+}	0.000	0.103	0.065	0.049	0.101	0.043	0.108	0.143
	C site =	**5.000**	**5.000**	**5.000**	**5.000**	**5.000**	**5.000**	**5.000**	**5.000**
	Fe^{2+}								
	Mn^{2+}								
	Ca^{2+}	1.824	1.773	1.864	4.902	1.779	1.834	1.744	1.743
	Na^{+}	0.176	0.227	0.136	0.098	0.221	0.166	0.256	0.257
	B site =	**2.000**	**2.000**	**2.000**	**2.000**	**2.000**	**2.000**	**2.000**	**2.000**
	Na^{+}	0.41	0.339	0.447	0.545	0.347	0.416	0.331	0.342
	K^{+}	0.252	0.26	0.239	0.266	0.268	0.171	0.253	0.26
	A site =	**0.662**	**0.599**	**0.686**	**0.811**	**0.615**	**0.587**	**0.584**	**0.602**

Table 5.7

Composition of amphibole determined by electron microprobe.

	Sample	87-32-01	87-34-03	87-34-03	87-34-03	87-34-3	87-34-03	88-16-4a	88-16-4a
	Lithology type	pxt/gb contact replacement	pxt/gb contact replacement	pxt/gb contact replacement	pxt/gb contact replacement	pxt/gb contact vein	pxt/gb contact pegmatitic	hb gabbro acicular	hb gabbro acicular
	Target no.	126	117	119	120	121	127	131	132
Weight %	SiO_2	42.4	40.9	41.5	40.5	40.8	42.3	40.1	40.2
	TiO_2	2.22	2.25	2.10	2.14	2.11	2.01	3.17	3.28
	Al_2O_3	11.4	12.7	11.7	12.6	12.7	12.0	13.8	13.7
	Fe_2O_3	4.4	8.4	8.4	8.0	8.0	6.8	2.1	2.1
	FeO	7.5	7.9	8.0	7.4	7.4	6.3	8.0	8.0
	MnO	0.28	0.21	0.31	0.29	0.21	0.26	0.09	0.13
	MgO	14.0	11.0	11.1	11.7	11.8	13.3	14.8	15.0
	CaO	11.8	11.7	12.0	11.9	12.0	12.0	12	11.7
	Na_2O	2.13	2.05	1.93	1.98	2.09	2.12	2.7	2.76
	K_2O	1.03	1.38	1.31	1.29	1.35	0.94	0.32	0.34
Total		96.8	98.0	97.7	98.3	98.0	97.8	97.6	98.7
100Mg/(Mg+Fe)		68	56	55	58	59	65	73	73
Molecular proportions	Si^{4+}	6.257	6.041	6.142	6.013	6.017	6.183	5.903	5.907
	$^{iv}Al^{3+}$	1.743	1.959	1.858	1.987	1.983	1.817	2.097	2.093
	T site =	**8**	**8**	**8**	**8**	**8**	**8**	**8**	**8**
	$^{vi}Al^{3+}$	0.236	0.253	0.184	0.219	0.225	0.251	0.298	0.28
	$^{vi}Fe^{3+}$	0.488	0.934	0.936	0.894	0.888	0.748	0.233	0.232
	Ti^{4+}	0.246	0.25	0.234	0.239	0.234	0.221	0.351	0.363
	Mg^{2+}	3.073	2.422	2.449	2.59	2.594	2.898	3.248	3.286
	Fe^{2+}	0.924	0.976	0.99	0.919	0.913	0.77	0.87	0.839
	Mn^{2+}	0.033	0.026	0.039	0.037	0.026	0.032	0	0
	Ca^{2+}	0.000	0.139	0.168	0.102	0.120	0.080	0.000	0.000
	C site =	**5.000**	**5.000**	**5.000**	**5.000**	**5.000**	**5.000**	**5.000**	**5.000**
	Fe^{2+}							0.115	0.144
	Mn^{2+}	0.002						0.011	0.016
	Ca^{2+}	1.862	1.713	1.735	1.791	1.776	1.799	1.893	1.842
	Na^{+}	0.136	0.287	0.265	0.209	0.024	0.201	0.000	0.000
	B site =	**2.000**	**2.000**	**2.000**	**2.000**	**2.000**	**2.000**	**2.019**	**2.002**
	Na^{+}	0.472	0.3	0.289	0.361	0.574	0.4	0.771	0.786
	K^{+}	0.194	0.26	0.247	0.244	0.254	0.175	0.003	0.064
	A site =	**0.666**	**0.560**	**0.536**	**0.604**	**0.828**	**0.575**	**0.781**	**0.898**

Table 5.7

Composition of amphibole determined by electron microprobe.

	Sample	87-34-03	87-32-01	87-32-01	87-32-01	87-32-01	87-18-01
	Lithology type	fibrous	fibrous	fibrous	fibrous	fibrous	fibrous
	Target no.	114	128	129	130	130.5	135
Weight %	SiO_2	52.1	53.9	53.3	53.3	51.1	51.3
	TiO_2	0.07	0.01	0.07	0.12	0.00	0.10
	Al_2O_3	2.7	1.9	2.26	2.29	3.32	2.97
	Fe_2O_3	0.0	0.0	0.0	0.0	0.0	
	FeO	11.7	10.9	11.9	10.7	10.3	11.0
	MnO	0.52	0.38	0.35	0.44	0.24	0.76
	MgO	16.2	17.0	16.2	17.3	17.4	16.5
	CaO	12.4	12.3	12.2	12.4	12.1	12.3
	Na_2O	0.56	0.46	0.66	0.62	0.75	0.38
	K_2O	0.10	0.12	0.18	0.14	0.14	1.35
Total		96.4	97.2	97.1	97.4	96.1	95.8
100Mg/(Mg+Fe)		70	73	70	73	75	73
Molecular proportions	Si^{4+}	7.617	7.767	7.714	7.666	7.505	7.588
	$^{iv}Al^{3+}$	0.383	0.233	0.286	0.334	0.495	0.412
	T site =	**8**	**8**	**8**	**8**	**8**	**8**
	$^{vi}Al^{3+}$	0.079	0.086	0.1	0.054	0.08	0.104
	$^{vi}Fe^{3+}$						
	Ti^{4+}	0.008	0.001	0.008	0.013		0.011
	Mg^{2+}	3.531	3.652	3.495	3.709	3.809	3.624
	Fe^{2+}	1.382	1.261	1.397	1.224	1.111	1.261
	Mn^{2+}	0	0	0	0	0	0
	Ca^{2+}	0.000	0.000	0.000	0.000	0.000	0.000
	C site =	**5.000**	**5.000**	**5.000**	**5.000**	**5.000**	**5.000**
	Fe^{2+}	0.049	0.053	0.043	0.063	0.154	0.094
	Mn^{2+}	0.064	0.046	0.043	0.054	0.03	0.095
	Ca^{2+}	1.943	1.899	1.892	1.911	1.904	1.942
	Na^{+}	0.000	0.002	0.022	0.000	0.000	0.000
	B site =	**2.056**	**2.000**	**2.000**	**2.028**	**2.088**	**2.131**
	Na^{+}	0.159	0.127	0.163	0.173	0.214	0.109
	K^{+}	0.019	0.022	0.033	0.026	0.026	0.036
	A site =	**0.144**	**0.149**	**0.196**	**0.172**	**0.212**	**0.169**

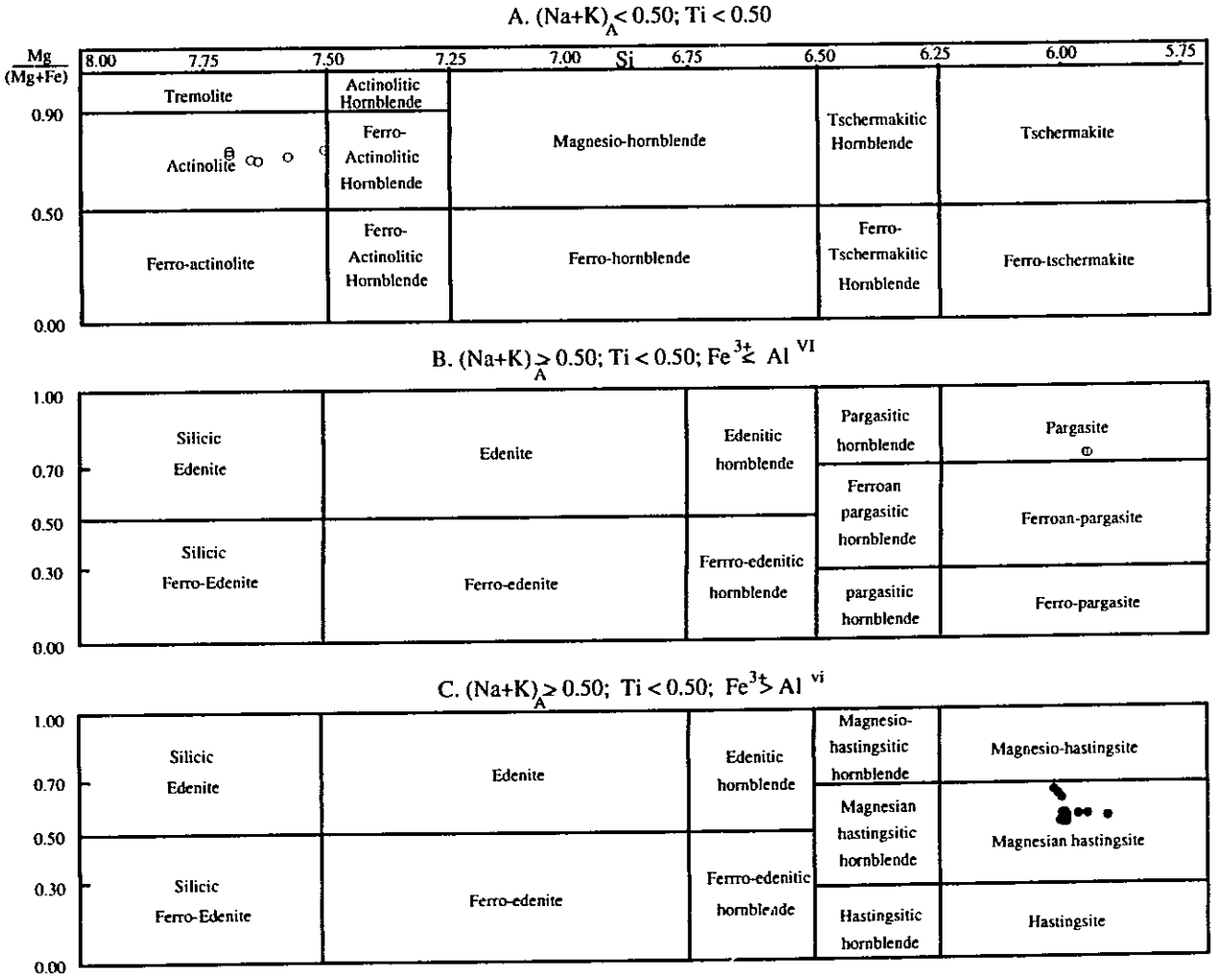

Figure 5.16. Classification of calcic amphiboles from the Tulameen complex (from Rock and Leake, 1984).
○=Fibrous secondary amphibole ●=Replacement, vein and pegmatitic amphibole ◎=Acicular amphibole

and high $Fe^{3+}/(Fe^{3+}+Fe^{2+})$ (0.97 and 0.52). Magnesium ratios, 100Mg/(Mg+Fe), are variable from 55 to 68. All but two of these replacement amphiboles plot within Rock and Leake's (1984) field for magnesio-hastingsite (Fig. 5.16). Analyses from sample JR-32-01 plot in the field for magnesio-hastingsitic hornblende.

b) Vein and pegmatitic amphibole:

The coarse-grained bladed and large poikilitic amphibole, that occurs in irregular, vein-like concentrations, at the contact between the ultramafic and gabbroic rocks, is indistinguishable in composition from the replacement-type of amphibole, which occurs within the same thin-sections. All analyses of this vein amphibole are magnesio-hastingsite to magnesio-hastingsitic hornblende in composition (Fig. 5.16), characterized by low SiO_2 (39.2 to 42.2 wt. %), high Al_2O_3 (11.8 to 13.9 wt. %), CaO (11.7 to 12.0) and low TiO_2 (2.08 to 2.22 wt. %). A chemical zonation from core to rim was detected in sample 87-34-03, demarked by a slight increase in SiO_2 (39.2 to 40.3 wt. %) and decrease in Al_2O_3 (13.9 to 12.8 wt. %).

c) Acicular amphibole:

The amphibole that constitutes the main mafic phase in a modally-layered hornblende gabbro, is characterized by an acicular habit, green-brown pleochroism and green-brown core to rim colour zonation. The microprobe analyses (targets 131 and 132; Table 5.7) reveal higher Al_2O_3 (13.7 to 13.8 wt. %) and TiO_2 (3.17 to 3.28 wt. %) and lower SiO_2 (40.1 to 40.2 wt. %) and K_2O (0.32 to o.34 wt. %) than the replacement or vein amphibole. A lower $Fe^{3+}/^{vi}Al$ contents makes these amphiboles pargasites, as opposed to magnesio-hastingsites (Fig. 5.16).

d) Fibrous amphibole:

The fourth type of amphibole analyzed from rocks of the Tulameen complex is a yellow to blue-green pleochroic fibrous mineral which forms a rim around relict pyroxene cores in all

of the pyroxene-bearing rocks. This variety is an aluminum-poor, calcium-rich amphibole, with 100Mg/(Mg+Fe) of 70-73 and is classified as actinolite (Rock and Leake, 1984).

Interpretation of amphibole analyses:

The similarity in composition between the amphibole formed at the expense of pyroxene, and those occurring as veins and pegmatitic bodies at the periphery of the ultramafic rocks, is interpreted as reflecting their formation as post-cumulus phases in both cases. The replacement of diopside by patchy grains of amphibole is well documented in ultramafic and mafic cumulate rocks in arc-related igneous complexes (Arculus and Wills, 1980; Conrad and Kay, 1984 and Foden and Green, 1992). Amphibole in arc plutonic rocks also occurring as xenocrysts, phenocrysts and xenoliths in mafic island arc lavas, is of the pargasite and magnesio-hastingsite variety, distinguished by low SiO_2, and high Al_2O_3, CaO and alkalies (Fig. 5.17). Although there is a consensus that hornblende is a postmagmatic phase that replaced pyroxene, as it became unstable during the cooling and equilibration of the the ultramafic and mafic cumulate rocks with ascent into shallower crustal levels, views differ as to the nature of the phase with which the pyroxene is in reaction. Charlton (1979) attributed the formation of hornblende-rich rocks, which occur along the periphery of the Ironside Mountain complex, to the reaction between hot clinopyroxene-rich ultramafic to gabbroic crystal mushes and meteoritic water, introduced along the margins of the cooling pluton. Taylor and Noble (1969), James (1971), Snoke et al.(1982) and Best (1975) favor an hydrous intercumulate silicate melt as the reactant. According to Wallace and Green (1991), the formation of pargasitic amphibole by Al, Ti, Fe and Na metasomatism of diopside is a natural consequence of the crystallization of a water-bearing, alkali-rich melt during the upwards migration and solidification of water-bearing ultramafic assemblages. This view is in agreement with a chemical reaction derived by Taylor and Noble (1969) for the formation of hornblende in Alaskan-type complexes.

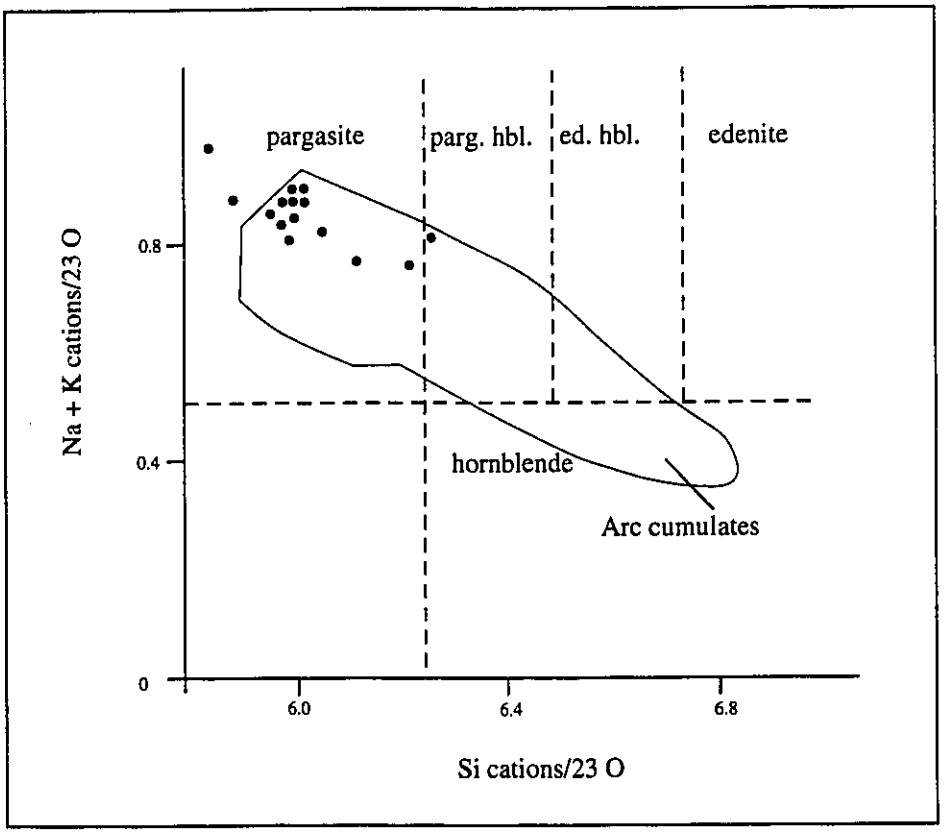

Figure 5.17. Plot of Tulameen hornblendes with respect to the compositional field of hornblende in arc cumulates (from Beard and Barker, 1989).

$$\mathbf{76Px} + 7Mt + 8Al_2O_3 + Na_2O + 0.3K_2O + 1.7H_2O = \mathbf{87Hb} + 7CaO$$

(Taylor and Noble, 1969)

Springer (1989) interprets the subsolidus replacement of pyroxene by hornblende in the Pine Hill intrusive complex as indicating the progressive fluid enrichment of the parent melt. On the basis of textural evidence, he argues that hornblende (and biotite) occurred in equilibrium with a residual (intercumulus) hydrous fluid phase as opposed to an intercumulus silicate melt. Drawing from his observations of peripheral pegmatitic hornblende bodies in the Skaergaard and Duke Island ultramafic to gabbroic bodies, Irvine (1986) proposed that hornblende originated by infiltration metasomatism of the pyroxene-rich cumulates by upward seepage of silicate liquid and associated vapors from the feeder system. The nature of the infiltrating fluids—hydrothermal or intercumulate silicate melts—is uncertain (Irvine, 1986). Recently, Foden and Green (1992) have proposed a model to account for the occurrence of amphiboles (of the pargasite-hastingsite group) in mafic island arc lavas and Alaskan-type zones ultramafic complexes by the reaction between cooling hydrous mafic liquid and anhydrous ferromagnesian phases (either earlier formed olivine and clinopyroxene cumulates or peridotite wall rock). The stability of the amphibole phase, determined by experiments in the system high-Al basalt (HAB)-water (Foden and Green, 1992) is optimized by isobaric, equilibrium crystallization in a closed system at upper mantle (25-30 km) depths.

The replacement of tremolite fringed-diopside crystals by unaltered hornblende (plate 2.2) indicates that the formation of hornblende followed the alteration of diopside to tremolite.

The association of abundant apatite crystals and lenses of magnetite with the pegmatitic hornblende-rich rocks, indicates the presence of a volatile phase during the formation of hornblende. The magnesio-hastingsite of the Tulameen complex is considered to form at near-magmatic temperatures, suggested by the high crystallization temperatures experimentally produced for magnesio-hastingsite (775-1050°C; Wones and Gilbert, 1981) and an Ar-Ar

hornblende plateau age of 207.5 Ma (McDougall, 1974; recalculated using new decay constants from Steiger and Jäger, 1977) which is contemporaneous with the U-Pb crystallization age for the syenodiorite of ~ 210 Ma.

The acicular pargasitic amphibole in the layered gabbro is interpreted as magmatic amphibole which crystallized in a hydrous basaltic dyke. The high Cr, V, Ni contents support a primary magmatic origin for this amphibole.

Discussion of chemical petrology and mineralogy of the Tulameen complex

The most striking feature of the chemical petrology and iron-magnesium silicate mineralogy of the Tulameen complex is the significance of H_2O in its genesis. Evidence for high H_2O contents include the enrichment of aqueous mobile elements (Ba, Sr, K, Rb) in the whole rock chemistry as well as the order of crystallization and chemistry of the major phases. Magnesium-rich olivines and clinopyroxenes dominate the mineralogy of the cumulate rocks. Early crystallizing cumulus chromite—which contains inclusions of primary hydrous silicate phases (Talkington et al., 1986)—pyroxenes and post-cumulate hornblende are characterized by high ferric iron contents which suggests the oxidation of iron and early crystallization of Fe^{3+}-rich oxides by elevated water contents Another compelling clue for the involvement of water is the aluminum-enrichment trend observed in the pyroxenes which has been interpreted by Conrad and Kay (1984) as reflecting crystallization of pyroxene from progressively more hydrous melts.

Water not only enhances partial melting in the subduction zone by depressing the liquidus temperatures of the anhydrous phases (Wyllie, 1979), but also facilitates the transport of the mobile trace elements (LILE, LREE; Tastumi et al., 1986; Tatsumi, 1989) which give island arc magmas their distinctive chemical signature. The effect of the elevated water activity in subduction-zone generated mafic magmas has dramatic effects on the mineral compositions and crystallization sequence. Addition of water lowers the $aSiO_2$ in the melt which enhances

the stability fields of olivine and diopside relative to enstatite and plagioclase (Yoder and Tilley, 1962; Loucks, 1990). The high aAl_2O_3 in the hydrous melt stabilizes high-Ca pyroxene by the formation of Ca-Tschermak's molecule (Sisson and Grove, 1993). Arc cumulate suites—in particular Alaskan-type complexes, Aleutian plutonic suite and the Tulameen complex—are exquisite examples in nature of these experimentally deduced relations. More recently, attention has been focused on arc cumulates as natural evidence for the processes involved in subduction-zone magmatism and their possible role in the genesis of andesite in arc environments (Foden and Green, 1992; Sisson and Grove, 1993; Draper and Johnston, 1992; Brophy, 1988)

Figure 5.18 shows the interpreted tectonic setting of the Tulameen complex as an island arc. It is proposed, that following extraction of the parental magma from the hydrated mantle wedge, olivine, clinopyroxene and spinel fractionated to form the ultramafic cumulate rocks in a deeper magma chamber below the crust-mantle boundary. The unzoned, uniform composition of olivine and clinopyroxene suggests equilibrium crystallization and slow cooling of the cumulates. As the magma body cooled, the earlier formed clinopyroxene and olivine crystals entered a reaction relationship with the hydrous melt (Foden and Green, 1992; Wallace and Green, 1991) or infiltrating fluid (Irvine, 1986), and produced pargasite. Plagioclase crystallization, inhibited by the presence of water (Foden and Green, 1992), was suppressed until the H_2O content of the magma decreased, the $aSiO_2$ increased or the magma body ascended and ponded at a lower pressure within the plagioclase stability field (approximately 2.5 kb at 5 wt. % H_2O content of the magma; Foden and Green, 1992).

Alternatively, the Tulameen complex may be a composite pluton made up of ultramafic cumulates from a deeper magma chamber juxtaposed during deformation of the arc against a shallower level (feldspar-rich) pluton.

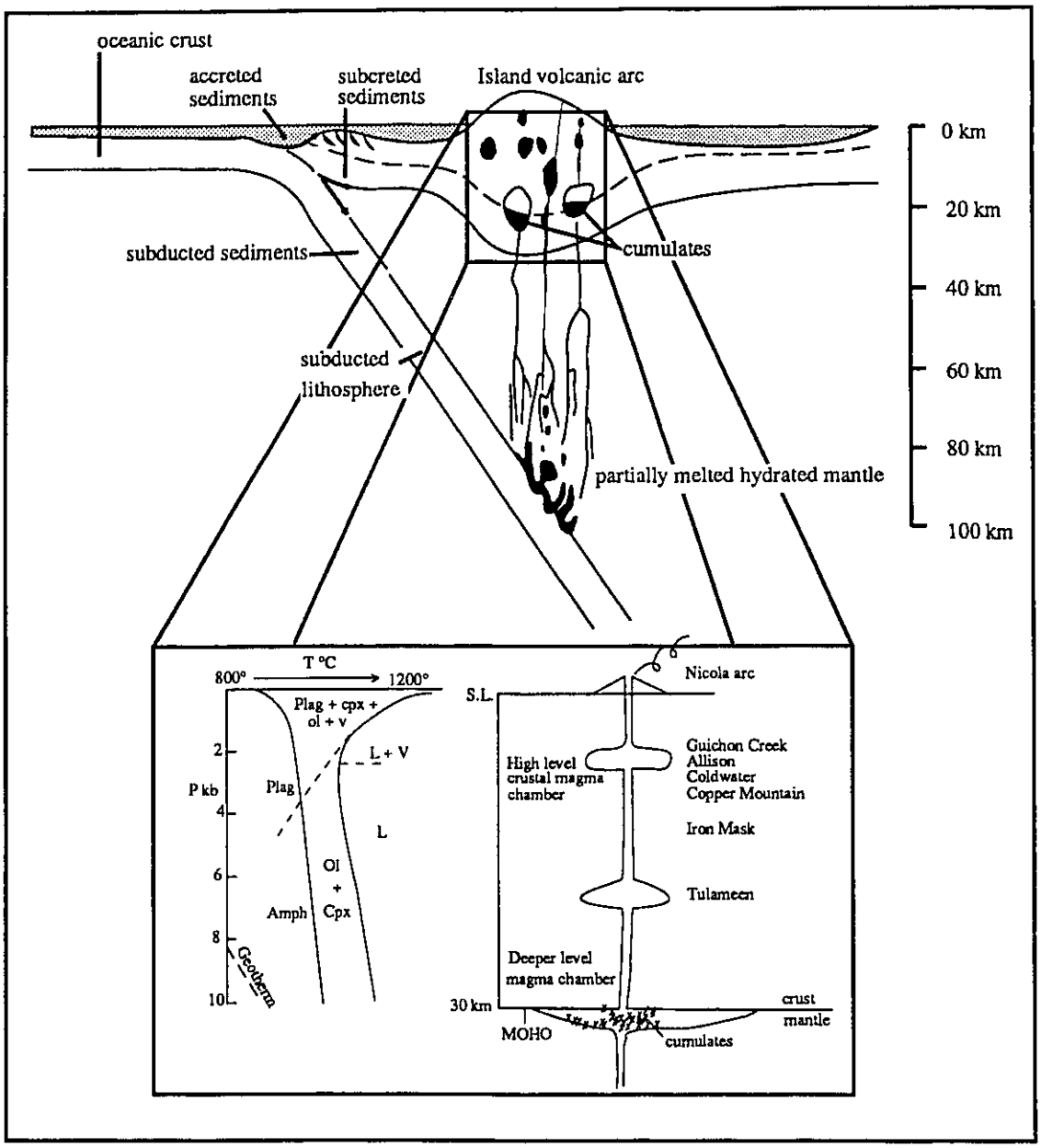

Figure 5.18. Interpreted tectonic setting of the Tulameen complex. The simplified crustal section of an island arc (modified after Wilson, 1989) illustrates the polybaric nature of magmatism above a subduction zone. The generalized phase diagram (modified after Foden and Green, 1992) relates to the high-Al basalt system with 5% H_2O. The mineral chemistry of the Tulameen complex is consistent with crystallization at mid-crustal levels. Also shown is a diagrammatic plutonic stratigraphy for the Nicola arc during its Late Triassic to Early Jurassic evolution.

Conclusions.

The mineral chemistry of the mafic silicate phases of the Tulameen complex has provided the most insight into the petrogenesis of the ultramafic to syenodioritic body. The chemical trends observed in olivine, diopside and hornblende are consistent with the crystallization of the Tulameen complex in a hydrous environment, under relatively high fO_2. Trace element chemistry of the representative rock-types exhibit a subduction-zone signature and rare earth element patterns indicate a calc-alkaline affinity of the magma.

The interpreted crystallization age of 209.9 ± 4.7 Ma (U-Pb zircon) for the syenodiorite is a minimum crystallization age for the Tulameen complex. An ^{40}Ar-^{39}Ar hornblende plateau age of 207.4 Ma , obtained by McDougall (1974) on the syenogabbro, implies that the feldspathic part of the Tulameen complex cooled below 550°C (the closure temperature of hornblende for argon; McDougall and Harrison, 1988) shortly after the crystallization of the syenodiorite. The U-Pb zircon age confirms the contemporaniety between the Tulameen complex and the several other calc-alkaline to alkaline plutons— characterized by low initial $^{87}Sr/^{86}Sr$ ratios (0.7036-0.7039; Preto et al., 1979; Mortimer, 1987) and K-Ar and Rb-Sr isochron ages ranging from 205-220 Ma (Armstrong, 1988)—spatially associated with the Nicola Group. These Late Triassic to Early Jurassic plutons have been interpreted by Mortimer (1987) as representing the final culmination of Nicola-related magmatism. K-Ar cooling ages of 210-190 Ma (Mortimer et al., 1990) from sericites in structurally-controlled mineralized veins associated with the dextral Lornex and Highland Valley faults—which control the emplacement of the 210 ± 3 Ma (Mortimer et al., 1990) Guichon Creek batholith—suggest that the demise of Nicola arc coincided with deformation.

The schematic cross-section of the Nicola arc, during the Late Triassic to Early Jurassic, shown in Fig. 5.17, depicts a complex plumbing system with ponding of magma at various levels of the crust. The polybaric evolution of the Nicola arc is interpreted from

contemporaneous alkaline and calc-alkaline magmatism and exposures of mantle-derived ($^{187}Os/^{186}Os$ =1.011-1087; Hattori and Hart, 1992) ultramafic cumulates of the Tulameen complex. According to experimental work by Foden and Green (1992), andesitic liquids in arcs are derived by the reaction between early formed arc cumulates and cooling hydrous mafic liquid. Pressure, temperature and water content of the magma can dictate the composition of the derived liquids. At deeper crustal pressures (10 kb) and hydrous conditions (~5% H_2O), clinopyroxene is the stable Fe-Mg silicate phase and the liquids produced by the reaction between the clinopyroxene-rich cumulates and hydrous basaltic melt will be less silica-rich that the liquids produced from cumulates crystallized at lower pressures (5-7.5 kb) within the olivine and clinopyroxene stability fields. The more alkaline, clinopyroxene-rich plutons (Tulameen, Copper Mountain and Iron Mask) may represent a deeper magma source than the calc-alkaline plutons (Guichon Creek, Allison and Coldwater).

The faulted margins of the Tulameen complex, lack of metamorphic aureole within the country rocks, the absence of Tulameen dykes within the Nicola Group rocks, and inclusions of country rock at the margins of the plutonic body, all indicate that the Tulameen complex has been tectonically transported relative to its original setting. The margins of the Tulameen complex are northwest-striking mylonitic shear zones—characterized by sub-horizontal stretching lineations—which extend along strike of the ultramafic-syenodioritic body and envelope several smaller ultramafic bodies along strike to the northwest and southeast of the Tulameen complex. The sense of shear along the northwest-trending ductile faults is dextral.

The difference in K-Ar hornblende data between the Tulameen complex (196-208; Roddick and Farrar, 1971) and the Eagle plutonic complex and bordering schists (110.5 ± 2, 117 ± 4 and 130 ± 4 Ma; Greig et al., 1992; Fig. 4.1) and structural fabrics (i.e. northeasterly-verging contractional structures with west to southeast directed lineations in the Eagle shear zone versus consistent northwest directed stretching lineations measured in the mylonitic shear

zones in the Tulameen area (Fig. 3.3) implies that the Eagle and Tulameen complexes have experienced different structural and thermal histories prior to the middle Cretaceous. It is postulated that the formation of the northwest-trending ductile fabric in the Tulameen complex is genetically unrelated to the Middle Jurassic deformation associated with the Eagle shear zone, as proposed by Greig (1992). If deformation of the Tulameen complex is syn-intrusive—as suggested by the closed system behavior of the hornblendes for argon (McDougall, 1974) and confinement of the post-cumulus hornblende to the ductile structures—the dextral shearing of the Tulameen complex may represents a deeper structural equivalent of the dextral faulting associated with the emplacement of the Guichon Creek batholith (Hollister et al., 1975).

Tertiary brittle faults disrupt all units within the Hope-Princeton area and have further modified the map pattern of the Tulameen complex.

References.

Akrigg, G.P.V. and Akrigg, H.B. 1969. 1001 British Columbia place names. Discovery Press, Vancouver.

Akrigg, G.P.V. and Akrigg, H.B. 1970. British Columbia Chronicle 1847-1987, Gold & Colonists. Discovery Press, Vancouver.

Aoki, K.I. 1971. Petrology of mafic inclusions from Itinome-gata, Japan. Contributions to Mineralogy and Petrology, 30: 314-331.

Aoki, K.I. and Kushiro, I. 1968. Some clinopyroxenes from ultramafic inclusions in Dreiser Welher, Eifel. Contributions to Mineralogy and Petrology, 18: 326-337.

Arculus, R.J. and Wills, K.J.A. 1980. The petrology of plutonic blocks and inclusions from the Lesser Antilles Island arc. Journal of Petrology, 21: 743-799.

Armstrong, R.L. 1988. Mesozoic and early Cenozoic magmatic evolution of the Canadian Cordillera; In Processes in Continental Lithosphere Deformation. Edited by S.P. Clark. Jr., B.C. Burchfiel, and J. Suppe. Geological Society of America, Special Paper 218 , pp 55-91.

Barr, D.A., Fox, P.E., Northcote, K.E. and Preto, V.A. 1976. The alkaline suite porphyry deposits—a summary. In Deposits of the Canadian Cordillera. Edited by A. Sutherland Brown. Canadian Institute of Mining and Metallurgy, Special Volume 15, pp. 359-367.

Bau, M. and Knittel, U. 1993. Significance of slab-derived partial melts and aqueous fluids for the genesis of tholeiitic and calc-alkaline island-arc basalts: Evidence from Mt. Arayat, Philippines. Chemical Geology, 105: 233-251.

Beard, J.S. and Barker, Fred 1989. Petrology and tectonic significance of gabbros, tonalites, shoshonites and anorthosites in a late Paleozoic arc-root complex in the Wrangellia terrane, southern Alaska. Journal of Geology, 97: 667-683.

Bence, A.E., Cameron, K. and Papike, J.J. 1970. Sector zoning in calcic clinopyroxenes. Transactions of the American Geophysical Union, 51: 435.

Best, M.G. 1975. Amphibole-bearing cumulate inclusions, Grand Canyon, Arizona and their bearing on silica-undersaturated hydrous magmas in the upper mantle. Journal of Petrology, 16: 212-236.

Brophy, J.G. 1988. Basalt convection and plagioclase retention: a model for the generation of high-alumina basalt. Journal of Geology, 98: 319-329.

Brown, G.E. 1982. Olivines and silicate spinels. In Orthosilicates. Edited by: P.H. Ribbe. Reviews in Mineralogy, 5: 275-365.

Bryan, L. 1981. Backroads of British Columbia. Sunflower Books, Vancouver.

Burns, L.E. 1985. The Border Ranges ultramafic and mafic complex, south-central Alaska: cumulate fractionates of island-arc volcanics. Canadian Journal of Earth Sciences, 22: 1020-1038.

Butler, J.R. 1989. Review and classification of ultramafic bodies in the Piedmont of the Carolinas. In Ultramafic rocks of the Appalachian Piedmont. Edited by Geological Society of America Special Paper, 231: 19-32.

Cabri, L.J., Owens, D.R. and LaFlamme, J.H.G. 1973. Tulameenite, a new platinum-iron-copper mineral from placers in the Tulameen River area, British Columbia. Canadian Mineralogist: 12: 380-384.

Cameron, M. and Papike, J.J. 1981. Structural and chemical variations in pyroxenes. American Mineralogist, 66: 1-50.

Campbell, R.B. and Tipper, H.W. 1971. Geology of Bonaparte Lake map-area, British Columbia. Geological Survey of Canada, Memoir 249.

Camsell, C. 1913. Geology and Mineral Deposits of the Tulameen District, British Columbia. Geological Survey of Canada, Memoir 26.

Charlton, D. 1979. Geology of part of the Ironside Mountain quadrangle, northern California, Klamath Mountains. Ph.D thesis, University of California, Santa Barbara.

Clark, T. 1980. Petrology of the Turnagain ultramafic complex, northwestern British Columbia. Canadian Journal of Earth Sciences, 17: 744-757.

Coleman, M.E. and Parrish, R.R. 1991. Eocene dextral strike-slip and extensional faulting in the Bridge River terrane, southeastern British Columbia. Tectonics, 10: 1222-1258.

Coleman, R.G. 1977. Ophiolites: Ancient oceanic lithosphere? New York, Springer-Verlag, 229 p.

Coleman, R.G. and Keith, T.E. 1971. A chemical study of serpentinization, Bruno Mountains, California. Journal of Petrology, 12: 311-328.

Conrad, W.K. and Kay, R.W. 1984. Ultramafic and mafic inclusions from Adak Island: Crystallization history, and implications for the nature of primary magmas and crustal evolution in the Aleutian arc. Journal of Petrology, 25: 88-125.

Dawson, G.M. 1879. Report on exploration in the southern portion of British Columbia. Geological Survey of Canada, Report of Progress for 1877-1878, pp. 1B-173B.

Debari, S.M. and Coleman, R.G. 1989. Examination of the deep levels of an island arc: evidence from the Tonsina ultramafic-mafic assemblage, Tonsina, Alaska. Journal of Geophysical Research, 94: 4373-4391.

Debari, S.M., Kay, S.M. and Kay, R.W. 1987. Ultramafic xenoliths from Adagdak volcano, Adak, Aleutian Islands, Alaska: Deformed igneous cumulates from the Moho of an Island arc. Journal of Geology, 95: 329-342.

Deer, W.A., Howie, R.A. and Zussman, J. 1978a. Orthosilicates. Rock-forming minerals, Volume 1A, 2d edition. John Wiley and Sons, New York.

Deer, W.A., Howie, R.A. and Zussman, J. 1978b. Single-chain silicates. Rock-forming minerals, Volume 2A, 2d edition. John Wiley and Sons, New York.

Donaldson, J.R. 1973. The petrology of the coal from the Blakeburn strip mine in the Tulameen coal area, British Columbia. Geological Survey of Canada, Paper 72-39.

Downes, M.J. 1974. Sector and auxillatory zoning in calcic augites from Mt. Etna, Sicily. Contributions to Mineralogy and Petrology, 47: 187-196.

Dowty, E. 1976. Crystal structure and crystal growth: II. Sector growths in minerals. American Mineralogist, 61: 460-469.

Draper, D.S. and Johnston, A.D. 1992. Anhydrous phase relations of an Aleutian high-MgO basalt: an investigation of the role of olivine-liquid reaction in the generation of arc high-alumina basalts. Contributions to Mineralogy and Petrology, 112: 501-519.

Duda, A. and Schmincke, H.-U. 1987. Polybaric differentiation of alkali basaltic magmas: evidence from green-core clinopyroxenes (Eifel, FRG). Contributions to Mineralogy and Petrology, 91: 340-353.

Duncan, A. M. 1974. Chemical variation of clinopyroxene phenocrysts from trachybasaltic lavas from Mt. Etna. Mineralogical Magazine, 43: 765

Eastwood, G.E.P. 1959. Magnetite in Lodestone Mountain stock. British Columbia Department of Mines, Annual Report, 1960, pp 39-53.

Eastwood, G.E.P. 1961. Tulameen: Lawless Creek area. British Columbia Ministry of Mines, Annual Report, 1960, pp.42-55.

Eldson, R. 1971.Clinopyroxenes from the upper layered series Kap Edvard Holm, East Greenland. Mineralogical Magazine, 38: 49-57.

Ewing, T.E. 1980. Paleogene tectonic evolution of the Pacific northwest. Journal of Geology, 88: 619-638.

Ferguson, A.K. 1973. On hourglass-sector zoning in clinopyroxene. Mineralogical Magazine, 39: 321-325.

Ferguson, A.K. 1978. Ca-enrichment in olivines from volcanic rocks. Lithos, 11: 189-194.

Findlay, D.C. 1963. Petrology of the Tulameen Ultramafic Complex, Yale District, British Columbia. Ph.D. thesis, Queen's University, Kingston, Ontario.

Findlay, D.C. 1969. Origin of the Tulameen ultramafic-gabbro complex, southern British Columbia. Canadian Journal of Earth Sciences, 6: 399-425.

Fleet, M.E. 1975. Growth habits of clinopyroxene. Canadian Mineralogist, 13: 336-341.

Foden, J.D. and Green, D.H. 1992. Possible role of amphibole in the origin of andesite: some experimental and natural evidence. Contributions to Mineralogy and Petrology, 109: 479-493.

Frebold, H. and Tipper, H.W. 1969. Lower Jurassic rocks and fauna near Ashcroft, British Columbia and their relation to some granitic plutons. Geological Survey of Canada Paper 69-23.

Friedman, R.M. and van der Heyden, P. 1992. Late Permian U-Pb dates for the Farwell and Northern Mt. Lytton plutonic bodies, Intermontane belt, British Columbia. In Current research part A. Geological Survey of Canada, Paper 92-1A, pp. 137-144.

Gabrielse, H. (Comp.) 1992. Structural styles, Chapter 17 in Geology of the Cordilleran Orogen in Canada. Edited by H. Gabrielse and C.J.Yorath. Geological Survey of Canada, Geology of Canada, no.4, pp. 571-675.

Gabrielse, H. and Yorath, C.J. 1992. Tectonic synthesis, Chapter 18 in Geology of the Cordilleran Orogen in Canada. Edited by H. Gabrielse and C.J.Yorath. Geological Survey of Canada, Geology of Canada, no.4, pp. 677-705.

Gibb, F.G.F. 1973. The zoned clinopyroxenes of the Shiant Isles Sill, Scotland. Journal of Petrology, 4: 203-230.

Gill, J.B. 1981. Orogenic andesites and plate tectonics. Springer-Verlag, New York, N.Y.

Goodharzi, F. and Van Der Flier-Keller. 1988. Organic petrology and depositional environment of a coal-bearing section from Blakeburn open cast mine in Tulameen, British Columbia. In Current research, part E, Geological Survey of Canada, Paper 88-1E, pp. 85-90.

Gray, F., Page, N.J., Carlson, C.A., Wilson, S.A. and Carlson, R.R. 1986. Platinum-Group element geochemistry of zoned ultramafic intrusive suites, Klamath Mountains, California and Oregon. Economic Geology, 81: 1252-1260.

Greig, C.J. 1992. Jurassic and Cretaceous plutonic and structural styles of the Eagle plutonic complex, southwestern British Columbia, and their regional significance. Canadian Journal of Earth Sciences, 29: 793-811.

Greig, C.J., Armstrong, R.L., Harakal, J.E , Runkle, D. and van der Heyden, P. 1992. Geochronometry of the Eagle plutonic complex and the Coquihalla area, southwestern British Columbia. Canadian Journal of Earth Sciences, 29: 812-829.

Greig, J.C. 1989. Geology and Geochronology of the Eagle plutonic complex, Coquihalla Area, Southwestern British Columbia. M.Sc. thesis, University of British Columbia, Vancouver.

Grove, T.L. and Bence, A.E. 1977. Experimental study of pyroxene-liquid interaction in quartz-normative basalt 15597. Proceedings of the 8th Lunar Science Conference : 1549-1579.

Hargraves, R.B., Hollister, L.S. and Otalora, G. 1970. Compositional zoning and its significance in pyroxenes from three coarse-grained lunar samples. Science, 176: 631-633.Harkins, E. and Hollister, L.S. 1977. Sector-zoning of clinopyroxene from a weakly metamorphosed diabase. American Mineralogist, 62: 390-394.

Harkins, E. and Hollister, L.S. 1977. Sector zoning of clinopyroxene from a weakly metamorphosed diabase. American Mineralogist, 62: 390-394.

Hart, S.R. and Dunn, T. 1993. Experimental cpx/melt partitioning of 24 trace elements. Contributions to Mineralogy and Petrology, 113: 1-8.

Hattori, K. and Hart, S.R. 1991. Osmium-isotopic ratios of platinum-group minerals associated with ultramafic intrusions: Os-isotopic evolution of the oceanic mantle. Earth and Planetary Science Letters, 107: 499-514.

Henderson, P. 1984. Rare earth element geochemistry. Edited by P. Henderson. Elsevier, Amsterdam. 510 p.

Himmelberg, G.R., Loney, R.A. and Craig, J.T. 1986. Petrogenesis of the ultramafic complex at Blashke Island, Southeast Alaska. United States Geological Survey, Bulletin 1662, 14 p.

Himmelberg, G.R., Loney, R.A. and Nabelek, P.L. 1987. Petrogenesis of gabbronorite at Yakobi and northwest Chichagof Islands, Alaska. Geological Society of America, Bulletin 98: 265-279.

Hollister, L.S. and Garcanz, A.Z. 1971. Compositional sector zoning in clinopyroxene from the Narce area, Italy. American Mineralogist 56: 959-979.

Hollister, L.S. and Hargraves, R.B. 1970. Compositional zoning and its significance in pyroxenes from two coarse-grained Apollo 11 samples. Apollo 11 Lunar Science Conference 1, pp. 541-550.

Hollister, V.F., Allen, J.M., Anzalone, S.A. and Seraphim, R.H. 1975. Structural evolution of porphyry mineralization at Highland Valley, British Columbia. Canadian Journal of Earth Sciences, 12: 807-820.

Hopson, C.A., Mattinson, J.M. and Pessagno, E.A. Jr. 1981. Coast Range ophiolite, Western California. In The Geotectonic development of California. Edited by W.G. Ernst. Prentice Hall, New Jersy.

Idiz, E.F. 1981. Geology of the Marble Canyon plutonic complex, Inyo County, California. M.Sc. thesis, University of California, Los Angeles.

Irvine, T.N. 1967. Chromian spinel as a petrogenetic indicator. II. Petrologic applications. Canadian Journal of Earth Sciences, 2: 648-672.

Irvine, T.N. 1974. Petrology of the Duke Island ultramafic complex, southeastern Alaska. Geological Society of America, Memoir 138.

Irvine, T.N. 1976. Alaskan-type ultramafic-gabbro bodies in the Aiken Lake, McConnel Creek, and Toodoggone map-areas. Geological Survey of Canada Paper 76-1A: 76-81.

Irvine, T.N. 1982. Terminology for layered intrusions. Journal of Petrology, 23: 127-162.

Irvine, T.N. 1986. Layering and related structures in the Duke Island and Skaergaard Intrusions: Similarities, differences and origins. In Origins of Igneous Layering. Edited by Ian Parsons. D. Reifel Publishing Company, Dordrecht, Holland: 185-246.

Jackson, E.D. and Thayer, T.P. 1972. Some criteria for distinguishing between stratiform, concentric and alpine peridotite-gabbroic complexes. 24th International Geological congress, Montreal. Proceedings Section 2: 289-296.

James, O.B. 1971. Origin and emplacement of the ultramafic rocks of the Emigrant Gap area, California. Journal of Petrology, 12: 523-560.

Kay, R.W. and Senechal, R.G. 1976. The rare earth geochemistry of the Troodos ophiolite complex. Journal of Geophysical Resources, 81: 964-970.

Kay, S. M., Kay, R.W., Citron, G.P. and Perfit, M.R. 1990. Calc-alkaline plutonism in the intraoceanic Aleutian arc, Alaska. In Plutonism from Antarctica to Alaska. Edited by Kay, S.M. and Rapela, C.W. Geological Society of America Special Paper 241: 233-255.

Kelemen, P.B., Johnson, K.T.M., Kinzler, R.J. and Irving, A.J. 1990. High-field-strength element depletions in arc basalts due to mantle-magma interaction. Nature, 345: 521-524.

Kemp, J.F. 1902. The geological relations and distribution of platinum and associated metals. United States Geological Survey, Bulletin 193.

Krogh, T.E. 1982. Improved accuracy of U-Pb ages by the creation of more concordant systems using an air abrasion technique. Geochemica et Cosmochemica Acta, 46: 637-649.

Kushiro, I. 1960. Si-Al relation in clinopyroxenes from igneous rocks. American Journal of Science, 258: 548-554.

Larson, L.M. 1981. Sector-zoned aegerine from the Illmaussaq alkaline intrusion, South Greenland. Contributions to Mineralogy and Petrology, 76: p. 285-291.

Larson, L.M., 1976. Clinopyroxenes and co-existing mafic minerals from the alkaline Illmaussaq intrusion. Journal of Petrology, 17: 258-290.

LeBas, M.J. 1962. The role of aluminum in igneous clinopyroxenes with relation to their parentage. American Journal of Science, 260: 267-288.

Leterrier, J., Maury, R.C., Thonon, P., Girard, D. and Marchal, M. 1982. Clinopyroxene composition as a method of identification of the magmatic affinities of paleovolcanic series. Earth and Planetary Science Letters, 59: 139-154.

Leung, I.S. 1974. Sector-zoned titanaugites: Morphology, crystal chemistry and growth. American Mineralogist, 59: 127-138.

Lippard, S.J., Shelton, A.W. and Gass, I.G. 1986. The Ophiolite of Northern Oman. The Geological Society, Memoir 11.

Loney, R.A. and Himmelberg, G. R. 1992. Petrogenesis of the Pd-rich intrusion at Salt Chuck, Prince of Wales Island: an early Paleozoic Alaskan-type ultramafic body. Canadian Mineralogist, 30: 1005-1022.

Loucks, R.R. 1990. Discrimination of ophiolitic from nonophiolitic ultramafic-mafic allochthons in orogenic belts by the Al/Ti ratio in clinopyroxene. Geology, 18: 346-349.

MacKenzie, G.C. 1920. An investigation of certain Canadian platinum and manganese resources. Canadian Institute of Mining and Metallurgy, 22: 305-319.

MacLellan, H.E. and Taylor, R.P. 1989. Geology and geochemistry of the Burnthill Granite and related W-Sn-Mo-F mineral deposits, central New Brunswick. Canadian Journal of Earth Sciences, 26: 499-511.

McClelland, W.C., Gehrels, G.E. and Saleeby, J.B. 1992. Upper Jurassic-Lower Cretaceous strata along the Cordilleran Margin: Implications for the accretionary history of the Alexander-Wrangellia-Peninsular terrane. Tectonics, 11: 823-834.

McCulloch, M.T. and Gamble, J.A. 1991. Geochemical and geodynamical constraints on subduction zone magmatism. Earth and Planetary Science Letters, 102: 358-374.

McDougall, I. 1974. The $^{40}Ar/^{39}Ar$ method of K-Ar age determination of rocks using HIFAR reactor. Atomic Energy in Australia, 17: 9-18.

McDougall, I. and Harrison, T.M. 1988. Geochronology and thermochronology by the $^{40}Ar/^{39}Ar$ Method. Oxford University Press, New York.

Mertie, J.B. Jr. 1969. Economic geology of platinum metals. United States Geological Survey, Bulletin 918.

Mielke, J.E. 1979. Composition of the Earth's crust and distribution of the elements. In Review of research on modern problems in geochemistry. Edited by F.R. Siegel.

International Association for Geochemistry and Cosmochemistry. UNESCO. pp. 13-37.

Molly, E.N. 1959. Platinum deposits of Ethiopia. Economic Geology, 54: 467-477.

Monger, J.W.G. 1985. Structural evolution of the southwestern Intermontane belt, Ashcroft and Hope map areas, British Columbia. In Current research, part A. Geological Survey of Canada, Paper 85-1A, pp. 349-358.

Monger, J.W.G. 1986. Geology between Harrison Lake and Fraser River, Hope map area, southwestern British Columbia. In Current research, part A. Geological Survey of Canada, Paper 86-1B, pp. 699-706.

Monger, J.W.G. 1989a. Geology of Hope and Ashcroft map areas, British Columbia. Geological Survey of Canada, Maps 41-1989 and 42-1989, scale 1:250 000.

Monger, J.W.G. 1989b. Overview of Cordilleran Geology. In Western Canada Sedimentary Basin, a case history. Edited by Brian D. Ricketts. Canadian Society of Petroleum Geologists, Calgary.

Monger, J.W.H., Price, R.A. and Tempelman-Kluit, D.J. 1982. Tectonic accretion and the origin of two major metamorphic and plutonic welts in the Canadian Cordillera. Geology, 12: 70-75.

Moore, J.M. 1989. Geology along the lithoprobe transect between the Guichon Creek Batholith and Okanagan Lake. In Geological Fieldwork 1988, Paper 1989-1, British Columbia Ministry of Energy, Mines and Petroleum Resources, pp 93-98.

Morgan, J.W. and Wandless, G.A. 1980. Rare earth elements in some hydrothermal minerals: evidence for a crystallographic control. Geochimica and Cosmochimica Acta, 44: 473-980.

Morimoto, I.N. 1988. Nomenclature of pyroxenes. Mineralogical Magazine, 52: 535-550.

Mortensen, J.K., Roddick, J.C. and Parrish, R.R. 1992. Evidence for high levels of unsupported radiogenic ^{207}Pb in zircon from a granitic pegmatite: Implications for interpretation of discordant U-Pb Data. EOS Spring Meeting, p. 370.

Mortimer, N. 1986. Late Triassic, arc-related, potassic igneous rocks in the North American Cordillera. Geology, 14: 1035-1038.

Mortimer, N. 1987. The Nicola Group: Late Triassic and Early Jurassic subduction-related volcanism in British Columbia. Canadian Journal of Earth Sciences, 24: 2521-2536.

Mortimer, N., van der Heyden, P., Armstrong, R.L. and Harakal, J. 1990. U-Pb and K-Ar dates related to the timing of magmatism and deformation in the Cache Creek terrane and Quesnellia, southern British Columbia. Canadian Journal of Earth Sciences, 27: 117-123.

Mossman, D. 1973. Geology of the Greenhills ultramafic complex, Bluff Peninsula, Southland, New Zealand. Geological Society of America Bulletin, 84: 39-62.

Murray, C.G. 1972. Zoned ultramafic complexes of the Alaskan-type: Feeder pipes of andesitic volcanoes: Studies in Earth and Space Sciences, Hess Volume. Geological Society of America, Memoir 132, pp 313-335.

Nakamura, Y. 1973. Origin of sector zoning in igneous clinopyroxenes. American Mineralogist, 58: 986-990.

Nakamura, Y. and Coombs, D.S. 1973. Clinopyroxene in the Tawhiroho tholeiitic dolerite at Moeraki, northeastern Otago, New Zealand. Contributions to Mineralogy and Petrology, 42: 213-228.

Nixon, G.T. and Rublee, V.J. 1988. Alaskan-type ultramafic rocks in British Columbia: new concepts of the structure of the Tulameen complex. In Geological Fieldwork, 1987. British Columbia Ministry of Energy, Mines and Petroleum Resources, Paper 1988-1: pp 281-294.

Nixon, G.T., Cabri, L.J. and LaFlamme, J.H.G. 1990. Platinum-group-element mineralization in lode and placer deposits associated with the Tulameen Alaskan-type complex, British Columbia. Canadian Mineralogist, 28: 503-535.

Noble, J.A. and Taylor, H.P. Jr. 1960. Correlation of the ultramafic complexes of southeastern Alaska with those of other parts of North America and the world. International Geological Congress, 21st Session Report, 13: 188-197.

O'Brien, J.A., Gehrels, G.E. and Monger, J.W.H. 1992. U-Pb geochronology of plutonic clasts from conglomerates in the Ladner and Jackass Mountain groups and the Peninsula Formation, southwestern British Columbia. In Current research, part A. Geological Society of Canada, Paper 92-1A, pp. 209-214.

O'Neill, J.J. and Gunning, H.C. 1934. Platinum and allied metal deposits of Canada. Canada Department of Mines, Economic Geology Series, no. 13.

Onuki, H. 1963. Petrology of the Hyachine ultramafic complex in the Kitakami Mountainland, northern Japan. Tohoku University Science Report, series 3, volume 8, number 3: 241-295.

Palmer, A.R. 1983. The Decade of North American Geology 1983 Geologic Time Scale. Geology, 11: 503-504.

Papike, J. J. 1980. Pyroxene mineralogy of the moon and meteorites. In Pyroxenes. Edited by C.T. Prewitt. Reviews in Mineralogy, 7.: 495-525.

Parrish, R.R. and Monger J. W.H. 1992. New U-Pb dates from southwestern British Columbia. In Radiogenic Age and Isotopic Studies: Report 5. Geological Survey of Canada, Paper 91-2, p. 87-108.

Parrish, R.R. and Wheeler, J.O. 1983. A U-Pb zircon age of the Kuskanax batholith, southeastern British Columbia. Canadian Journal of Earth Sciences, 20: 1751-1756.

Parrish, R.R., Carr, S.D. and Parkinson, D.L. 1988. Eocene extensional tectonics and geochronology of the southern Omineca belt, British Columbia and Washington. Tectonics, 7: 181-212.

Parrish, R.R., Roddick, J.C., Loveridge, W.D. and Sullivan, R.W. 1987. Uranium-Lead analytical techniques at the geochronology laboratory; Geological Survey of Canada, Paper 87-2, p. 3-7.

Pearce, J.A. 1983. Role of the sub-continental lithosphere in magma genesis at active continental margins. In Continental Basalts and Magma Xenoliths. Edited by C.J. Hawkesworth and M.J. Norris. Shiva Publication Ltd., Chesire, U.K..

Preston, J. 1966. An unusual hourglass structure in augite. American Mineralogist, 51: 1227-1253.

Preto, V.A. 1977. The Nicola Group: Mesozoic volcanism related to rifting in southern British Columbia. In Volcanic regimes in Canada. Edited by W.R.A. Baragar, L.C. Coleman and J.M. Hall. Geological Association of Canada, Special Paper 16, pp. 39-57.

Preto, V.A., Osatenko, M.J., McMillan, W.J. and Armstrong,R.L. 1979. Isotopic dates and strontium isotopic ratios for plutonic and volcanic rocks in the Quesnel trough and Nicola belt. Canadian Journal of Earth Sciences, 16: 1658-1672.

Price, R.A., Monger, J.W.H. and Roddick, J.A. 1985. Cordilleran Cross-Section; Calgary to Vancouver. In Field Guides to Geology and Mineral Deposits in the southern Canadian Cordillera. Edited by D. Tempelman-Kluit, Geological Society of America Cordilleran Section Meeting, Vancouver, B.C. May, 1985.

Raicevic, D. and Cabri, L.J. 1976. Mineralogy and concentration of Au- and Pt-bearing placers from the Tulameen River area in British Columbia. Canadian Institute of Mining and Metallurgy, Bulletin 69, no. 770: 111-119.

Read, P. B. and Okulitch, A.V. 1977. The Triassic unconformity of south central British Columbia. Canadian Journal of Earth Sciences, 14: 1127-1145.

Reitz, A. 1986. Geology and petrology of the northern San Emigdio plutonic complex, San Emigdio mountains, southern California. M.Sc. thesis, University of California, Santa Barbara.

Rice, H.M. 1947. Geology and Mineral deposits of Princeton map-area, British Columbia. Geological Survey of Canada, Memoir 243.

Rock, N.M.S. 1982. Chemical mineralogy of the Monchique alkaline complex, south Portugal. Contributions to Mineralogy and Petrology, 81: p. 64-78.

Rock, N.M.S. and Leake, B.E. 1984. The International Mineralogical Association amphibole nomenclature scheme: computerization and its consequences. Mineralogical Magazine, 48: 211-227.

Roddick, J.C. and Farrar, E. 1971. High initial argon ratios in hornblendes. Earth and Planetary Science Letters, 12: 208-214.

Rowins, S.M., Lalonde, A.E. and Cameron, E.M. 1991. Magmatic oxidation in the syenitic Murdock Creek Intrusion, Kirkland Lake, Ontario: Evidence from the ferromagnesian silicates. Journal of Geology, 99: 395-414.

Rublee, V.J. 1986. Occurrence and distribution of platinum-group elements in British Columbia. British Columbia Ministry of Energy Mines and Petroleum Resources, Open File 1986-7.

Rublee, V.J. 1989. The structural control of the Tulameen complex and outlying ultramafic rocks (92H/7,10). British Columbia Ministry of Energy, Mines and Petroleum Resources, Exploration in B.C., 1988: pages B71-B81.

Saleeby, J. 1992. Age and tectonic setting of the Duke Island ultramafic intrusion, southeast Alaska. Canadian Journal of Earth Sciences, 29: 506-522.

Sato, H. Tchoua, F. and Kusakabe. 1991. Olivine phenocrysts in some Cameroonian basalts: implications for primary magma composition. Mineralogy and Petrology 44: 253-269.

Saunders, A.D., Tarney, J. and Weaver, S.D. 1980. Transverse geochemical variations across the Antarctic peninsula: Implications for the genesis of calc-alkaline magmas. Earth and Planetary Science Letters, 46: 344-360.

Shervais, J.W. 1982. Ti-V plots and the petrogenesis of modern and ophiolitic lavas. Earth and Planetary Science Letters, 59: 101-108.

Simkin, T. and Smith, J.V. 1970. Minor element distribution in olivine. Journal of Geology, 78: 304-325.

Simpson, C. 1986. Determination of movement sense in mylonites. Journal of Geological Education, 34: 246-261.

Simpson, C. and Schmid, S.M. 1983. An evalutation of criteria to deduce the sense of movement in sheared rocks. Geological Society of America Bulletin, 94: 1281-1288.

Sisson, T. W. and Grove, T.L. 1993. Experimental investigations of the role of H_2O in calc-alkaline differentiation and subduction zone magmatism. Contributions to Mineralogy and Petrology, 113: 143-166.

Smith D. and Lindslay, D.H. 1971. Chemical variations in pyroxene and olivine from Picture Gorge Basalt. Carnegie Institute of Washington Year Book 69, pp 269-274.

Smith, T.E., Huang, C.H., Walawender, M.J., Cheung, P. and Wheeler, C. 1983. The gabbroic rocks of the peninsular ranges batholith, southern California: Cumulate rocks associated with calc-alkaline basalts and andesites. Journal of Volcanology and Geothermal Research, 18: 249-278.

Snoke, A.W., Quick, J.E. and Bowman, H.R. 1981. Bear Mountain igneous complex, Klamath Mountains California: an ultrabasic to silicic calc-alkaline suite. Journal of Petrology, 22: 501-552.

Snoke, A.W., Sharp, W.D., Wright, J.E. and Saleeby, J.B. 1982. Significance of mid-Mesozoic peridotitic to dioritic intrusive complexes, Klamath Mountains-western Sierra Nevada, California. Geology, 10: 160-166.

Springer, R.K. 1989. Mineralogy of a layered gabbro deformed during magmatic crystallization, western Sierra Nevada foothills, California. American Mineralogist, 74 : 101-112.

St. Louis, R.M. 1984. Geochemistry of the platinum group elements in the Tulameen ultramafic complex, British Columbia. M.Sc. thesis, University of Alberta, Edmonton.

St. Louis, R.M., Nesbit, B.E. and Morton, R.D. 1986. Geochemistry of platinum-group elements in the Tulameen ultramafic complex, southern British Columbia. Economic Geology, 81: 961-973.

Steiger, R.H. and Jäger, E. 1977. Subcommission on geochronology: convention of the use of decay constants in geo- and cosmochronology. Earth and Planetary Science Letters, 36: 359-362.

Stormer, J.C. Jr. 1972. Mineralogy and petrology of the Raton-Clayton volcanic field, northeastern New Mexico. Geological Society of America Bulletin 83: 3299-3320.

Stormer, J.C. Jr. 1973. Calcium zoning in olivine and its relationship to silica activity and pressure. Geochemica and Cosmochemica Acta, 37: 1815-1821.

Streckeisen, A. 1976. To each plutonic rock its proper name. Earth-Science Reviews, 12: 1-33.

Strong, D.F. 1969. Formation of hourglass structure in augite, Mineral Magazine, 37: 472-479.

Takahashi, E. 1986. Genesis of calc-alkali andesite magma in hydrous mantle-crust boundary: Petrology of lherzolite xenoliths from the Ichinomegata crater, Oga peninsula, northeast Japan, Part II. Journal of Volcanology and Geothermal Research, 29: 355-395.

Talkington, R.W., Watkinson, D.H., Whittaker, P.J. and Jones, P.C. 1986. Platinum group element-bearing minerals and other solid inclusions in chromite of mafic and ultramafic complexes: Chemical composition and comparisons. In Metallogeny of basic and ultrabasic rocks. Theophrastus Publications, S.A. Athens:223-247.

Tatsumi, Y. 1989. Migration of fluid phases and genesis of basalt magmas in subduction zones. Journal of Geophysical Research, 94: 4697-4707.

Tatsumi, Y., Hamilton, D.L. and Nesbitt, A.W. 1986. Chemical characteristics of the fluid phase released from the subducted lithosphere and the origin of arc magmas: evidence from high pressure experiments and natural rocks. Journal of Volcanology and Geothermal Research, 29: 293-309.

Taylor, H.P. Jr. 1967. The zoned ultramafic complexes of southeastern Alaska. In Ultramafic and related rocks. Edited by P.J. Wyllie. John Wiley and Sons, New York.

Taylor, H.P. Jr. and Noble, J.A. 1960. Origin of the Ultramafic complexes in southeastern Alaska. International Geological Congress, 21st Session Report, 13: 175-187.

Taylor, H.P. Jr. and Noble, J.A. 1969. Origin of magnetite in the zoned ultramafic complexes of southeastern Alaska. In Magmatic ore deposits: a symposium. Edited by H.D.B. Wilson. Monograph 4, Economic Geology, pp. 209-230.

Thompson, R.N. 1972. Oscillary and sector zoning in augite from a Vesuvian lava. Carnegie Institute Year Book, 71: 463-470.

Thompson, R.N., Morrison, M.A., Hendry, G.L. and Parry, S.J. 1984. An assessment of the relative roles of crust and mantle in magma genesis: an elemental approach. Philosophical Transactions of the Royal Society of London, series A, 310: 549-590.

Thorkelson, D.J. and Smith, A..D. 1989. Arc and intraplate volcanism in the Spences Bridge Group: Implications for Cretaceous tectonics in the Canadian Cordillera. Geology, 17: 1093-1096.

Travers, W.B. 1978. Overturned Nicola and Ashcroft strata and their relation to the Cache Creek Group, southwestern Intermontane belt, British Columbia. Canadian Journal of Earth Sciences, 15: 99-116.

Travers, W.B. 1982. Possible large-scale overthrusting near Ashcroft, British Columbia: implications for petroleum prospecting. Bulletin of Canadian Petroleum Geology, 30: 1-8.

Travers, W.B. 1987. Cache Creek-Ashcroft area, western Intermontane belt, British Columbia. Geological Society of America Centennial Field Guide-Cordilleran Section, pp. 407-412.

Verhoogen, J. 1962. Distribution of titanium between silicates and oxides in igneous rocks. American Journal of Science, 260: p. 211-220.

Wager, L.R. and Brown, G.M. 1968. Layeried igneous rocks. Oliver and Boyd, Edinburgh. 588 p.

Wakita, H. Rey, P. and Schmitt, R.A. 1971. Abundances of the 14 rare-earth elements and 12 other trace-elements in Apollo 12 samples: five igneous and one breccia rock and five soils. Proceedings of the 2nd Lunar Science Conference: 1319-1329.

Walawender, M.J. and Smith, T.E. 1979. Geochemical and petrological evolution of the basic plutons of the Peninsular ranges batholith, southern California. Journal of Geology, 88: 233-242.

Wallace, M.E. and Green, D.H. 1991. The effect of bulk rock composition on the stability of amphibole in the upper mantle: Implications for solidus positions and mantle metasomatism. Mineralogy and Petrology, 44: 1-21.

Wass, S.Y. 1973. The origin and petrogenetic significance of hour-glass zoning in titaniferous clinopyroxene. Mineralogical Magazine, 39: 133-144.

Williams, V.E. and Ross, C.A. 1979. Depositional setting and coal petrology of Tulameen coalfield, southcentral British Columbia. American Association of Petroleum Geologists, 63: 2058-2069.

Wilson, M. 1989. Igneous petrogenesis. Unwin Hyman, London. 466 p.

Wones, D.R. and Gilbert, M.C. 1981. Amphiboles in the igneous environment; In Amphiboles: Petrology and experimental phase relations. Edited by D.R. Veblin and P.H. Ribbe. Reviews in Mineralogy, 9B: 355-390.

Woodhead, J. Eggins, S. and Gamble, J. 1993. High field strength and transition element systematics in island arc and back-arc basins: evidence for multi-phase extraction and a depleted mantle wedge. Earth and Planetary Science Letters, 114: 491-504.

Wyllie, P.J. 1979. Magmas and volatile components. American Mineralogist, 64: 469-500.

Yoder, H.S. Jr and Tilley, C.E. 1962. Origin of basalt magmas: an experimental study of natural and synthetic rock systems. Journal of Petrology, 3: 342-532.

Mineral compositions: Olivine

Target no.	61	62	64	65	66	67	68	83	85	69
Sample	87-01-02	87-01-02	87-01-02	87-29-01	87-29-01	87-32-08	87-32-08	87-32-08	87-32-08	87-29-09
Lithology	dunite	dunite	dunite	wehrlite	wehrlite	ol. cpxt.	ol. cpxt.	ol. cpxt.	ol. cpxt	cpxt. dyke
Electron microprobe olivine analyses.										
SiO2	41.4	41	41	41.1	41.4	40.3	40.7	40.1	39.7	40.5
FeO*	10.2	10.3	10.2	9.3	9.2	13.6	13.3	13.8	13.5	12.1
MnO	0.23	0.22	0.24	0.21	0.19	0.23	0.23	0.23	0.24	0.26
MgO	49.1	49.1	49.4	49.6	49.6	46.5	46.8	46.5	47.4	47.6
NiO	0.12	0.13	0.12	0.12	0.01	0.13	0.11	0.12	0.11	0. 10
CaO	0.22	0.22	0.22	0.14	0.12	0.01	0.02	0.00	0.03	0.00
Total	101.3	100.9	101.2	100.5	100.3	100.8	101.1	100.7	101.1	100.6
Numbers of cations on the basis of 4 oxygens.										
Si	1.0043	0.9972	0.9942	1.0004	1.0064	0.9966	1.0016	0.992	0.9763	0.9968
Fe	0.2072	0.2098	0.2071	0.1896	0.1873	0.2817	0.274	0.2859	0.278	0.2494
Mn	0.0047	0.0450	0.0049	0.0043	0.0039	0.0048	0.0048	0.0048	0.005	0.0054
Mg	1.7756	1.7802	1.7857	1.7997	1.7973	1.7141	1.7168	107148	1.7377	1.7464
Ni	0.0023	0.0025	0.0023	0.0023	0.0020	0.0026	0.0022	0.0024	0.0022	0.002
Ca	0.0057	0.0057	0.0057	0.0037	0.0031	0.0003	0.0005	0.0000	0.0008	0.0000
% Forsterite	89	89	89	90	90	86	86	86	86	87

* All Fe as FeO

Mineral compositions: Olivine

Target no.	72	73	74	75	76	77	79	80	81
Sample	87-29-09	87 -29-09	88-16-2a	88-16-2a	88-16-2a	88-16-2a	87-28-01	87-28-01	87-28-01
Lithology	cpxt. dike	cpxt. dyke	ol. cpxt.	ol. cpxt.	ol. cpxt.	ol. cpxt.	gabbro	gabbro	gabbro
				Electron microprobe olivine analyses.					
SiO2	39.8	40.3	40.3	40.4	39.6	40.4	38.2	38.3	38.4
FeO*	12.5	12.5	13.7	13.7	13.5	13.9	22.7	22.9	22.2
MnO	0.26	0.21	0.25	0.25	0.23	0.26	1.25	1.13	1.11
MgO	46.5	47.3	46.2	46.6	46.3	46.4	38.1	38.5	39.6
NiO	0.11	0.11	0.13	0.11	0.11	0.11	0.03	0.04	0.04
CaO	0.01	0.02	0.02	0.03	0.01	0.02	0.06	0.07	0.06
Total	99.1	100.5	100.6	101.1	99.8	101	101	100.9	101.4
				Numbers of cations on the basis of 4 oxygens.					
Si	0.9958	0.9945	0.9993	0.9961	0.9882	0.9972	0.9952	0.9911	0.9841
Fe	0.2619	0.2583	0.2845	0.2829	0.2821	0.2873	0.4953	0.4963	0.4765
Mn	0.0055	0.0044	0.0053	0.0052	0.0049	0.0054	0.0276	0.0248	0.0241
Mg	1.7343	1.7400	1.7078	1.7128	1.7223	1.7073	1.4796	1.4851	1.5128
Ni	0.0022	0.0022	0.0026	0.0022	0.0022	0.0022	0.0276	0.0008	0.0008
Ca	0.0003	0.0005	0.0005	0.0008	0.0003	0.0001	0.0017	0.0019	0.0016
% Forsterite	87	87	85	86	86	85	74	74	75

* All Fe as FeO

Mineral compositions: Clinopyroxene.

Target no.	009	011	020	022	0 91	023	024	026	013	014
Spot no.	2	3	3	6	4	1	1	2	3	8
(notes)										
Sample	87-29-01	87-29-01	87-29-09	87-29-09	87-29-09	88-16-2a	88-16-2a	88-16-2a	87-32-08	87-32-08
Lithology	peridotite	peridotite								
SiO2	53.6	52.8	52.9	52.7	52.0	52.4	52.0	51.1	52.3	52.1
TiO2	0.06	0.00	0.11	0.16	0.13	0.24	0.13	0.10	0.13	0.26
Al2O3	0.88	0.66	1.23	1.26	1.23	1.52	1.56	1.69	1.12	1.44
FeO*	2.25	1.89	3.37	3.16	2.96	3.88	3.74	4.09	3.45	3.55
MnO	0.02	0.02	0.08	0.10	0.10	0.10	0.10	0.12	0.12	0.02
MgO	17.2	17.4	16.9	17.0	17.7	16.7	16.8	16.7	17.0	16.8
CaO	24.6	24.8	23.5	23.8	23.6	23.2	23.4	23.4	23.6	23.2
Na2O	0.40	0.29	0.26	0.26	0.25	0.33	0.27	0.36	0.19	0.25
K2O	0.01	0.00	0.00	0.03	0.00	0.03	0.00	0.03	0.00	0.00
Total	99.0	97.9	98.3	98.6	98.1	98.6	98.1	97.6	97.9	97.8

Mineral compositions: Clinopyroxene.

Target no.	093	094	015	016	017	087	027	028	029
Spot no.	8	8	2	3	4	5	1	1	2
(notes)									
Sample	87-32-08	87-32-08	87-29-08	87-29-08	87-29-08	87-29-08	88-16-05	88-16-05	88-16-05
Lithology									
SiO2	51.5	53.4	52.4	51.9	52.1	52.2	48.4	48.4	49.3
TiO2	0.16	0.18	0.18	0.22	0.27	0.16	0.55	0.60	0.63
Al2O3	1.44	1.38	1.90	2.16	2.16	2.03	5.36	4.86	4.87
FeO*	3.88	3.69	3.66	4.35	4.13	3.98	6.67	6.73	6.91
MnO	0.09	0.02	0.15	0.13	0.09	0.10	0.24	0.25	0.25
MgO	17.2	47.0	16.3	15.9	15.9	16.1	13.7	13.4	13.5
CaO	23.6	23.6	24.1	23.5	23.7	23.8	21.9	21.4	21.6
Na2O	0.26	0.32	0.31	0.30	0.29	0.36	1.02	1.18	1.04
K2O	0.03	0.00	0.00	0.00	0.02	0.00	0.06	0.04	0.00
Total	98.1	99.6	99.0	98.5	98.8	98.8	98.1	96.8	98.2

Mineral compositions: Clinopyroxene.

Target no.	001	002	003	004	005	006	007	008	055
Spot no.	1	3	3	8	8	9	9	9	8
(notes)		(rim)	(core)	(basal sect.)	(prism)	(basal)	(prism)	(centre)	(prism)
Sample	87-28-01	87-28-01	87-28-01	87-28-01	87-28-01	87-28-01	87-28-01	87-28-01	87-28-01
Lithology									
SiO2	49.5	49.4	49.0	50.3	49.1	49.0	48.9	49.2	49.2
TiO2	0.62	0.57	0.63	0.38	0.61	0.55	0.59	0.45	0.67
Al2O3	5.27	5.12	4.36	3.22	4.86	4.61	5.25	4.64	5.48
FeO*	7.17	7.21	6.95	6.29	6.51	7.07	7.18	6.87	6.89
MnO	0.41	0.23	0.26	0.23	0.21	0.28	0.21	0.22	0.22
MgO	13.2	13.2	13.8	14.8	13.9	14.1	13.2	14.0	12.7
CaO	21.4	21.1	21.6	22.1	21.6	21.8	21.5	21.9	21.4
Na2O	1.36	1.13	1.06	0.82	1.12	0.82	1.21	0.90	1.30
K2O	0.01	0.02	0.01	0.05	0.00	0.00	0.02	0.02	0.02
Total	99.0	98.0	97.9	98.2	98.2	98.3	98.0	98.3	98.0

Mineral compositions: Clinopyroxene.

Target no.	056	057	058	059	102	104	108	031	032
Spot no.	8	8	8	8	8	8	1	1	1
(notes)	(basal)	(basal)	(prism)	(prism)	(saganitic)	(saganitic)	(saganitic)	(saganitic)	recryst.
Sample	87-28-01	87-28-01	87-28-01	87-28-01	87-28-01	87-28-01	87-34-02	87-15-05	87-15-05
Lithology									
SiO2	51.2	49.4	49.2	49.5	49.8	49.8	50.5	50.9	50.6
TiO2	0.46	0.64	0.74	0.56	0.70	0.57	0.32	0.50	0.43
Al2O3	3.24	5.34	5.40	5.33	4.81	4.74	2.78	3.40	3.51
FeO*	6.16	7.39	7.08	7.01	6.41	6.99	8.06	5.73	5.85
MnO	0.28	0.39	0.26	0.27	0.21	0.31	0.29	0.21	0.20
MgO	14.1	12.8	12.7	12.7	14.1	13.7	13.1	15.0	15.3
CaO	22.1	21.3	21.5	21.1	21.8	22.0	23.4	23.1	23.2
Na2O	0.86	1.24	1.25	1.38	0.90	1.01	0.51	0.25	0.26
K2O	0.00	0.00	0.00	0.03	0.00	0.01	0.01	0.00	0.01
Total	98.5	98.6	98.2	97.9	98.8	99.6	99.3	99.2	99.3

Mineral compositions: Clinopyroxene.

Target no.	049	050	051	034	036	037	038	136	039
Spot no.	4	5	6	3	5	3	4	1	1
(notes)			(near hb)	relict core	relict core				(basal sect.)
Sample	87-34-03	87-34-03	87-34-03	87-21-03	87-21-03	87-18-01	87-18-01	87-18-01	88-16-4a
Lithology			contact	monzosyenite	monzosyenite				
SiO2	50.8	51.4	50.1	51.7	52.1	51.6	51.1	51.6	52.0
TiO2	0.32	0.27	0.35	0.43	0.26	0.36	0.34	0.30	0.35
Al2O3	2.21	1.95	2.27	2.12	2.09	1.73	2.02	1.73	2.37
FeO*	8.84	8.65	8.78	6.88	6.53	7.60	8.20	7.99	5.21
MnO	0.24	0.31	0.29	0.65	0.43	0.58	0.54	0.60	0.10
MgO	12.4	12.9	12.7	14.9	15.4	14.1	14.0	14.5	16.9
CaO	22.9	22.9	23.0	21.5	21.9	22.6	22.3	22.2	21.4
Na2O	0.46	0.55	0.56	0.59	0.52	0.47	0.48	0.49	0.17
K2O	0.00	0.01	0.00	0.00	0.00	0.00	0.01	0.00	0.00
Total	98.2	99.0	98.7	98.8	99.3	99.3	99.0	99.4	98.5

Mineral compositions: Clinopyroxene.

Target no.	040	041	042	044	045	052	053
Spot no.	1	1	1	3	3	7	8
(notes)	(prism sect.)	(basal sect.)	(prism sect.)	(basal sect.)	(prism sect.)		
Sample	88-16-4a	88-16-4a	88-16-4a	88-16-4a	88-16-4a	87-18-0	87-18-0
Lithology							
SiO2	48.0	50.6	47.3	50.9	48.4	51.1	51.1
TiO2	0.76	0.41	1.16	0.31	0.56	0.13	0.14
Al2O3	5.16	3.58	6.04	2.22	4.81	1.03	1.05
FeO*	6.01	6.18	7.11	5.21	6.00	9.16	9.27
MnO	0.13	0.16	0.10	0.13	0.15	0.35	0.45
MgO	14.1	15.7	13.8	16.6	14.4	12.9	12.9
CaO	22.2	21.4	22.1	21.6	21.9	23.2	23.0
Na2O	0.22	0.21	0.22	0.21	0.29	0.46	0.44
K2O	0.00	0.00	0.00	0.00	0.00	0.00	0.01
Total	96.7	98.3	97.9	97.3	96.7	98.4	98.7